

Therapy and mechanism of Mendelian eye diseases

Yi-Ting Tsai

Submitted in partial fulfillment of the
requirements for the degree of
Doctor of Philosophy
under the Executive Committee
of the Graduate School of Arts and Sciences

COLUMBIA UNIVERSITY

2018

© 2018
Yi-Ting Tsai
All rights reserved

Abstract

Therapy and mechanism of Mendelian eye diseases

Yi-Ting Tsai

Retinal degenerative diseases cause varying degrees of irreversible vision loss in millions of people worldwide. Common to all retinal degenerative diseases is the malfunction or demise of photoreceptor cells or its supportive cells, retinal pigment epithelium cell in the retina. A considerable part of these diseases were resulted from the inherited mutations of essential genes expressed in these retinal cells. The understanding of pathologic mechanism as well as developing of therapeutic treatment for these diseases were discussed in this study.

A cutting-edge therapeutic genome editing technology is studied in the first part of study. This technology was invented to treat retinitis pigmentosa via engineered nucleases, which has great clinical potential for autosomal dominant genetic disorders that were previously irreparable by conventional gene therapy interventions. Though customizable gene editing tools can be engineered to target specific mutation sites, however it is too daunting for diseases like retinitis pigmentosa, a progressive retinal degenerative condition associated with more than 150 mutations in the rhodopsin gene alone. Here in this study, we present an “ablate-and-replace” combination strategy that 1) destroys expression of the endogenous gene by CRISPR/Cas9 in a mutation-independent manner, and 2) enables expression of wild-type protein through exogenous cDNA. As proof of concept, we show that our CRISPR-based therapeutic machinery

efficiently ablates *mRho* in vivo, and when combined with gene replacement therapy, ameliorates rod photoreceptor degeneration and improves visual function in two genetically distinct autosomal dominant retinitis pigmentosa animal models. This mutation-independent, ablate-and-replace strategy represents the first electrophysiological recovery by a CRISPR-mediated therapy in an autosomal dominant disorder and it offers a clinically relevant, universal strategy to overcome allelic heterogeneity in debilitating inherited conditions.

For the second part of the study, gene editing technology was used to study the pathogenesis of Doyme honey comb dystrophy, another Mendelian disease with extensive similarities to age-related macular degeneration. This monogenic disorder is caused by a unique point mutation on an extracellular matrix protein *EFEMP1*, expressed by retinal pigment epithelium cell. To precisely gauge the physiological effect resulted from this mutation, CRISPR-mediated gene correction was used to create isogenic cell pairs from patient donated tissue-derived stem cells. These stem cells were differentiated into retinal pigment epithelium cell before analysis. We found unfolded protein response and immune response were not involved in the pathogenesis, which contradicts existing theories. Via proteomics analysis, we found expression level of a cholesterol catabolic enzyme was affected by the *EFEMP1* mutation while those proteins controlling the cholesterol transport remains constant. This result provides supportive evidence to explain the aberrant intracellular accumulation of cholesterol found in patient retinal pigment epithelium cells. This imbalance in lipid homeostasis also suggests Doyme honey comb dystrophy is a retinal pigment epithelium cell-autonomous disease.

Table of Contents

LIST OF FIGURES	iv
ACKNOWLEDGEMENTS	vii
CHAPTER 1: BACKGROUND OF OPHTHALMOLOGY, DISEASES AND POTENTIAL TREATMENTS	1
I. THE EYE AND THE RETINA	1
• BRIEF OVERVIEW OF THE EYE AND THE RETINA	1
• PHOTOTRANSDUCTION CASCADE	4
II. EYE DISEASES	11
• RETINAL DEGENERATION	11
• RETINITIS PIGMENTOSA	12
• DOYNE HONEY COMB DYSTROPHY	17
III. THERAPY FOR GENETIC DISEASES	21
• BRIEF OVERVIEW OF CURRENT EXPERIMENTAL THERAPIES	21
• GENE THERAPY	25
• GENE EDITING	26
• ADENO-ASSOCIATED VIRAL VECTORS	31
• GENE THERAPY CLINICAL TRIALS	39
CHAPTER 2: ESTABLISHMENT OF CRISPR-MEDIATED GENE ABLATION	41

I.	INTRODUCTION	41
II.	RESULT	45
III.	DISCUSSION	50
CHAPTER 3: ESTABLISHMENT OF AAV VECTORS AND SUBRETINAL INJECTION OF GENE		
THERAPY VECTORS		
		51
I.	INTRODUCTION	51
II.	RESULT	52
III.	DISCUSSION	65
CHAPTER 4: TEST OF ABLATE-AND-REPLACE VECTORS IN PRE-CLINICAL MODELS OF		
RETINITIS PIGMENTOSA		
		66
I.	INTRODUCTION	66
II.	RESULT	68
III.	DISCUSSION	76
IV.	FUTURE DIRECTIONS	78
CHAPTER 5: MATERIAL AND METHODS (FIRST PART)		
		79
CHAPTER 6: ESTABLISHMENT OF GENE CORRECTION TOOLSET FOR DOYNE HONEY		
COMB DYSTROPHY		
		85
I.	INTRODUCTION	85
II.	RESULT	86

III.	DISCUSSION	95
CHAPTER 7: IPSC REPROGRAMING AND RPE DIFFERENTIATION		96
I.	INTRODUCTION	96
II.	RESULT	97
III.	DISCUSSION	102
CHAPTER 8: PHENOTYPING OF PATIENT IPSC-DERIVED RPE		103
I.	INTRODUCTION	103
II.	RESULT	104
III.	DISCUSSION	112
IV.	FUTURE DIRECTIONS	115
CHAPTER 9: MATERIAL AND METHODS (SECOND PART)		116
Reference		122

LIST OF FIGURES

Figure 1. Structure of the retina	1
Figure 2. The phototransduction signaling	6
Figure 3. Repair of DNA double strand break	27
Figure 4. Components of CRISPR technology: Cas9 protein and gRNA	28
Figure 5. Subretinal and intravitreal injection	36
Figure 6. Illustration of Ablate-and-Replace gene therapy strategy	44
Figure 7. Illustration of double (CRISPRd) or single (CRISPRs) gRNA strategies to specifically ablate mouse <i>Rho</i> exon 1	45
Figure 8. Modified pX459 vectors for CRISPRd and CRISPRs	46
Figure 9. Genetic and expression outcomes following CRISPRd- vs CRISPRs-mediated gene editing	47
Figure 10. Validation of m <i>Rho</i> exon 1 truncation	48
Figure 11. Schematic summary of the basic outcomes produced by CRISPRd- and CRISPRs-mediated gene editing	49
Figure 12. Schematic design of primers to generate truncated <i>Rho</i> promoter with different length	52
Figure 13. Plasmid expressing transcription factors CRX, NRL and NR2E3	53
Figure 14. Testing of <i>Rho</i> promoter reporter	54
Figure 15. Different <i>Rho</i> promoters exhibit similar driving efficiency	55
Figure 16. Schematic of experimental (AAVs-Cas9+GR) and control (AAVs-Cas9+SR) AAV2/8 vector pairs	56

Figure 17. Conventional gene replacement therapy vs CRISPRd plus gene replacement, compound therapy for a heterozygous loci	57
Figure 18. The gRNAs sequences, their targeting sites on <i>mRho</i> and the corresponding sites on <i>hRHO</i>	58
Figure 19. Representative data of <i>in vitro</i> SpCas9/gRNA cutting	58
Figure 20. Experimental scheme and timeline for subretinal injection of dual AAV vectors in right eyes of wild-type C57BL/6J mice	59
Figure 21. Representative data of Cas9-immunostaining in retinal flat mount	60
Figure 22. Representative data of PCR analysis of retinal genomic DNA from AAVs-Cas9+GR-injected right eyes and uninjected, fellow (left) eyes	60
Figure 23. Representative data of mRho gene ablation validated by Sanger sequencing of PCR amplicon from Fig. 22	61
Figure 24. Gene ablation and replacement are co-localized in rod photoreceptors <i>in</i> <i>vivo</i>	62
Figure 25. Schematic of two different AAVs distribution scenarios	65
Figure 26. The amino acids of P23 and D190 on Rho structure	67
Figure 27. Experimental and disease progression timelines	69
Figure 28. Therapeutic effect of <i>Rho</i> ^{P23H/P23H} mice	70
Figure 29. Therapeutic effect of <i>Rho</i> ^{P23H/+} mice	73
Figure 30. Therapeutic effect of <i>Rho</i> ^{D190N/+} mice	75
Figure 31. gRNA targeting sites	86
Figure 32. <i>In vitro</i> gRNA targeting	87
Figure 33. Donor template design	88

Figure 34. Optimization of nucleofection program	90
Figure 35. Sequencing result of iPSC colonies after gene correction	94
Figure 36. Immunostaining of TRA-1-60 and SOX2	97
Figure 37. Immunostaining of SSEA4 and OCT4	98
Figure 38. iPSC culture of RPE differentiation before and after colonial enrichment	99
Figure 39. Morphology of iPSC-derived RPE after 200 days of differentiation	100
Figure 40. Immunostaining of RPE marker. Anti-BEST1 (red) and DAPI (blue) were used to stain iPSC-derived RPE	101
Figure 41. Real-time analysis of unfolded protein response biomarkers	104
Figure 42. ELISA analysis of pro-inflammatory cytokines	106
Figure 43. Proteomics analysis on patient-iPSC-derived RPEs by LC-MS/MS	108
Figure 44. Volcano plot comparing proteomic profiles between patient and wildtype iPSC-derived PREs	109
Figure 45. Volcano plot comparing proteomic profiles between gene-corrected and mutant iPSC-derived RPEs	110
Figure 46. Protein level changes after gene correction	111
Figure 47. Hypothesis illustration of potential mechanism resulting intracellular lipid accumulation	113
Figure 48. Medium and components used for RPE differentiation	118
Figure 49. Primers list for real-time PCR	121

ACKNOWLEDGEMENTS

I would first like to thank my advisor, Dr. Stephen Tsang for his guidance and mentorship over the years. He provided an excellent environment for me to broaden my sight in science. He taught me how to think about science, how to do science, and especially, how to argue science. It has been an honor to work in his lab. I am also grateful to my thesis committee members and other faculty mentors for their insightful suggestions and helpful advice throughout my PhD research. I also like to thank my colleagues and lab mates who have provided remarkable support and collaboration to my research. Finally, I would like to thank my wife Wen-Hsuan, who has provided me through moral and intellectual support in my work.

THE EYE AND THE RETINA

BRIEF OVERVIEW OF THE EYE AND THE RETINA

The eye is a sophisticated organ that provides information on the shape, light intensity, and color reflected from objects. The eye ball can be divided into two segments: anterior and posterior parts. The anterior segment comprises of the cornea, lens, iris and ciliary body, while the posterior segment consists vitreous, retina, and choroid. The eye ball can also be divided into three layers: the outermost layer for protection layer (sclera and cornea), the middle layer, the nutritive layer (the choroid, ciliary body and iris), and the innermost layer, neural sensory layer (the retina). Each layer has its importance; however, the focus in this section will be the retina.

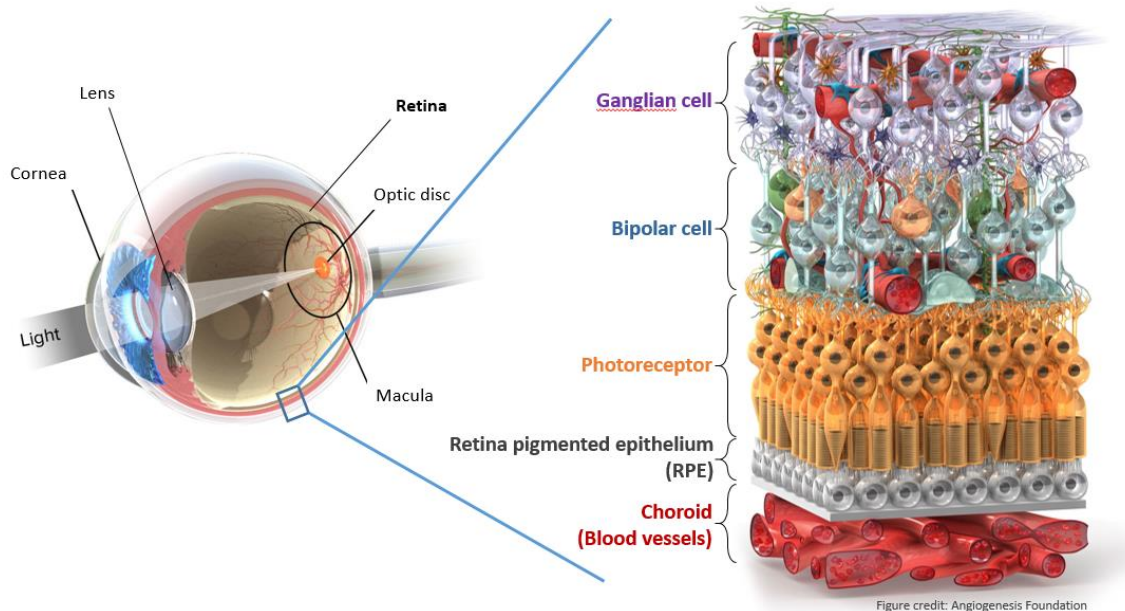


Figure 1. Structure of the retina. (Figure credit: Angiogenesis Foundation)

The retina is like the film or CCD of the camera. Retina contains at several types of different neuron cells that form more than 30 distinct synapses with one another (Fig. 1). The primary light sensitive neurons, called the photoreceptor cells, lie in the outermost layer of retina. The other retina cells, in order from the photoreceptor cells inwards: Müller glial cells, amacrine cells, bipolar neurons, horizontal cells, and the innermost ganglion cells¹. A layer of pigmented epithelium cells called retinal pigment epithelium (RPE) lies outwards to photoreceptor layer. RPE nourishes retinal visual cells, and is firmly attached to the underlying choroid and overlying retinal visual cells. RPE cells help nutrients and oxygen exchange from the choroid to photoreceptor.

The photoreceptor cells are very essential neuronal cells that can be divided into four counterparts: the outer segment (OS), inner segment (IS), soma, and a synaptic terminal for neurotransmission to the second-order cells of the retina. There are two types of photoreceptor, the rod and cone cells. Rod cells comprise approximately 97% of the total retinal photoreceptors, whereas cone cells make up the only 3% of the retinal photoreceptor cells in both mouse and human retinas. The IS segment in both of the rod and cone cells contains ribosomes, mitochondria, and ER membranes that are used to assemble and transport opsin molecules to the OS discs. In the rod cells, the OS features invaginations of the plasma membrane at its base, which makes detached stacks of disc structures. As for the cones, the discs remain attached to the OS membrane. The RPE cell pseudopodia continually renews these OS discs by separating the distal disc from the four remaining stack. These shed discs are then phagocytosed by RPE and degraded. This process can keep the photoreceptor cell OS length constant.

Each photoreceptor cell features a specific role for the type and amount of light that results in its unique signaling response. Rod cells are sensitive photoreceptors that respond to single photons of light. Therefore, they are active in dim-light settings and thus enable for night-time vision. Rods principally have a response range of three orders of magnitude, up to 10,000 photons per second (mesopic vision), at that point they saturate²⁻⁴. Once the rods saturate, the cones begin to activate (photopic vision). By shifting their operating curves, cones take the human eye out to more than ten billion photons per second.

There are completely different variations of cone cells, each accountable for sensing different wavelengths of light, and thus granting day-time, sight. In humans, there are three kinds of cone cells: the S-cones, L-cones, and M-cones. The macula, a central region of the retina, is enriched in cone cells, causing the cones to be accountable for the central visual field whereas the rod cells comprise the majority of the peripheral visual field^{2, 3, 5}. Using the photoreceptor cells' sensitivity to photons, the retina takes responsibility for two major functions of vision. One, it transduces photons into neural signals; and second, these neural signals are then transmitted to the brain in a manner within which the brain will acknowledge and decipher the visual image. Retinal circuits transform patterns of light and darkness on the photoreceptor mosaic of the retina, and these patterns result in repetitive discharges from a two-dimensional array of ganglion cells to the brain. Over the past years, progress has been done in understanding the mechanisms of neurocircuitry and phototransduction in the retina. No feedback from the brain to the retinal cells occurs during the visual process, and thus the phototransduction

signaling cascade in the photoreceptor rods and cones is of high importance to provide correct visual images.

PHOTOTRANSDUCTION CASCADE

The photoreceptor cells contain opsins within the OS discs, which are photosensitive pigments that photoactivate once light exposure. Every OS disc contains several million opsin molecules. These photoexcited opsins then stimulate the plasma membrane of the photoreceptors to trigger signals that are transmitted through the inner retina, to the optic nerve, and on to the brain. In the dark, there is a current that flows from the IS to the OS of the photoreceptor cell. After light exposure, the OS undergoes a process, known as the phototransduction cascade that interrupts this cell current. This cascade happens on the stacks of disc membranes and results in altered cyclic guanosine monophosphate (cGMP) levels in the photoreceptor OS. The fluctuation in cGMP levels in the photoreceptor transmits the light response signal from the OS discs to the cell membrane of the photoreceptor cell⁶. This process is rigorously regulated by numerous molecules, each of which is responsible for the activation, deactivation, and adaptation of the phototransduction cascade in the photoreceptor cell. The phototransduction cascade is activated once light is absorbed by a molecule in the OS of the photoreceptor, known as rhodopsin (RHO). Rho protein is a seven-loop transmembrane G-protein coupled receptor that contains a protonated Schiff base with a lysine side chain. This lysine side chain is covalently conjugated to an 11-cis chromophore^{7, 8}. A photochemical event happens after light sensation to the photoreceptor cells that causes the geometrical

photoisomerization of the pigment 11-cis retinylidene chromophore into an all-trans configuration⁹. After light stimulation, this pigment will no longer be photoactivated. Therefore, a mechanism exists within the retina to regenerate these light-sensing pigments. The all-trans retinylidene is isomerized back into the 11-cis configuration, to produce a pigment that can be photoactivated by light. This whole process is known as the visual cycle.

In the vertebrate, the Schiff base link between the chromophore and opsin is hydrolyzed, that permits for free all-trans retinal to be discharged. This is a process called bleaching⁹. This all-trans retinal is then reduced within the photoreceptor cell by NAD(P)H-dependent retinol dehydrogenases (RDHs) to yield all-trans retinol, otherwise referred to as vitamin A. All-trans-retinol is transferred into the RPE cell layer to be esterified by lecithin: retinol acyltransferase (LRAT) for storage⁹. In the RPE cells, stored all-trans retinyl esters are isomerized to 11-cis retinol by retinal pigment epithelial 65 kilodalton (RPE65) protein. This happens in a complex enzymatic reaction that involves the concurrent hydrolysis of the ester moiety. The 11-cis retinol is then converted to 11-cis retinal. 11-cis retinal then passes out of the RPE and into the outer segment of the photoreceptor cell to bind to opsin and form the RHO molecule.

While there are three unique opsins in cone cells, the RHO gene encodes the sole opsin in rod cells. RHO is firstly synthesized and modified by N-Glycosylation into the endoplasmic reticulum. In Golgi apparatus, proteins are further assembled into vesicles, to be exported from the inner segment of photoreceptor through the connecting cilium into the outer segment, where rhodopsin proteins (RHO) are directly integrated into the

disc membranes. RHO is a special G protein-coupled receptor, with seven trans-membrane domains, which can be assembled with the 11-cis-retinal chromophore (derivative of vitamin A), to function. When the photon enters into the retina, photons are captured by the 11-cis-retinal. This molecule will undergo a conformational change (isomerization) to all-trans-retinal isomer. This reaction is the first step of phototransduction cascade (Fig. 2).

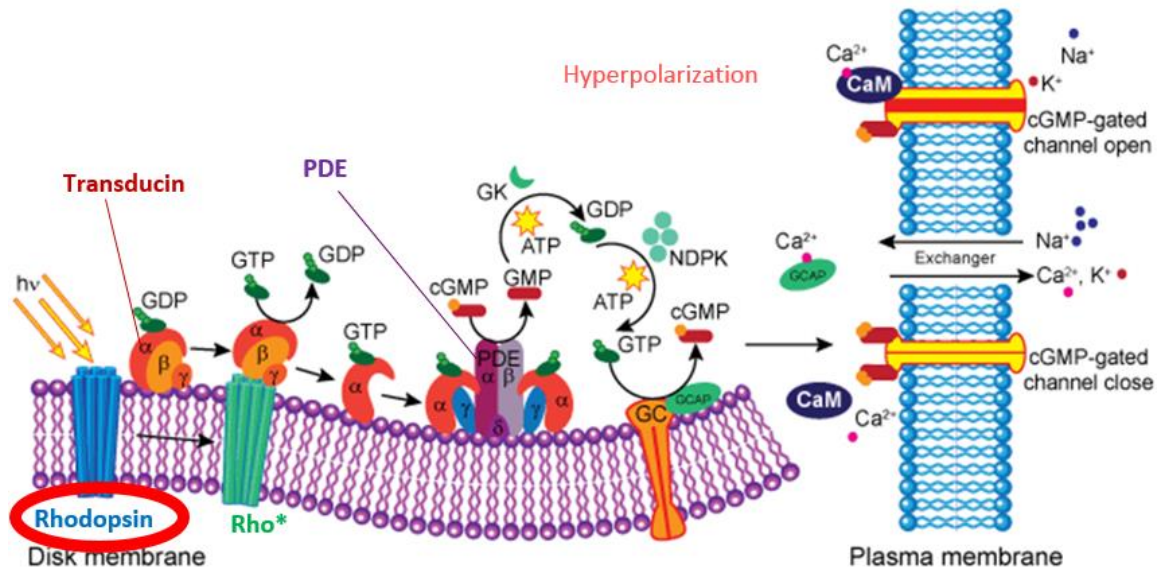


Figure 2. The phototransduction signaling.

Light causes this RHO molecule to an activated state with conformational change. This product is called metarhodopsin II (Rh*). Rh* next activates it downstream molecules transducin (Gtαβγ). Gtαβγ are heterotrimeric G-proteins which can act by exchanging

guanosine diphosphate (GDP) for guanosine triphosphate (GTP)¹⁰. This activation by Rh* causes GTP to bind to the G α subunit of G $\alpha\beta\gamma$. Then, this G α -GTP dissociates from the G $\beta\gamma$ portions of G $\alpha\beta\gamma$. Once dissociation, the G α -GTP binds to the inhibitory γ subunits of cyclic guanosine monophosphate (cGMP)-phosphodiesterase 6 (PDE6).

PDE6 is a heterotetrameric protein consisting of a catalytic α -subunit, a catalytic β -subunit, and two inhibitory γ -subunits within the rod photoreceptor cell. In the cone, PDE6 consists of a catalytic dimer that contains two identical α' subunits, instead of the α and β subunits found in the rod. In addition, the γ' inhibitory subunits of the cone PDE6 differ slightly in size and amino acid composition from the rod γ inhibitory PDE6 subunits⁶. PDE6 is highly essential in the phototransduction cascade, because it is the primary regulator of cytoplasmic cGMP concentration in the photoreceptor cells. In the dark, PDE6 is in an inactive form, with the γ inhibitory subunits attached (PDE6 $\alpha\beta\gamma$), and cGMP level inside the photoreceptor cell OS is high (several micromolars)⁶. This permits for cGMP-gated Na⁺/Ca²⁺ ion (CNG) channels in the plasma membrane to stay open, allowing a current to circulate through the photoreceptor cell.

After light stimulation of the phototransduction cascade, the binding of G α -GTP on the γ -subunits of PDE6 eliminates the inhibition on the catalytic α - and β -subunits of PDE^{10, 11}. The activated PDE6 hydrolyzes cGMP, breaking it down and lowering its concentration within the photoreceptor cell. This light-activated PDE is about three hundred times greater active than in its basal state, swiftly breaking down the cyclic nucleotide levels¹². The fast reduction of cGMP within the photoreceptor cell after light stimulation of the phototransduction cascade causes the CNG channels located in the

plasma membrane to shut. Consequently, the levels of Na^+ and Ca^{2+} into the cytoplasm are decreased, causing the rod cell to become hyperpolarized. Hyperpolarization of the rod cell causes it to lower glutamate at its synaptic terminal to signal to the other neuronal cells of the retina and on to the optic nerve and the brain.

After light stimulation, the phototransduction cascade has to undergo deactivation to return cGMP to its basal levels. The photoexcited Rh^* is inactivated via the phosphorylation of threonine and serine residues at its carboxyl tail by a rhodopsin-specific kinase known as G protein-dependent receptor kinase I (GRK1)¹³. This phosphorylated rhodopsin ($\text{Rh}^*\text{-P}$) has greater efficiency binding toward a molecule called arrestin (Arr; also known as S-antigen), instead of $\text{Gt}\alpha$. Arr inhibits the removal of the phosphate groups on $\text{Rh}^*\text{-P}$ ¹⁴. This hastily reduces the amount of dephosphorylated, active Rh^* available for the activation of $\text{Gt}\alpha$ and the rest of the phototransduction cascade.

Moreover, $\text{Gt}\alpha$ has intrinsic GTPase activity to inactivate itself after its binding to the γ inhibitory subunits of PDE6¹². The PDE6 $\alpha\beta$ catalytic subunits re-associate with the two PDE6 γ subunits for inactivation of the PDE6 complex while retinal guanylate cyclases (Ret GC-1 and Ret GC-2) become activated and reproduce cGMP within the photoreceptor cell¹³. The recovery of the basal cGMP concentration in the photoreceptor cell re-opens the CNG channels. The deactivation process is now complete. Activation of the phototransduction cascade begins again while $\text{Rh}^*\text{-P}$ -Arr binds to 11-cis retinal which releases the molecule from Arr. The $\text{Rh}^*\text{-P}$ is then dephosphorylated by phosphatase 2A and the light/dark activation/deactivation cycle can continue in the photoreceptor cell.

In addition to the activation and deactivation of the phototransduction cascade, there is also the photoreceptor adaptation to constant light stimulus. As formerly referred to, light stimulation of the phototransduction cascade ends in the closure of the CNG channels in the photoreceptor OS. This induces a decline in Ca^{2+} influx into the photoreceptor. Intracellular Ca^{2+} levels act to inhibit the guanylate cyclases (Ret GC-1 and Ret GC-2). Consequently, Ret GC-1 and Ret GC-2 are activated when light stimulates the phototransduction cascade and Ca^{2+} levels reduce within the cell¹⁵⁻¹⁷. This occurs through the stimulation of Ret GC-1 and Ret GC-2 with the aid of the guanylate cyclase activating proteins (GCAP-1/p-20 and GCAP-2/p24). These guanylate cyclases work to create more cGMP to counteract the reduction in cGMP by PDE6 after the activation of the phototransduction cascade.

Additionally, a molecule known as recoverin then mediates the Ca^{2+} sensitivity of GRK1 phosphorylation of Rh^* . For that reason, extended light leads to a decrease in Ca^{2+} levels and induces GRK1 activity by decreasing recoverin's inhibition of GRK1¹⁵⁻¹⁷. Furthermore, the CNG channel, accountable for the ionic current of the photo-response, binds a molecule called calmodulin at high levels of Ca^{2+} , and extended light reduces calmodulin binding and leads to a decline in the channel affinity for cGMP. This causes the channel to re-open at lower levels of cGMP than it would in dark environment.

Lastly, light adaptation results in a greater inhibition of the PDE6 enzyme to permit for a speedy reduction in the hydrolysis of cGMP. Ca^{2+} -sensitive members of the protein kinase C family phosphorylate the two PDE6 γ subunits. This phosphorylation site is blocked while the γ subunits are bound to PDE6 $\alpha\beta$, but light activation of the

phototransduction cascade allows for $G\alpha$ -GTP to discharge the γ inhibitory subunits from the PDE6 $\alpha\beta$ complex. After GTP hydrolysis, free PDE6 γ are then phosphorylated by members of the protein kinase C family at threonine 35, which permits them to re-bind to PDE6 $\alpha\beta$ and cause a stronger inhibition of the catalytic activity of PDE6.

Any alterations of the phototransduction cascade, such as changes affecting the renewal and shedding of the photoreceptor OS or visual transduction, or even retinol metabolism can have a remarkable impact on the retinal integrity. Mutations within any of the related molecules accountable for those visual processes may cause numerous types of retinal and RPE degenerative conditions. The majority of retinal degenerations are caused by gene defects, leading to a lower protein levels or incorrect protein functions. For instance, the inability of the RPE to phagocytose the photoreceptor OS causes a type of autosomal recessive retinitis pigmentosa (arRP). This disease and other retinal degenerative diseases, are a common healthcare issue in the world¹⁸.

EYE DISEASES

RETINAL DEGENERATION

Unfortunately, retinal degeneration is a common occurrence in the world. The loss of sight affects about 3.4 million people in the United States. Alone and is predicted to increase over the years¹⁹. Visual impairment ranks merely behind arthritis and cardiovascular disease with respect to disease impact on function in the elderly. In fact, visual loss is frequently considered by patients to be their dominant health issue, even in the presence of other chronic disabling disorders²⁰. Patients experience a loss of quality of life, as they require assistance in daily tasks such as walking, reading, or driving.

There is great genetic and allelic heterogeneity of the several retinal dystrophies. These conditions have been categorized using age of onset, electrophysiological and psychophysical studies. However, those classifications can be ambiguous as there are comparable clinical presentations in retinal degenerations arising from different genetic mechanisms. For example, RP can be caused by both mutations within proteins of the phototransduction cascade, such as RHO or PDE6, and also by mutations within rod OS membrane proteins, such as peripherin^{21, 22}. Moreover, different mutant alleles at the identical locus can cause diverse clinical manifestations of disease. For instance, mutations in the β subunit of PDE6 can cause different kinds of retinal degenerative diseases: such as congenital stationary night blindness or RP^{21, 22}. Currently, the most accurate method of classification is based on the specific molecular genetic defect, and genetic testing is becoming a common practice utilized by clinicians to improve their clinical diagnosis.

RETINITIS PIGMENTOSA

As mentioned, photoreceptor neurodegenerative diseases have great impacts on both patients and society. Unfortunately, there is no cure^{18, 23-26}. One of the most devastating photoreceptor degenerative diseases is retinitis pigmentosa (RP), which is the focus of this study. RP is the most common cause of hereditary blindness in the world, affecting about 1:3000 people^{18, 26}. There are various forms of RP, including autosomal dominant (15-20% of cases), autosomal recessive (20-25% of cases), and X-linked (10-15%). The remaining 40-55% of cases is currently of unclassified inheritance^{23, 26-30}. Those unclassified RP patients are typically due to the absence of familial histories, and are denoted as simplex RP. Most simplex RP cases are believed to be autosomal recessive³⁰. Autosomal dominant forms of RP are generally the mildest, with onset that can occur as late as 50 years of age. Autosomal recessive, however, are more severe and disease onset normally occurs during the first decade of life^{26, 30}. Moreover, RP can be secondary in etiology and is involved in more than 30 disease syndromes.

Genetically, most forms of RP are monogenic, even though there have been cases of digenic-diallelic and digenic-triallelic inheritances. Due to RP being both locus heterogenous and phenotypically heterogenous, mutations in no single gene are known to cause greater than 10% of 14 cases of RP³⁰. In 2013, there are 45 genes mapped that cause non-syndromic forms of RP, although there is likely to be many more genes responsible for this disease as about 200 more genes have already been identified that are involved in retinal disease²⁶.

Gene	Estimated Proportion of adRP Attributed to Mutations in This Gene	Protein
<i>RHO</i>	30-40%	Rhodopsin
<i>PRPF31</i>	5%-10%	U4/U6 small nuclear ribonucleoprotein Prp31
<i>PRPH2</i>	5%-10%	Peripherin-2
<i>RPI1</i>	3%-4%	Oxygen-regulated protein 1
<i>IMPDH1</i>	2%-3%	Inosine-5'-monophosphate dehydrogenase 1
<i>PRPF8</i>	2%-3%	Pre-mRNA-processing-splicing factor 8
<i>KLHL7</i>	1%-2%	Kelch-like protein 7
<i>NR2E3</i>	1%-2%	Photoreceptor-specific nuclear receptor
<i>CRX</i>	1%	Cone-rod homeobox protein
<i>PRPF3</i>	1%	U4/U6 small nuclear ribonucleoprotein Prp3
<i>TOPORS</i>	1%	E3 ubiquitin-protein ligase Topors
<i>CA4</i>	Rare	Carbonic anhydrase 4
<i>NRL</i>	Rare	Neural retina-specific leucine zipper protein
<i>ROM1</i>	Rare	Retinal outer segment membrane protein 1
<i>RP9</i>	Rare	Retinitis pigmentosa 9 protein
<i>RDH12</i>	Unknown	Retinol dehydrogenase 12
<i>SNRNP200</i>	Unknown	U5 small nuclear ribonucleoprotein 200 kDa helicase
<i>AIPL1</i>	Rare	Aryl-hydrocarbon-interacting protein-like 1
<i>BEST1</i>	Rare	Bestrophin- 1
<i>PRPF6</i>	Rare	Pre-mRNA-processing factor 6
<i>RPE65</i>	Rare	Retinoid isomerohydrolase
linked to 6q23; gene not identified	Linkage in one family	not identified
<i>GUCA1B</i>	4%-5% in Japan; rare in UK	Guanylyl cyclase-activating protein 2
<i>FSCN2</i>	3% of Japanese with adRP; otherwise rare	Fascin-2
<i>SEMA4A</i>	3%-4% in Pakistan	Semaphorin-4A

Table 1. Genes associated with autosomal dominant retinitis pigmentosa (adRP).

Adapted from sph.uth.edu/retnet/ and Fahim et al., GeneReviews, 1993²³.

In RP, the progressive atrophy of the rod photoreceptor cells results in the secondary death of the cones. Affected individuals will present with night blindness,

tunnel vision, and eventual loss of central vision when cone cells degenerate. This photoreceptor cell death has been thought to result from a caspase-dependent apoptotic mechanism, as was observed in animal models of retinal dystrophies^{31, 32}. However, there have been recent research suggesting that other disease pathways, such as calpain-mediated cell death or proteasome activity, may be responsible for the degeneration of the photoreceptor cells^{13, 33, 34}. Although it stays to be elucidated which death mechanism leads to the loss of the photoreceptors, RP can be categorized into three stages of clinical disease.

In stage I of RP, patients usually present with night blindness. While some patients ignore this symptom, and typically will not recognize the disease phenotype until the teenage years, when they attend evening events. There are not any visual defects presented in the daylight, and patients have normal life activities. Only the electroretinogram (ERG), a clinical test that measures the electrophysiological response of the retinal cells to flashes of varying light intensities, will display a loss of visual response at this time^{27, 29}. Hence, at the early disease stage most patients will not be clinically diagnosed with RP.

In the mid-stage of RP, patients will have difficulty performing nighttime activities, such as driving, and will become aware of a loss of their peripheral visual field even in the daylight. Moreover, patients may become photophobic, especially in regards to diffuse light, such as cloudy weather days^{27, 29}. This imposes difficulty reading and performing daily activities. At this stage, patients notice the disease phenotype, visit a clinician, and are generally diagnosed with RP.

At the clinic, fundus examination will show the presence of bone-spicule shaped pigment deposits in the mid-periphery of the retina, along with retinal pigment epithelial atrophy. Narrowing of the retinal vessels is also obvious at this time. ERG examination will display an attenuated visual response in the cone cells, and a complete loss of visual response under scotopic, dark-adapted conditions^{27,29}. This phenomenon reflects the loss of the majority of the rod photoreceptor cells.

In the final stage of RP, the clinical manifestations that occur in the mid-stage of the disease will worsen until the patients have lost their ability to perform daily tasks on their own, without assistance from others. They will then continue to deteriorate until the loss of their central visual field, rendering them blind. This disease not only affects the patient and their cherished ones, but society as a whole. RP patients have progressively declining vision that inevitably leads to blindness, and society is confronted with the high costs of caring for each of these visually handicapped persons for the remainder of their lives.

RP is arguably one of the best model for studying neurodegenerative diseases, for three main reasons. First of all, the basic pathogenic process in RP, that of rod cell atrophy leading to a secondary, non-autonomous death of the cone cells, is generalizable to other types of retinal degenerative diseases, such as age-related macular degeneration (AMD) or even normal aging¹³.

Secondly, many mouse models now exist for mutations in Rho leading to RP, which is the most common cause of autosomal dominant RP¹³. Third, in contrast to mouse

models of EYS³⁵ or ABCA4³⁶, common photoreceptor degenerative diseases in which the mouse model does not mimic human disease, these mouse models with loss of function of Rho mimic the human phenotype^{37, 38}.

More than 120 single nucleotide mutations have been reported in RHO gene, each of them can lead to retinal degeneration. Within those RHO mutation-induced retinal degeneration, most of them can cause autosomal dominant retinitis pigmentosa (adRP), but also sometimes autosomal recessive RP (arRP) or congenital stationary night blindness. These mutations are homogeneously distributed on RHO gene. Every mutation can cause disease through different mechanisms. These pathogenesis based on diverse RHO mutations can be classified into several groups.

Classification	Behaviour	Site of point mutation	Misfolds
Class I	Fold normally but are not transported to the outer segment	L328, T342, Q344, V345, A346, P347	No
Class II	Are retained in the ER and cannot easily reconstitute with 11- <i>cis</i> -retinal	T17, P23, G51, T58, V87, G89, G106, C110, L125, A164, C167, P171, Y178, E181, G182, C187, G188, D190, H211, C222, P267, S270, K296	Yes
Class III	Affect endocytosis	R135	No
Class IV	Do not necessarily affect folding but affect rod-opsin stability and posttranslational modification	T4	No
Class V	Mutations show increased activation rate for transducin	M44, V137	No
Class VI	Show constitutive activation of opsin in the absence of chromophore and in the dark	G90, T94, A292,	No
Unclassified	No observed biochemical or cellular defect or not studied in detail	N15, Q28, L40, F45, L46, P53, G109, G114, S127, L131, Y136, C140, E150, P170, G174, P180, Q184, S186, T193, M207, V209, P215, M216, F220, E249, G284, T289, S297, E341	

Table 2. Classification of rhodopsin mutations. Adapted from Mendes et al., TRENDS in Molecular Medicine, 2005³⁹.

For instance, P23H mutation, which belongs to class II RHO mutations, has been described to be retained in the ER in cellular models^{40, 41}. This has been suggested to induce the unfolded protein response, which can lead to apoptosis⁴². This mechanism could be an explanation for photoreceptor degeneration, however this theory is still under debate in the *in vivo* context^{43, 44}.

Scientists and clinicians have started searching for therapeutic agents that will be effective in slowing the photoreceptor cell death, and/or curing the causative genetic defect.

DOYNE HONEY COMB DYSTROPHY

Doyme Honey Comb Dystrophy (DHRD) is an inherited condition that affects the eyes and causes vision loss. This disease was described initially in inhabitants or descendants of the Leventine valley of Tessin Canton in Southern Switzerland⁴⁵. A R345W mutation can be found in EGF Containing Fibulin Extracellular Matrix Protein 1 (EFEMP1) from all the DHRD patients^{46, 47}.

DHRD is characterized by small, round, yellow-white deposits known as drusen that accumulate between the retinal pigment epithelium (RPE, the nutritive layer of cells deep in the retina that helps maintain the function of the photoreceptor cells) and Bruch's membrane (BrM)⁴⁶⁻⁴⁸. The thin BrM is a pentalaminar matrix located between RPE and choroid. BrM is a semipermeable filtration barrier through which major metabolic exchange takes place⁴⁹. BrM has five layers (from the innermost to the outermost): the

RPE basement membrane, the inner collagenous zone, the elastic zone, the outer collagenous zone, and the choriocapillaris basement membrane. The inter fiber matrix of BrM is principally composed of heparin sulfate, chondroitin or dermatan sulfate. The chondroitin sulfate in BrM is believed to provide an electrolytic barrier to diffusion.

When DHRD progress over time, drusen may enlarge and come together, creating a honeycomb pattern. At this point, patients may start to notice changes in their visual acuity (the clarity or sharpness of vision)⁵⁰⁻⁵². Typically, people with DHRD do not have symptoms until 30-40 years of age. Early visual symptoms may include: decreased visual acuity; problems seeing color; relative scotomas (a defect in the visual field resulting in problems seeing objects of low brightness); photophobia (eye discomfort in bright light); and metamorphopsia (distorted vision). In the later stages of the condition, usually by the age of 40 to 50 years, one's central vision deteriorates. Additionally, absolute scotomas can develop. These visual defects (which are surrounded by normal visual field) are associated with total loss of vision within that specific area.

DHRD is usually characterized by slowly progressive loss of central visual acuity. To some extent, the degree of severity is associated with age. Mild cases are usually detected between 20 to 40 years of age⁵². They are characterized by normal vision and the presence of small, discrete drusen in the macula. More severe cases generally occur at or after 50 years of age and are associated with profound loss of visual acuity.

However, the severity of symptoms in DHRD can be variable. There are always exceptions to the "typical" age of onset and course of DHRD. For example, there have been

reports of people with DHRD in their sixties who still have good vision. In other affected people, their disease course may change to one of faster progression and severe visual loss if choroidal neovascularization (CNV) occurs^{48, 53-55}. CNV involves the growth of new blood vessels from the choroid into the subretinal space, and is a major cause of visual loss⁵⁶.

The importance of these diseases is due in large part to their close phenotypic similarity to age-related macular degeneration (AMD), a disorder with a strong genetic component that accounts for approximately 50% of registered blindness in the Western world⁵⁷⁻⁶⁰. Just as in ML and DHRD, the early hallmark of AMD is the presence of drusen⁶¹. Though in AMD, no genetic or other causative factor has been found.

The origin of drusen is still a mystery. Drusen is discrete extracellular deposits that commonly precede the development of AMD, and that are comprised of numerous cellular and inflammatory factors. Other than mutant EFEMP1 protein itself⁶², RPE basement membrane molecules such as collagen IV, VI, laminin, and heparan sulfate proteoglycans were found in drusen⁶³⁻⁶⁶. Other proteins such as vitronectin, MMP-7, TIMP-3, C3, and C5b-9 have also been reported^{67, 68}.

Lipid particles accumulate within Bruch's membrane in the exact location and prior to the development of basal deposits or drusen. This observation has led to the hypothesis that these lipid particles contribute to drusen formation during the development of AMD. Recent work suggests that the lipoprotein particles found within Bruch's membrane are distinct from plasma lipoproteins and have been found to contain

free and esterified cholesterol, phosphatidylcholine (PC), and apolipoprotein B100^{69, 70}. Curcio et al. found that esterified cholesterol comprised 60% of total cholesterol within these lipoproteins, and esterified cholesterol was 7-fold higher in the macula than periphery⁷¹. It has been speculated that membranous debris is membrane-bound packets of RPE cytoplasm released by the RPE⁷² or RPE basal in foldings disintegrating with age⁷³. This secretion of basement membrane-like material and lipid particles, may polymerize or condense to produce long spacing collagen and dense amorphous material, and finally, release of membranous debris forms large drusen⁷⁴.

THERAPY FOR GENETIC DISEASES

BRIEF OVERVIEW OF CURRENT EXPERIMENTAL THERAPIES

Patients with RP are not curable, and at this time there are not any standard treatments in clinical practice to halt the progression of photoreceptor degeneration and loss of vision. However, there are numerous methods being studied to try to slow down the rate of degeneration and allow for patients to extend the time in which they are able to maintain their central visual field. One approach used for patients with RP is to provide dark sunglasses for use outdoors, in order to block the amount of light to the photoreceptor cells^{26, 30}. Since a majority of RP cases are caused by mutations within the phototransduction cascade, which is activated by light, this decreases the effects of those mutations by limiting the light stimuli. Moreover, yellow-orange glasses block photophobic effects for patients and are suggested by some clinicians^{26, 30}. However, those methods for protecting the photoreceptor cells cannot offer a cure for the disease, and various other therapeutic options are being tested for RP patients.

A main research that was conducted examining the effects of vitaminotherapy for RP. Vitamin A was hypothesized to protect the photoreceptor cells through a trophic effect, and vitamin E via anti-oxidant protective effects^{26, 30}. Studies have shown that long-term supplementation of daily vitamin A was capable to slightly ameliorate the loss of visual function as observed by the cone ERG b-wave amplitude in RP patients. However, 400 units of vitamin E per day had unfavorable effects in RP patients^{23, 27, 30}. Since vitamin A is stored within the body, patients taking vitamin A supplementation at high doses have

to be monitored as well for potential toxicity, and clinicians debate the usefulness of this treatment.

Another method is to provide RP patients 1200mg/day of docosahexanoic acid (DHA) supplements in addition to the vitamin A supplementation, which showed an initial slowing of the disease progression in trials, but one which did not last in patients beyond two years of follow-up⁷⁵⁻⁷⁷. Moreover, patients with the ABCA4 gene mutation that leads to Stargardt's disease, another retinal degenerative disease, have negative effects after vitamin A supplementation⁷⁵⁻⁷⁷. Those are the most promising treatment options at this time for RP, and whether or not they will have any significant slowing of retinal degeneration is controversial.

Some other choice is to apply pharmacological treatments if the mechanism of degeneration is known for the patient. Animal studies have tested the use of calcium channel blockers to slow down RP progression. This is thought to be effective since increases in cGMP leads to a constant opening of the CNG channels and alters the ion current to cause photoreceptor cell death. However, those animal studies have shown limited success⁷⁵⁻⁷⁷. One of the promising pharmacological treatments analyzed the effects of 9-cis retinal in mouse models of Leber congenital amaurosis (LCA), an early-onset blinding disorder. LCA patients have mutations in RPE65, the isomerase that acts in the visual cycle for the conversion of all-trans retinyl esters to 11-cis retinal for binding to opsin. 9-cis retinal is assumed to be able to bind opsin and create a modified form of rhodopsin that can be activated by light and function in the phototransduction cascade. Delivery of 9-cis retinal to the Rpe65^{-/-} mouse model of LCA has restored rod cell function,

however further studies are necessary to determine the efficacy of rescue for this pharmacological treatment⁷⁵⁻⁷⁷.

Other pharmacological therapies include treating mouse models of Stargardt disease, a blinding disorder which is believed to involve the accumulation of bisretinoid lipofuscin in the RPE, with visual cycle inhibitors. Those studies have also found some slowing in the accumulation of lipofuscin, thought to lead to the RPE-related disease phenotype⁷⁵⁻⁷⁷. As more genetic mutations and mechanisms of retinal degenerative diseases are recognized, pharmacological treatments can become more targeted and better developed. These agents are promising, and may have the potential to be beneficial therapeutic options to decelerate the progression retinal degenerative diseases, such as RP.

Another treatment method is to use growth factors to form neuroprotection to the photoreceptor cells and thus limit photoreceptor degeneration. Animal models have shown therapeutic efficacy using an array of growth factors, including ciliary neurotrophic factor, brain-derived neurotrophic factor, and glial-derived neurotrophic growth factor⁷⁵⁻⁷⁷. However, these growth factors have to be introduced in situ to the animal, due to the short half-life of the growth factors. Many strategies are being developed for this drug delivery, such as gene transfer and the use of encapsulated cells placed into the vitreous cavity⁷⁵⁻⁷⁷. However, these growth can have side effects that include cataract, which could lead to a loss of vision. The application of ciliary neurotrophic factors is currently in phase I of human clinical trials for patients with RP; however it has been shown to lower the ERG

response in some animal models of retinal degeneration, suggesting a potential unwanted effect of the growth factor or delivery system⁷⁵⁻⁷⁷.

Besides treatments that may only decelerate the progression of retinal degeneration, scientists are also working on strategies to replace the already degenerated photoreceptor cells. One method in which to achieve this goal is to use retinal prosthetic devices. Those devices incorporate microphotodiode arrays that are able to capture light and stimulate the retina. They can be incorporated into the eye to act in the phototransduction cascade, or they can be included in sites accountable for later stages of the visual signaling cascade. Those sites include directly stimulating the optic nerve or the visual cortex of the brain. One of these early retinal prosthetic devices has been approved by the Federal Drug administration and is proven to be tolerated by the human patients after implantation⁷⁵⁻⁷⁷. However, these devices are not yet a standard therapy for RP, but further studies and improvements in the prosthetics can make them a feasible option.

Another method to replace the degenerated photoreceptor cells is to transplant cells from fetal or adult retina into patients. In current published cases, researches transplantation studies using photoreceptors allowed survival of the transplanted cells within the host diseased retinas, however they were not able to arrange and organize themselves to provide proper structure and synaptic connections⁷⁵⁻⁷⁷. An alternative therapy will be the use of stem cells, by using either embryonic or patient-derived induced pluripotent stem cells, to create sheets of cells or tissues for transplantation into patients with RP. Promising results from cell transplantation experiments have been found in

animal models of retinal degenerative diseases. RPE grafts have been proven to rescue both the Royal College of Surgeons (RCS) rat and the Rpe65^{-/-} mouse models^{78, 79}. Nevertheless, these therapies are still undergoing development and more studies have to be done before one can create a purified cell or tissue of interest *in vitro* that will be able to make all the essential synaptic connections *in vivo* after transplantation.

GENE THERAPY

Gene therapy has become a promising therapeutic tool for treating blindness due to inherited retinal degenerative diseases. Current technology has allowed for the elucidation of disease-causing alleles and specific genetic defects, which grants scientists the capability to create a gene therapy vector which can target those specific genes of interest. There are numerous vectors that can be applied for gene therapy, including both viral and non-viral vectors. Though usually, to maximize the transduction efficiency, viral vectors are used; although small molecules are now being created that have the potential to efficiently transfect the cells of the retina.

The first viral vector to be developed for use in gene therapy was the lentivirus. Lentiviruses were of interest because of the fact that they could hold approximately 9 kilobases (kb) of deoxyribonucleic acid (DNA), and more importantly, infect non-dividing cells, such as the photoreceptor cells^{13, 23, 75}. Lentiviral vectors take advantages of the human immunodeficiency virus (HIV) genome. Second and third generation lentiviruses are being developed, in which several regulatory proteins are deleted from the packaging

construct⁸⁰. At present, only the *in vivo* potential pathogenicity of the HIV-1 based viruses, such as lentiviruses, can be determined by *in vitro* tests, and more technical improvements and experimental studies of both efficiency and safety need be examined comprehensively before their clinical use.

GENE EDITING

For the treatment of dominant disease, a new approach has emerged that enables investigators to directly manipulate genes both *in vitro* and *in vivo*. This principal technology – usually referred to as “gene editing” or “genome editing” – is based on the application of engineered nucleases consist of sequence-specific, DNA-binding compartment fused to a DNA cleavage module^{128, 129}. These chimeric nucleases enable reliable and precise genetic modifications by introducing double-strand breaks (DSBs) on DNA at a designated site in the genome that can potentially stimulate the cellular DNA repair mechanisms, including non-homologous end joining (NHEJ) and homology-directed repair (HDR)^{128, 129}(Fig. 3). The versatility of this technology is enabled by the programmability of the DNA-binding ability that are obtained from zinc-finger (ZFN) and transcription activator-like effector (TALENs) proteins. In addition to those two technologies, investigators have also successfully developed a more efficient system using Clustered Regularly Interspaced Short Palindromic Repeats (CRISPR), which is a prokaryotic immune system that confers adaptive resistance to foreign genetic matters such as those double or single strand RNA and RNA present within plasmids and phages¹³⁰⁻¹³².

ZFNs were the first of the “genome editing” nucleases used in research. Zinc fingers are the most well-known DNA binding domain existed in eukaryotes. They typically are modules consist of around thirty amino acids that interact with nucleotide triplets. ZNFs have been engineered to recognize all of the 64 possible trinucleotide combinations^{128, 129, 133}. By stringing different zinc finger moieties, it is feasible to use ZNFs specifically target any specific sequence of DNA triplets. Each ZNF can recognize 3-6 nucleotide triplets. Because these nucleases can only function as dimers, pairs of ZNFs are necessary to carry out specifically targeting (one ZFN to recognize the sequence upstream and the other to recognize the downstream sequence of the site to be modified).

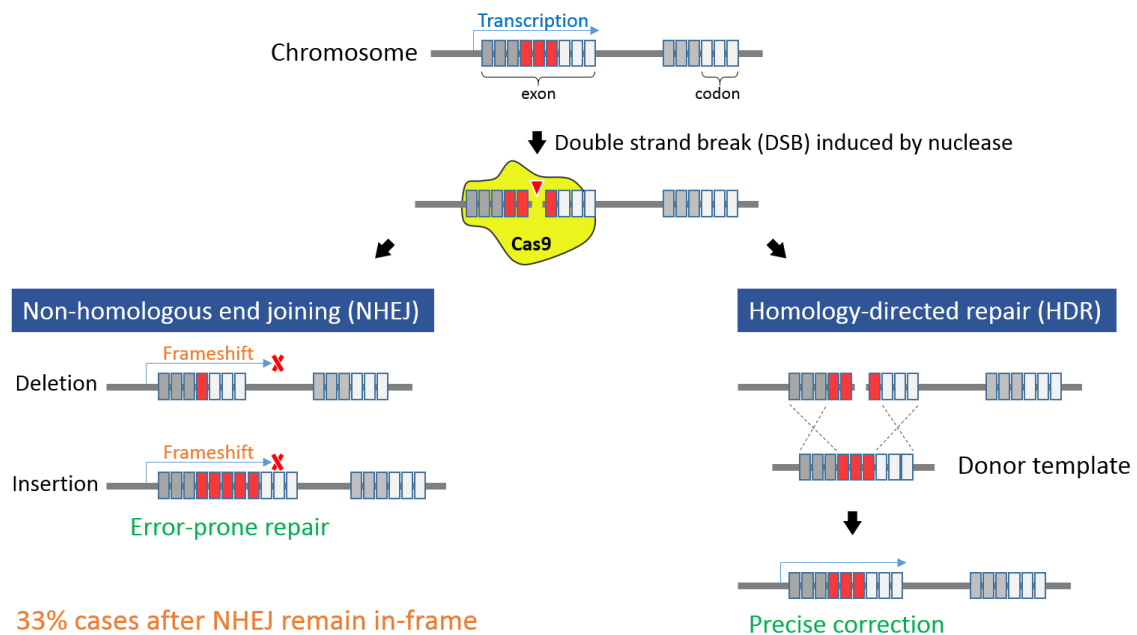


Figure 3. Repair of DNA double strand break

TALENs, on the other hand, is similar to ZNFs in that they use DNA binding motifs to guide the same non-specific endonuclease to cleave the DNA at a specific site in the genome¹³³. However, instead of recognizing DNA triplets, each TALENs domain recognizes a single nucleotide. The interactions between the DNA binding domains and their target nucleotides are less sophisticated than those between ZNFs and their target trinucleotides. This simplicity grants easier designing of TALENs in comparison to ZNFs¹³⁴-136.

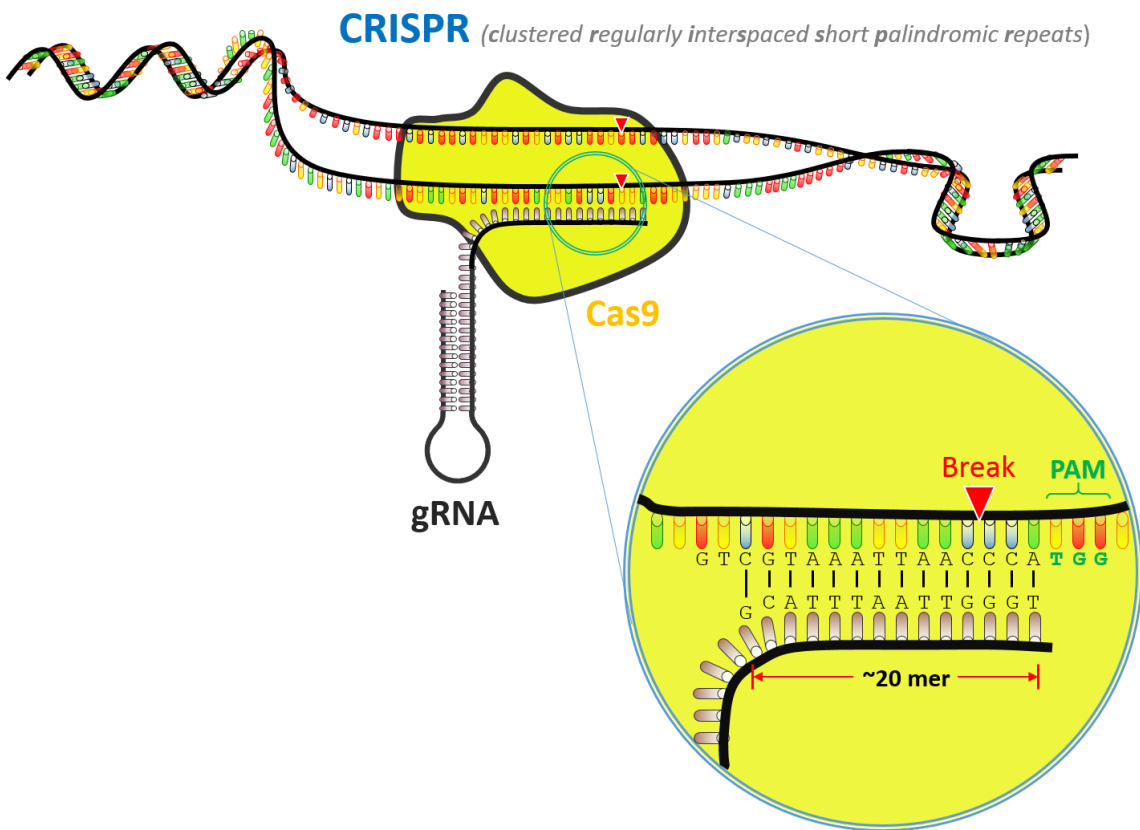


Figure 4. Components of CRISPR technology: Cas9 protein and gRNA.

CRISPR is the latest but most exciting development in genome editing technology. CRISPR are RNA-based prokaryotic defense mechanisms evolved to recognize and exclude foreign DNA from invading bacteriophages¹³⁷. CRISPR consists of an endonuclease called “Cas” that is directed to cleave a target sequence by a guide RNA (gRNA)¹³³(Fig. 4). Both the Cas endonuclease and the gRNA are naturally encoded in the bacterial genome, and this system can act synergistically to cleave any desired target site by engineering the sequence of the gRNA.

Just like the ZNF and TALEN systems, the CRISPR system can also be used to create double-strand break at a specific site. This break can then induce the occurrence of non-homologous end joining or homology-directed repair for the creation of desired mutation or gene correction^{130, 133}.

The CRISPR system provides several advantages over the ZNF and TALEN systems. First, as mentioned, it is restively easier to make the target design. Because the target specificity totally depends on RNA/DNA complex formation instead of protein/DNA recognition, gRNAs can be designed readily in a cost-efficient way to target almost any sequence in the genome^{130, 133}. Second, CRISPR has a higher efficiency among all three gene editing tools. DNA manipulation can be created by direct injection of Cas9 protein and gRNAs into developing mouse embryos. This method eliminates the laborious processes of transfecting and screening mouse ES cells that are required to generate targeted mutant mice using traditional homologous recombination techniques^{130, 133}.

And the last, CRISPR is possible to be multiplexed. Several mutations can be introduced in one or multiple genes at the same time by a single injection with multiple gRNAs.

All three gene editing technologies offer researchers with handy methods to develop mutant mouse or cell model for the studying of human disease, which were previously difficult to create by traditional gene targeting methods¹³⁸. However, all these three methods has some potential drawbacks. The most critical issue is off-target effect¹³⁸⁻¹⁴⁰. Unwanted mutation can be introduced at non-specific loci with similar, but not identical sequence to the target sites. These odd-targeting effects can be difficult to identify and usually require scanning of the whole genome for searching these mutations (usually by whole genome sequencing). Another disadvantage is the difficulty of delivery, especially for the purpose of gene therapy. For instance, the most widely-used Cas9, the SpCas9 is around 4 kb. For the packaging of the transgenes comprising Cas9 and associated gRNA can barely fit into an AAV vector. Efficient expression of those large nucleases for gene editing requires further development and improvement.

Despite these drawbacks, ZNFs, TALENs and especially the CRISPR/Cas systems are still so far the most powerful tools for manipulating the genomes. It can be expected refinements of these systems will continue to perfect genetic therapies for treating human diseases.

ADENO-ASSOCIATED VIRAL VECTORS

Most experiments utilize an adeno-associated virus (AAV) as the new standard for retinal gene therapy^{24, 81-84}. AAV is a non-enveloped, icosahedral-shaped member of the parvoviridae family; thus, it is a small virus with a virion about 25nm in diameter composed entirely of protein and DNA^{85, 86}. This fact means that AAV vectors are merely capable of packaging approximately 4.7 kb of DNA^{85, 87}. Hence, both the gene of interest and the promoter must fit this space requirement, making it a limiting factor of using AAV.

The AAV2 genome is the most widely studied, and is constituted of linear, single-stranded DNA containing 4679 nucleotides^{24, 81-88}. The AAV genome is composed of three open reading frames (ORFs) flanked by inverted terminal repeat (ITR) sequences that act as the viral origin of replication (ori) and packaging signal^{81, 82, 85}. AAV2 carries one ORF with two genes that encode four non-structural replication proteins (Rep40, Rep52, Rep68, and Rep78) and another ORF with three 60-mer capsid proteins (VP1, VP2, and VP3), together with the third ORF containing an assembly-activating protein which is flanked on each side by 145 base-pair ITRs^{85, 89, 90}. The two larger replication proteins, Rep68 and Rep78, play a role in many aspects of the AAV2 life cycle, including transcription, replication of the viral DNA, and site-specific integration into human chromosome 19. The other two smaller replication proteins are used for packaging of the DNA into the viral capsid^{85, 91}. The three capsid proteins have different translational start sites, even though they come from the same gene.

There are eleven known naturally occurring serotypes for AAV, and over 100 artificial variants⁸⁶. The capsid proteins can be found in distinctive configurations for the

various AAV serotypes, AAV1-9, however it is believed that they are found in a ratio of 1:1:10 VP1:VP2:VP3^{85, 92, 93}. These AAV capsid proteins determine its tropism (the ability to transduce specific cell types), permitting both cell surface receptor binding and the entry into the host cell nucleus⁸⁶. The mechanism by which AAV enters a host cell is through phagocytosis by receptor-mediated endocytosis^{85, 94}. There has been *in vivo* evidence supporting the use of both clathrin-coated pits and clathrin-independent carriers/glycosylphosphatidylinositol-anchored protein-enriched endosomal compartments for this process⁸⁶. The mechanism of cell entry for each AAV serotype remains to be studied.

After entry into the host cell, the capsid then leaves the endosome and gets into the nucleus. There has been evidence supporting both uncoating before nuclear entry, and uncoating after nuclear entry, and the exact timing of the uncoating of the capsid is yet to be clarified⁸⁶. Nevertheless, the localization to the host cell nucleus occurs via capsid protein VP1, which contains a phospholipase domain that allows for the escape from the endosome^{85, 95}. The N-termini of capsid proteins VP1 and VP2, which comprise nuclear localization signals, then direct the capsid to the host cell nucleus^{85, 96}. The genome is released in the nucleus by the capsids and converted to double-stranded DNA by means of the replication proteins and host cellular DNA synthesis machinery^{85, 86, 97}.

Without the presence of a helper virus, AAV enters a latent life-cycle and the DNA is retained in a circular episomal form in the nucleus, otherwise integrated into the human chromosome 19, at a specific locus termed AAVS1^{85, 98-101}. Due to the fact that AAV serotypes contain modifications in the capsid proteins, each serotype has diverse tropism

for different target cells and tissues. Hence, recombinant AAV vectors utilized in gene therapy have to be selected for their tropism to efficiently and effectively transduce the cell-type of interest. For instance, AAV1 was found to more effectively transduce muscle cells when compared to AAV2, and AAV5 to more effectively transduce the central nervous system in comparison to AAV2. These tissues are highly targeted by different serotype to treat disease, making these AAV serotypes thrilling for the potential of introducing gene therapy vectors to those tissues that were previously difficult for clinicians and researchers to treat with therapeutic agents.

The recombinant AAV used as a packaging vector for gene therapy has its viral compartments, the replication and capsid proteins, removed from the gene therapy virus. This makes the AAV non-pathogenic and theoretically safe for human clinical trials. The ITRs that flank the AAV genome are the only cis-acting elements in the AAV that are required for the genome replication, integration, and packaging of the capsid⁸⁵. Hence, the replication and capsid proteins flanked by the ITR sites are replaced with the promoter and gene of interest for gene therapy. The replication and capsid proteins are then expressed in trans in a separate plasmid that lacks the ITRs, preventing the formation of a viral AAV particle after delivery. The recombinant AAV vector is feasible transduce both dividing and non-dividing cells with stable transgene expression without the presence of a helper virus in post-mitotic tissue⁸⁶. These features make recombinant AAV a remarkable tool for gene therapy studies⁸⁵ and trials for human diseases.

However, science did not stop developing the AAV gene therapy vector system at this point. These recombinant AAV particles have been made more efficient using

numerous technological advances. One of these is the creation of self-complementary (sc) AAV vectors. In scAAV vectors, the terminal resolution site of one ITR has been removed, preventing the initiation of replication at this end^{85, 102}. This creates a single-stranded, inverted repeat viral genome with one wild-type ITR at one end and a mutated ITR in the center. This allows for the vector genome to fold after uncoating and creates a double-stranded, or self-complementary, genome.

These scAAVs, hence, do not require the host cell DNA synthesis machinery synthesize single-stranded DNA to double-stranded DNA before transcription and translation; they are incorporated with their DNA in the double-stranded form. There is a faster gene expression using scAAV vectors in comparison to recombinant AAV vectors, due to this skipped step in DNA synthesis, and these scAAV vectors have been found capable to transduce different cell types that previously did not express transgenes using the recombinant, single-stranded AAV vectors⁸⁵. However, these vectors are almost half the size (around 2.5 kb) of the recombinant AAVs, making them more restricting than recombinant AAV vectors due to DNA packaging constraints.

Scientists found another method in which to strengthen the recombinant AAV vectors. They created hybrid AAVs, in a procedure called “pseudotyping,” to create vectors that target specific cell types with greater efficiency. At the time, research had observed AAV gene therapy viruses to be restricted in regards to certain cells of interest. For instance, AAV2 vectors were the most carefully studied, and AAV2 vectors were used to efficiently transduce RPE cells in many animal models for several years. This made them an appealing therapeutic agent due to the fact they could potentially have a long-term

effect after a single administration of the vector into human patients¹⁰³. Even though AAV2 has been proven more effective for transduction of the RPE cells, it was not clearly shown to have a long-lasting effect on the photoreceptor cells^{104, 105}.

Hence, pseudotyping became a method to create AAV vectors that would more efficiently transduce the photoreceptor cells and other specific types which were not specifically targeted by AAV2. Pseudotyping relies on the recombinant AAV2 plasmid (with the ITRs from AAV2) and packages it into a capsid derived from another AAV serotype. This design puts the AAV2 replication genes downstream of the p19 promoter with the respective replication genes of another serotype followed after the promoter sequence^{85, 106}. These AAV vectors are named after the serotype 2 replication proteins (genome) and the serotype from the AAV serotype capsid proteins. For instance, a wild-type AAV2 capsid vector is typically written as “AAV2/2,” while the pseudotyped AAV with serotype 8 capsid for the gene therapy vector used in this study is written as “AAV2/8.”

This pseudotyping procedure grants advantages in the usage of AAVs in regards to improving gene therapy. For instance, the same vector genome, from AAV2, when packaged into the different AAV serotype capsids, the only difference between the pseudotyped AAV vectors is their viral capsid. This enables research to analyze each AAV serotypes *in vivo* and precisely determine its transgene expression efficiency and tissue tropism^{85, 106, 107}. The commonly used AAV serotype, AAV2/2, features a gradual increase in transgene expression over time, reaching plateau at approximately 2-4 months post-injection. In contrast, AAV2/1 or AAV2/5 vectors were able to initiate transgene expression much sooner, usually 3-4 days post-injection¹⁰³.

Besides the early gene expression feature, the different AAV serotypes and pseudotyped vectors were found to have diverse tropism, especially to different retinal cells. For instance, AAV2/4 is more efficiently to target the RPE cells than AAV2/2 or AAV2/5 when targeting both RPE and photoreceptors, while AAV2/8 has been found to have best efficiency targeting all the retinal cells (including photoreceptors, the RPE cells and the rest of the cells of the neural retina^{24, 81, 103, 104, 106, 107}. Thus, researchers can choose the AAV gene therapy vector based on the desired cell type that they are interested in targeting, and appropriate time frame they would like the transgene expression to initiate in the cell.

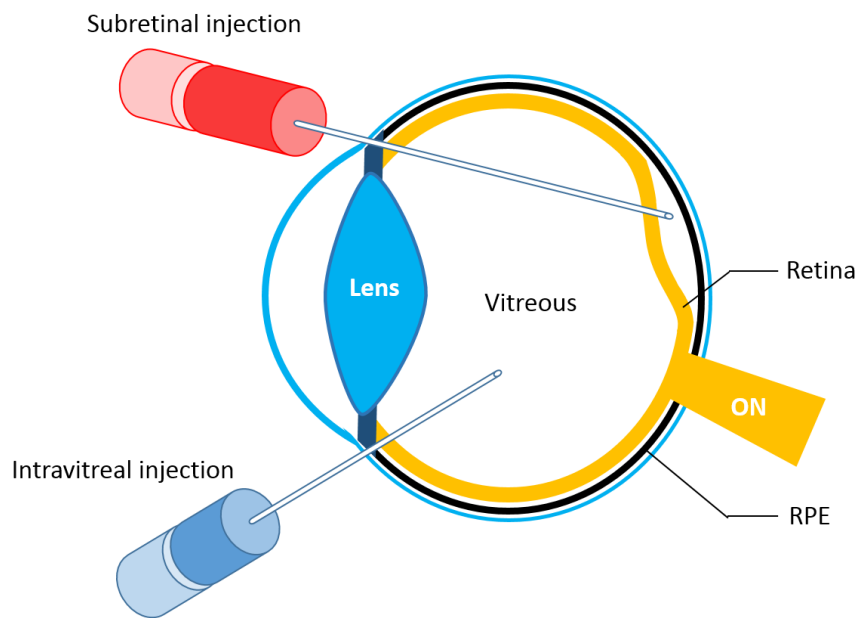


Figure 5. Subretinal and intravitreal injection.

For the drug delivery in retina, there are typically two main routes for viral administration by injection (Fig. 5): intravitreal and subretinal^{81, 92, 103}. Intravitreal injection introduces the AAV vector within the vitreous space of the eye, which permits viral delivery to the retinal ganglion cells or Müller glial cells. It is an ideal route for anti-angiogenic therapies for conditions such as diabetic retinopathy. Intravitreal injections are now standard practice by most ophthalmic clinicians^{81, 92, 103}. Currently, researchers are looking into developing AAV vectors that could pass through the complex retinal cell layers after intravitreal delivery¹⁰⁸. Unfortunately, currently there is no AAV serotype that can efficiently transduce the RPE or photoreceptor cells through intravitreal injection.

Subretinal injections are more optimal for the targeting of the RPE or photoreceptor cells. This method introduces the virus into the interspace between the RPE and photoreceptors, creating a temporary cavity with retinal detachment termed the “subretinal bleb.” This retinal detachment will naturally disappear after the diffusion of the viral agent^{92, 103}.

Subretinal injections are clinically used for human patients, but unlike intravitreal injections, this technique requires an invasive surgical procedure. In humans, the surgical procedure involves a partial vitrectomy to increase the volume of the AAV being injected, and also to balance intraocular pressure. However, it is not possible to carry out the vitrectomy procedure in mouse model. It is still possible to perform the subretinal injection on mice, but it requires careful skill and practice. Due to the small size of mouse eye ball, subretinal injection on mice usually has a successful rate at only 20%. In addition, the mouse eye has a much larger lens when comparing to humans. The lens must be

avoided during the surgical procedure otherwise can lead to cataract formation and a loss of vision. Therefore, for both mice and humans, the subretinal injection surgical procedure is typically more challenging than ordinary intravitreal injection and has a higher rate for surgical morbidities^{92, 103}. However, it is the best method for achieving efficient transduction on RPE and photoreceptor cells. Injections of the current established AAV serotypes into the subretinal space are capable to transduce the RPE cells with 100% efficiency in the location surrounding the subretinal bleb, and approximately 20-40% transduction efficiency of the photoreceptor cells in the area within the subretinal bleb, depending on the used AAV serotype for transgene delivery^{92, 103}.

Lastly, once the correct gene therapy vector has been selected, the method of administration determined, the clinician must then be concerned about safety issue. Immune response to the viral injections has become a concern following initial gene therapy trials on human patients. The gene therapy treatment itself may be successful, but when it comes to the adverse side effects, especially in young children, could potentially resulted in unwanted effects^{87, 109, 110}.

For gene therapy utilizing AAV viruses, since AAVs are generally non-pathogenic, safety concerns mainly only arise from whether or not the host will produce neutralizing antibodies to block virus transduction. Though neutralizing antibodies against AAV2 have been observed after the first injection of a gene therapy virus, but repeated ocular administration of the viral vectors in animal models does not arise obvious safe concern⁹².

¹¹¹. This could possibly be accredited to the retinal-blood barrier of the RPE and choroid, which makes the eye immune-privileged compared to other organs.

GENE THERAPY CLINICAL TRIALS

At present, there is no clinical trial for ADRP. There are currently several human clinical trials using AAV gene therapy in the eye for LCA disease, which is a recessive blinding disorder caused by a mutation in RPE65 (NCT00999609; NCT00821340; NCT01496040; NCT00481546). RPE65 is an isomerase in the visual cycle which converts all-trans retinyl esters to 11-cis retinal within the RPE to make 11-cis retinal available for photoreceptor OS to make a molecule of rhodopsin ^{13, 24, 81, 112}. RPE65 mutations account for around 5-10% of all LCA cases, and disease symptoms are present at birth or no later than the first months of life^{24, 81, 113-116}. Diagnosis of LCA is confirmed by ERG and pupillary responses to light^{85, 113-115}.

The LCA clinical trial was initially using a canine model with a mutation in RPE65. This model lacks functional RPE65 protein which is then supplemented by the delivery of the RPE65 cDNA packaged within the AAV2/2 virus. This gene replacement was also administered by injection of this viral vector into the subretinal space of the canine eye. Visual function was found restored in this canine model and has been sustained for more than 9 years at this time^{13, 24, 85, 103, 117-120}.

The LCA human clinical trial began in 2007. The LCA Phase I clinical trial consisted of three patients between 19-26 years of age⁸⁵. They all received a low dose injection of

the gene therapy virus in the eye for the estimation whether or not the viral gene therapy vector was safe in human. All three patients displayed improved vision in dim light settings in around two weeks after administration. Pupillary responses to light were also ameliorated in each of the three patient eyes injected with the gene therapy virus, becoming at least three times more sensitive to light than pre-treatment response. The efficacy of this gene therapy treatment was able to persist through the 1.5 year follow-up time-point^{85, 121}.

The 1.5 year data presented two essential benefits to AAV-mediated gene therapy research field. First, this trial confirmed that the transgene expression following AAV delivery is consistent in human patients over time and sustainable in the host cells. Second, the AAV2-mediated gene therapy to the retina does not cause a harmful immune response such as cytotoxic T-cell response in the patients⁸⁵. However, there were still unexpected findings from the clinical trials. None of the patients had improved ERGs response, in contrast to the canine models after gene therapy. This result suggests a possibility of unstoppable degeneration in the patients after treatment.

In addition to the eye, AAV-mediated gene therapy treatments have also been used for other human genetic diseases. Hemophilia B, which features an X-linked bleeding disorder caused by the deficiency of clotting Factor IX, has three independent phase I clinical trials using AAV2⁸⁵. This disease is a good target for gene therapy for monogenic cause, and as little as 1% increase in the physiological levels is able to improve the severe bleeding phenotype in human patients. The therapeutic effect has already been observed

after a single administration of AAV2/2 through muscle or liver injection on murine and canine models of hemophilia B^{85, 122-127}.

It is critical for scientists to determine which patients may benefit from gene therapy. For example, P23H mutation in *RHO* are the most common RP in North America³⁰. Therefore, there are many potential recipients who would be able to benefit from gene therapy specifically targeting this mutation. However, the disease phenotype resulted from this mutation is relative mild, and patient's vision remains acceptable until old age. In contrast, other more severe mutations such as *RHO*^{C110R} mutation or mutations within the PDE6 α or β subunit could serve as a better model³⁰. Patients with these mutations typically has early onset of disease in childhood. One limitation for the treatment of these patients would be the ability to diagnose these patients early enough to provide the treatment before everything is too late.

CHAPTER 2: ESTABLISHMENT OF CRISPR-MEDIATED GENE ABLATION

I. INTRODUCTION

Retinitis pigmentosa is an inherited disease characterized by bilateral degeneration of rod-cone photoreceptors, which ultimately leads to night blindness and progressive visual impairment¹⁴¹. The rod-specific light-sensitive pigment, rhodopsin (RHO), is a specialized G-protein coupled receptor that initiates phototransduction. Thus far, approximately 150 different mutations have been found in RHO, which account for 30% of dominant RP cases and 15% of all inherited retinal dystrophies. Two strategies are most commonly applied to treat autosomal dominant (ad) retinitis pigmentosa: expression of the wild-type RHO protein and elimination of the mutant protein¹⁴²⁻¹⁴⁴. The former strategy can be achieved by gene replacement, a well-established technology that uses viral vectors to introduce wild-type protein into cells of interest. While gene replacement itself may partially offset the adverse effects of dominant-negative proteins, it is powerless when used to counteract gain-of-function mutants^{142, 143}. The latter strategy, elimination of the mutant protein, could eradicate the bent causing the disease phenotype. However, this method also presents with its own set of challenging issues. For example, mRNA knockdown of pathologically mutant genes using either short interfering RNAs (siRNAs) or ribozymes only partially and transiently decreases mutant protein levels¹⁴⁵⁻¹⁴⁷. Moreover, these tools often exhibit poor specificity when distinguishing between mutant versus wild-type alleles due to the fact that most of the mutations in *RHO* are single-nucleotide mutations.

The new emerging gene ablation tool, clustered regularly interspaced short palindromic repeats (CRISPR), which involves the collaboration between Cas9 and a single guide RNA (abbreviated henceforth as “CRISPRs”), has been proposed to specifically destroy the mutant gene by targeting the unique mutation^{148, 149}. Traditionally, this gene ablation is performed by introducing a frameshifting nucleotide insertion or deletion (InDel) concomitantly with non-homologous end joining (NHEJ) at the CRISPRs-targeted site^{150, 151}. However, the drawbacks of CRISPRs are significant. For one, not every mutation is unique enough for CRISPRs, which involves highly allele-specific designs. Moreover, efficiency is compromised by the fact that most NHEJ results in precise ligation rather than the desired frameshifting InDels^{152, 153}. Last but not least, the costs of CRISPRs drug development are prohibitive given that the specificity of the guide RNA (gRNA) mandates separate clinical trials for each mutation, regardless of whether or not the mutations reside in the same gene¹⁴².

To address these issues, we present a two-pronged “ablate-and-replace” strategy that (1) destroys the expression of all endogenous chromosomal *Rho* genes in a mutation-independent manner using an improved, mutation-independent CRISPR/Cas9-based gene ablation technique and (2) enables expression of wild-type protein through exogenous cDNA (Fig. 6). For gene ablation, we utilize Cas9 and double gRNAs (abbreviated henceforth as “CRISPRd”) to create two double-strand breaks and, therefore, a large deletion that permanently destroys the targeted gene on both of the alleles. We combine this gene-ablation tool with gene replacement to deliver wild-type cDNA that

compensates for the lost endogenous RHO protein. We hypothesize that this toolset can be used to treat adRP caused by different types of *Rho* mutations.

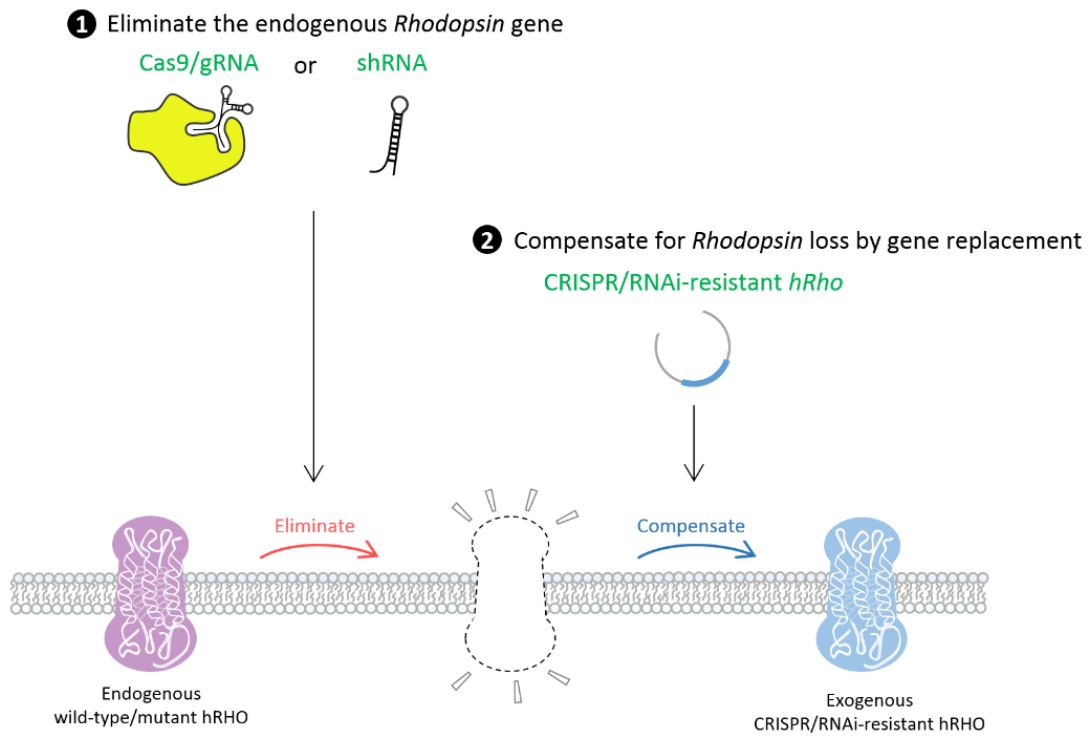


Figure 6. Illustration of Ablate-and-Replace gene therapy strategy.

II. RESULTS

To develop our CRISPRd gene excision tools, we first designed two gRNAs to target sequences in exon 1 of mouse *Rho*, leading to double-strand breaks 27 base pairs (bp) upstream (gRNA1) and 336 bp downstream (gRNA2) of the start codon (Fig. 7).

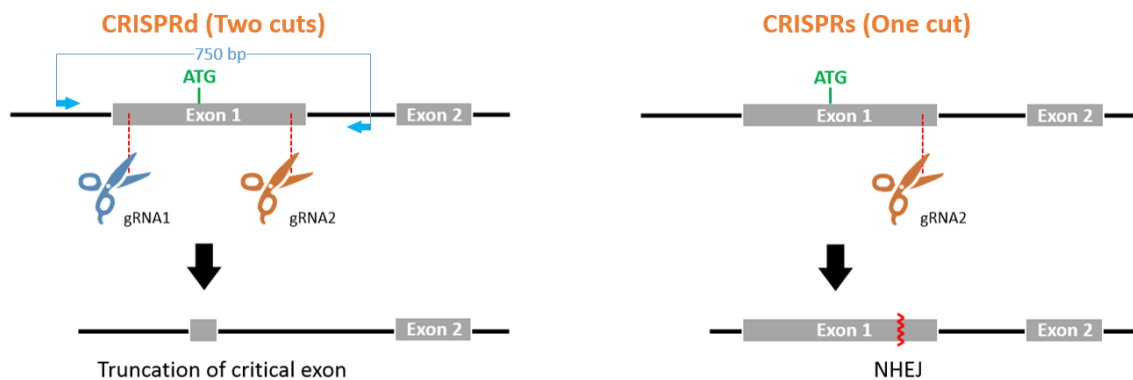


Figure 7. Illustration of double (CRISPRd) or single (CRISPRs) gRNA strategies to specifically ablate mouse *Rho* exon 1.

Of note, both sites are relatively void of pathogenic mutations and single nucleotide polymorphisms. To compare the gene-ablating efficiency of CRISPRd vs CRISPRs *in vitro*, we cloned gRNA1+2 or gRNA2 into respective modified pX459 vectors (Fig. 8) and transfected each respective plasmid into 3T3 fibroblasts.

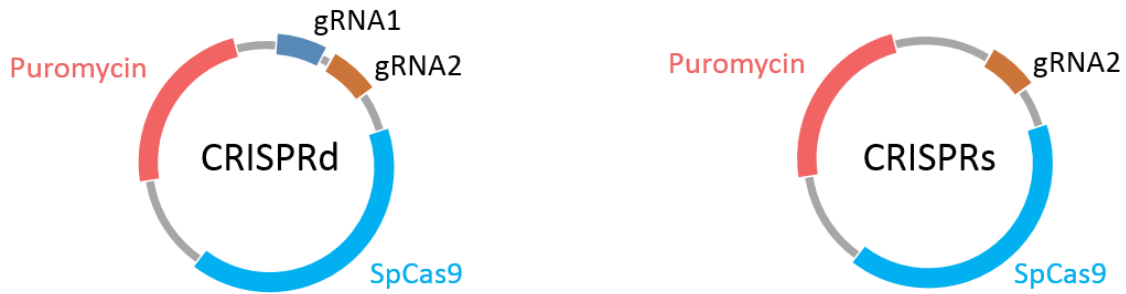


Figure 8. Modified pX459 vectors for CRISPRd and CRISPRs.

After two weeks of puromycin selection, the total genomic DNA was extracted for PCR. We expected that the CRISPRd and CRISPRs plasmids would respectively yield 5 and 2 gene editing scenarios (Fig. 9, type 1~5 and type 1~2), which would generate three gene expression outcomes: (1) normal/unaffected mouse *Rho* (*mRho*) expression resulting from either no editing or non-destructive NHEJ; (2) no *mRho* expression resulting from gene truncation or destructive NHEJ (frameshift); and (3) compromised expression resulting from non-destructive NHEJ at the 5'-untranslated site targeted by gRNA1.


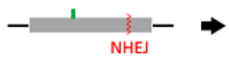

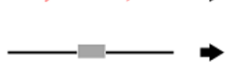

gene-editing scenario	genetic outcome	mRho expression	CRISPRd (%)	CRISPRs (%)
1 	-	unaffected	5.7	24.4
2 	in-frame frameshift	unaffected none	0 1.9	15.6 60.0
3 	insertion/deletion	unaffected or compromised	1.9	-
4 	in-frame frameshift	unaffected none	1.9 26.4	- -
5 	truncation	none	62.3	-

Figure 9. Genetic and expression outcomes following CRISPRd- vs CRISPRs-mediated gene editing.

We first examined genomic PCR products to grossly confirm genetic outcomes (Fig. 10).

CRISPRd (gRNA1+2) yielded a prominent 400-bp band that represents truncated *mRho* exon 1 (Fig. 9, row 5) and a minor 750-bp band that represents parental, full-length exon 1 (Fig. 9, row 1). In contrast, CRISPRs (using only gRNA2) generated just the 750-bp band. To more precisely gauge genetic outcomes and quantify their respective frequencies, PCR amplicons were subcloned using TA cloning for Sanger sequencing.

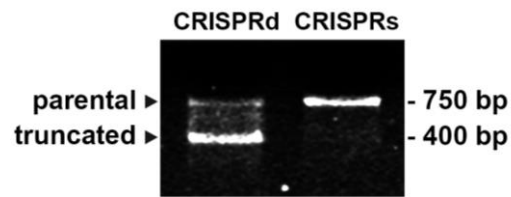


Figure 10. Validation of *mRho* exon 1 truncation. 3T3 cells were transfected with CRISPRd or CRISPRs plasmid (Fig. 8), and then submitted to 2 weeks of puromycin selection followed by genomic PCR (primers indicated in Fig. 7).

With CRISPRs, only 60.0 ± 9.9 % of the *mRho* gene was ablated due to destructive NHEJ resulting in frameshift mutations; in the remaining 40.0 ± 9.9 % of the gene that was not ablated, exon 1 was either intact (24.4%) or had in-frame mutations (15.6%) (Fig. 9 and 11 lower part). With CRISPRd, more than 90 ± 7.8 % of the *mRho* gene was ablated due to truncation (62.3%) or NHEJ-induced frameshift at the gRNA2 targeting site (28.3%) (Fig. 9 and 11 upper part). Similarly, with CRISPRd, only 5.7% of amplicons contained intact *mRho* sequence compared to 24% with CRISPRs, even after two weeks of puromycin selection (Fig. 9).

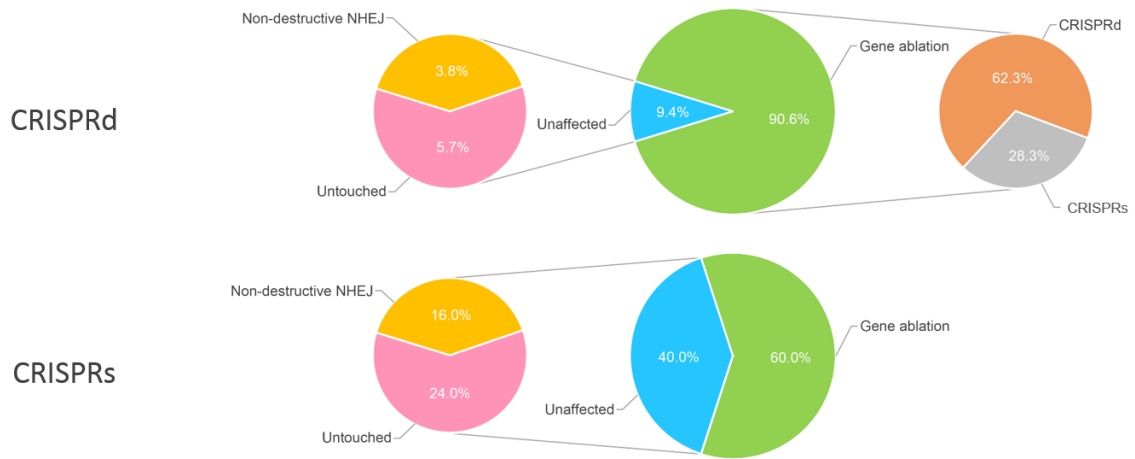


Figure 11. Schematic summary of the basic outcomes produced by CRISPRd- and CRISPRs-mediated gene editing.

III. DISCUSSION

Our experiments provide evidence for the superiority of CRISPRd over CRISPRs in many regards. Consistent with previous findings¹⁵⁴⁻¹⁵⁷, our Dideoxy-Sanger sequencing results showed that the induction rate of CRISPRd is higher than that of CRISPRs. These differences in outcome are most likely due to the fact that less than 0.1% of the NHEJ generates InDel¹⁵⁸. The production of destructive NHEJ may largely rely on repeated cutting. CRISPRd-induced truncation, on the other hand, is more independent of the error rate and only depends on the occurrence rate of NHEJ. Also, unlike homology-dependent repair, NHEJ is active in both dividing cells and non-dividing cells; thus, there is no limitation on cell cycle for our strategy¹⁵⁹. In addition, our results also demonstrate that CRISPRd can minimize the creation of secondary, in-frame mutations induced by NHEJ (CRISPRd 1.9% vs. CRISPRs 15.6%), which is essential for preventing the creation of more toxic *Rho* mutants via therapeutic genome editing.

CHAPTER 3: ESTABLISHMENT OF AAV VECTORS AND SUBRETINAL INJECTION OF GENE THERAPY VECTORS

I. INTRODUCTION

AAV vector has a packing capacity at around 4.5 kb, including ITR sequences. The SpCas9 cDNA is about 4.2kb^{98, 102, 103, 106}. To deliver the components for CRISPRd and the gene replacement *hRHO* cDNA, dual AAV vector system are necessary to encapsulate all the elements. The first AAV which express SpCas9 is driven by sCMV promoter, which is 173 bp long. The poly-A tail is a 49 bp long SV40 SPA sequence. The second virus is designed to express two gRNAs and the *hRHO* gene replacement. The gRNA is driven by U6 promoter and the whole gRNA expressing cassette (including the gRNA scaffold) is 346 bp long. And *hRHO* gene replacement sequence is placed next to the gRNA cassettes. The length of *hRHO* cDNA itself is 1047 bp. The promoter used to drive *hRHO* cDNA expression is a 2.2kb mouse *Rho* promoter.

II. RESULTS

To maximize the expression of *hRHO* gene replacement in the transduced photoreceptor, we truncated *mRho* promoter region to different lengths. From the longest 4.2 kb to 0.5 kb (Fig. 12).

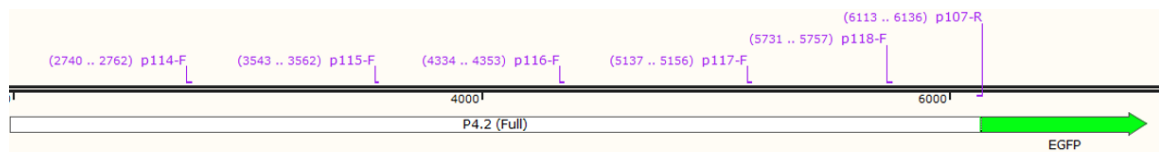


Figure 12. Schematic design of primers to generate truncated *Rho* promoter with different length.

Promoter with different length was cloned into pCDNA3.1 vector with EGFP cDNA as a reporter for gene expression. These plasmids were transduced into HEK293 cells for the evaluation of promoter strength. Since HEK293 cell line does not normally express transcription factors of *RHO* gene, a tripartite plasmid expressing human transcription factors NRL, CRX and NR2E3 (Fig. 13) was made and co-transfected into HEK293 along with the EGFP reporter plasmid.

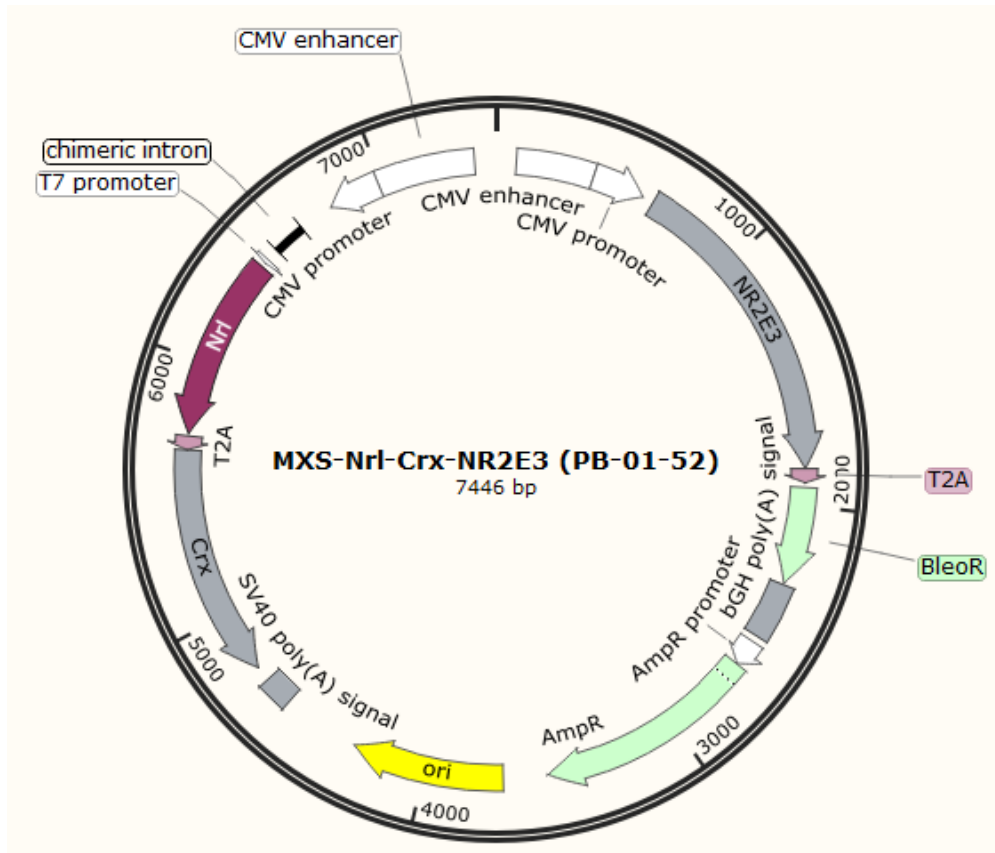


Figure 13. Plasmid expressing transcription factors CRX, NRL and NR2E3.

The HEK293 culture was incubated for 48 hours for protein expression before the fluorescence microscopy analysis. No any fluorescence was detected in transcription factors alone group (Fig 14, left column). Very little fluorescence was observed when using 4.2 kb *Rho* promoter to drive EGFP on HEK293 cells without the co-transfection of transcription factors (Fig 14, central column). As expected, when co-transfect both plasmids together into the cells, the fluorescence increased in intensity and quantity (Fig 14, right column).

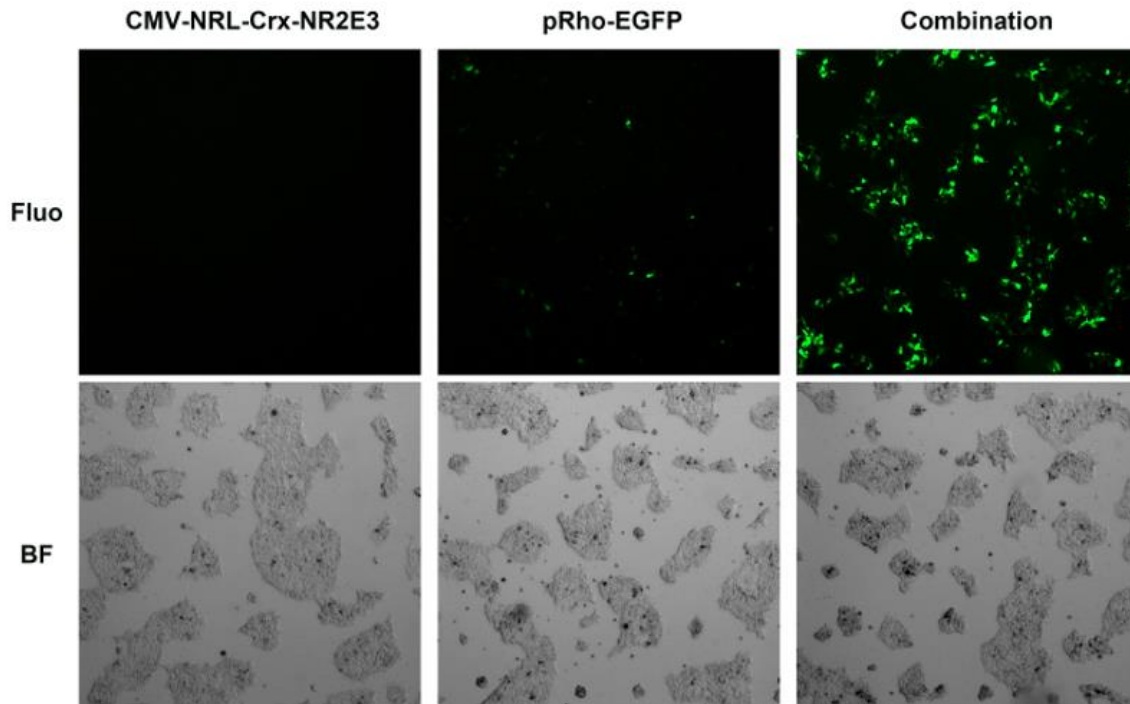
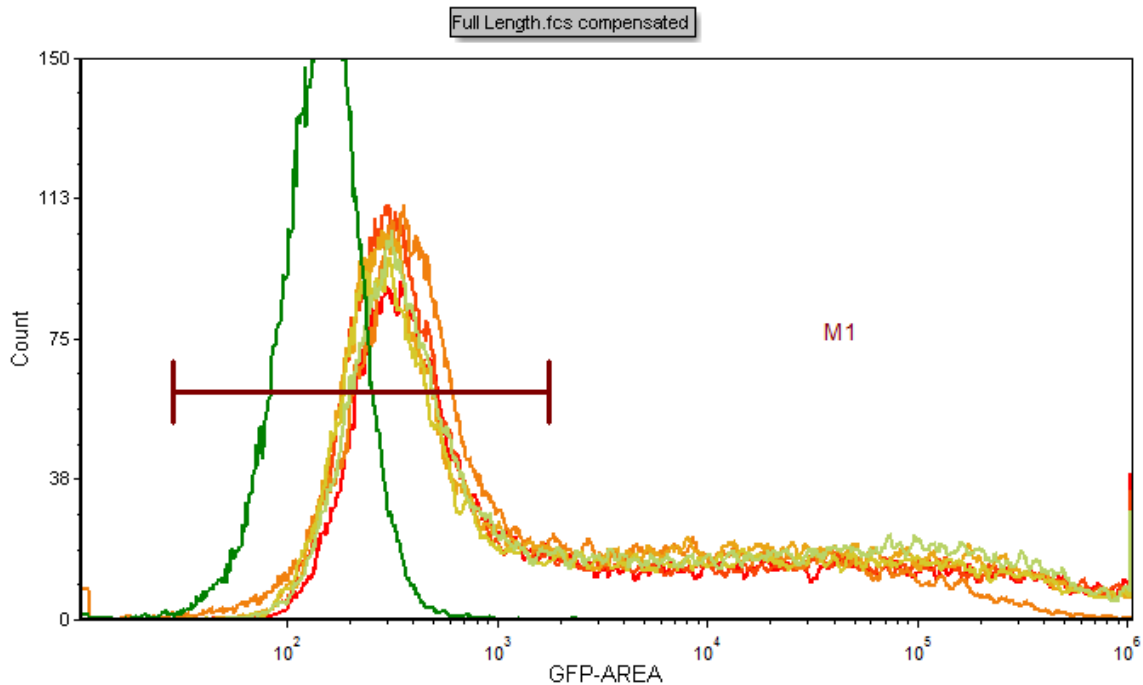


Figure 14. Testing of Rho promoter reporter. HEK293 cells were transfected with plasmid CMV-NRL-CRX-NR2E3, *pRho*-EGFP or both. The bright field and fluorescence were captured after 24 hours of transfection.

Flow cytometry was used to precisely compare the expression of fluorescence of EGFP driven by different length of the *mRho* promoters. Surprisingly, all the groups expressed similar fluorescence intensity (Fi. 15), no significant difference was detected in median and geometric mean values. Enhance, for the establishment of the gRNAs + gene replacement (GR) plasmid, the maximized length of *mRho* promoter is used.



Histogram #	Filename	Parameter	Low bound	High bound	# of Events	% of gated cells	Median	Geometric Mean	CV
1	Full Length.fcs compensated	GFP-AREA	28.97	1760.36	11035	59.28	353.00	378.32	71.80
2	114.fcs compensated	GFP-AREA	28.97	1760.36	13001	62.72	322.00	345.37	74.71
3	115.fcs compensated	FL2-HEIGHT	28.97	1760.36	13879	66.38	356.00	359.58	72.68
4	116.fcs compensated	GFP-AREA	28.97	1760.36	12580	58.23	313.00	341.75	77.75
5	117.fcs compensated	GFP-AREA	28.97	1760.36	11670	59.32	307.00	333.02	77.17
6	118.fcs compensated	GFP-AREA	28.97	1760.36	11823	56.18	335.00	359.96	73.82
7	Neg.fcs compensated	GFP-AREA	28.97	1760.36	15403	99.49	142.00	139.34	48.68

Figure 15. Different Rho promoters exhibit similar driving efficiency. FACS was used to measure the fluorescence emitted by HEK293 cells transfected with GFP-expressing plasmid driven by different lengths of *Rho* promoter.

To test our combination CRISPRd gene ablate-and-replace strategy *in vivo*, all components were cloned into two AAV 2/8 vectors (Fig. 16). Codon-optimized Cas9 cDNA driven by the sCMV promoter was packaged into one vector (AAV-Cas9), while the dual gRNA expression cassettes and human *RHO* (*hRHO*) cDNA (for xenogeneic gene

replacement) driven by a 2.2 kb *mRho* promoter were cloned into another (AAV-GR, stands for gRNA and *hRHO*).

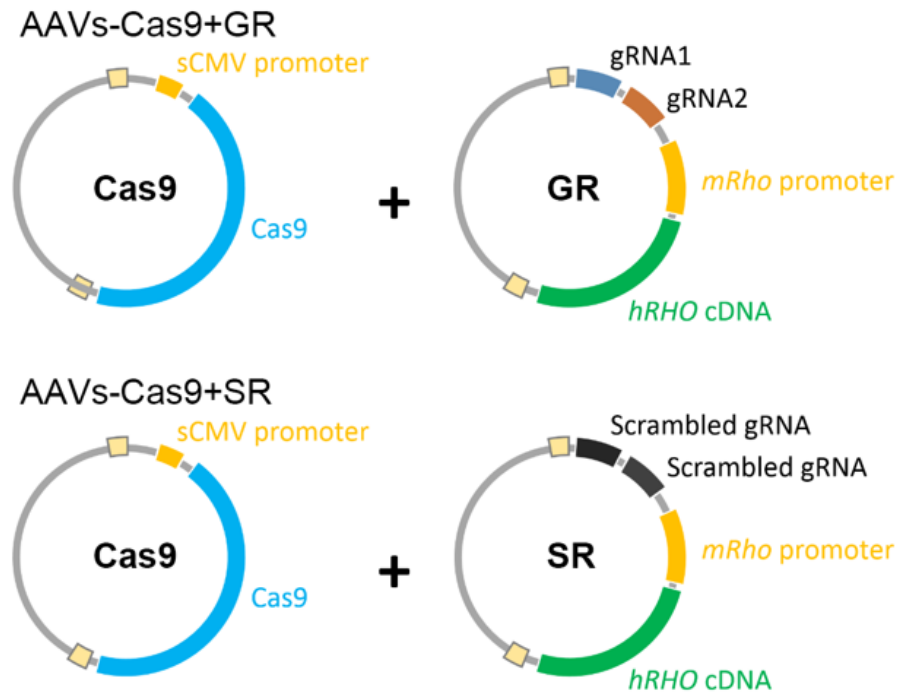


Figure 16. Schematic of experimental (AAVs-Cas9+GR) and control (AAVs-Cas9+SR) AAV2/8 vector pairs.

Thus, gene ablation could only occur in cells that took up both vectors (AAV-Cas9 + AAV-GR) while gene replacement could occur in any rod photoreceptors that took up just the *hRHO* cDNA-containing vector (AAV-GR). Since overexpression of wild-type *RHO* can, by itself, might slightly improve vision in *hRHO*^{P23H} transgenic mice¹⁴⁴, we designed a control AAV vector (AAV-SR, stands for scrambled gRNA and *hRHO*), in which both gRNAs

are replaced with scrambled sequences (Fig. 16); thus, in rods transfected with the AAVs-Cas9+SR vector pair, CRISPRd does not function, but xenogeneic gene replacement does (Fig. 17). Both gRNA1 and 2 were designed to specifically target *mRho*, not *hRHO* (Fig. 18).

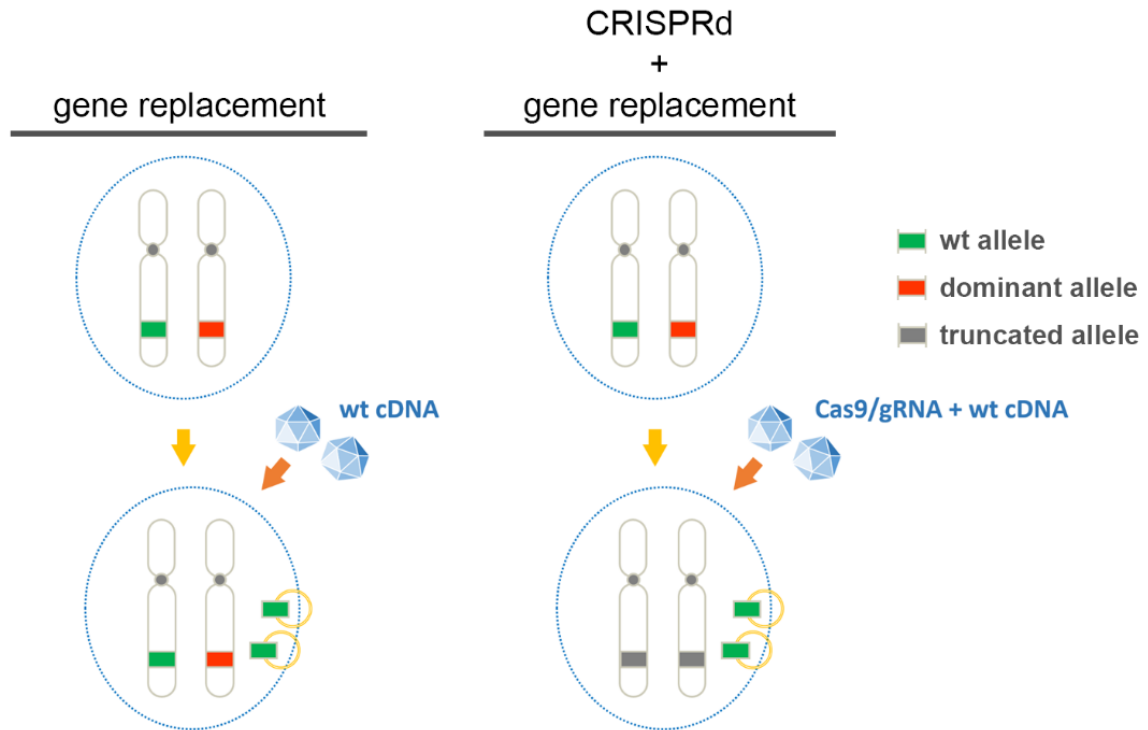


Figure 17. Conventional gene replacement therapy vs CRISPRd plus gene replacement, compound therapy for a heterozygous loci.

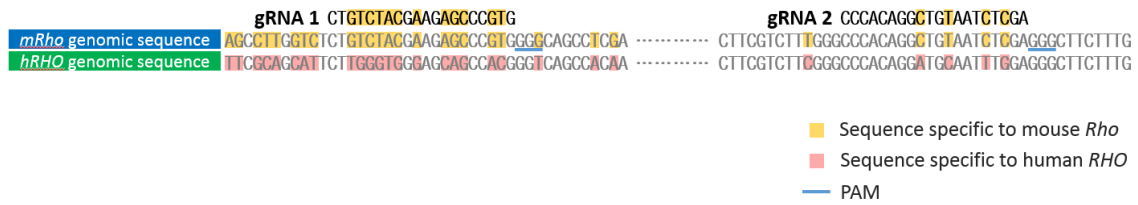


Figure 18. The gRNAs sequences, their targeting sites on *mRho* and the corresponding sites on *hRHO*. The two gRNA have 12 and 4 mismatches on *hRHO*, respectively.

The *hRHO* gene replacement was codon-modified by silent mutations to maximize the difference against gRNA targeting. Indeed, in an *in vitro*, cell-free assay, gRNA1 or gRNA2 each facilitated Cas9-mediated cleavage of *mRho*, but not *hRHO* (Fig. 19).

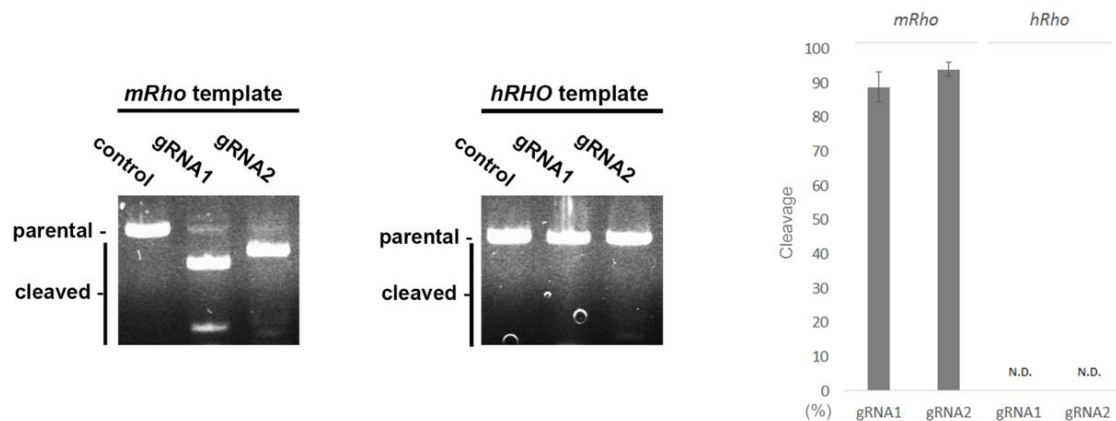


Figure 19. Representative data of *in vitro* SpCas9/gRNA cutting. In a cell-free assay, *mRho* vs *hRHO* DNA template was mixed with recombinant SpCas9 protein and a single gRNA: gRNA1, gRNA2, or control (scrambled gRNA). (n=3)

To validate that AAVs-Cas9+GR can mediate CRISPRd gene ablation *in vivo*, right eyes of wild-type C57BL/6J adult mice received a single, 1.5-microliter subretinal injection of AAVs-Cas9+GR (Fig. 20); as required by animal protocol, left eyes were uninjected, negative controls. Two weeks after the injection, retinæ were collected for analysis.

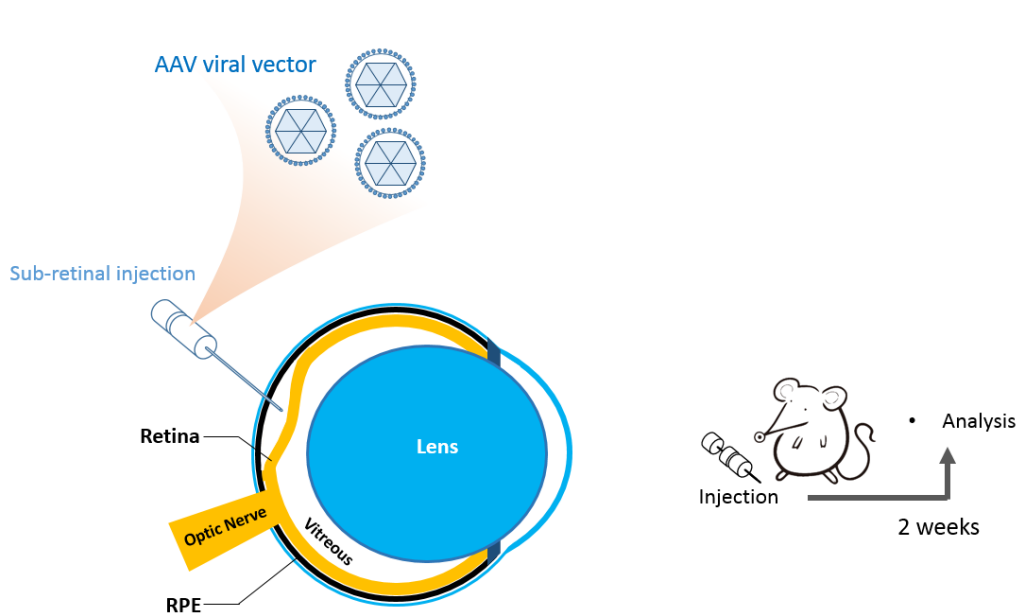


Figure 20. Experimental scheme and timeline for subretinal injection of dual AAV vectors in right eyes of wild-type C57BL/6J mice. (using a unique, posterior approach)

Cas9 immunostaining of whole, flat-mount retinæ revealed AAV-Cas9 transduction and expression in ~30% retinal cells (Fig. 21).

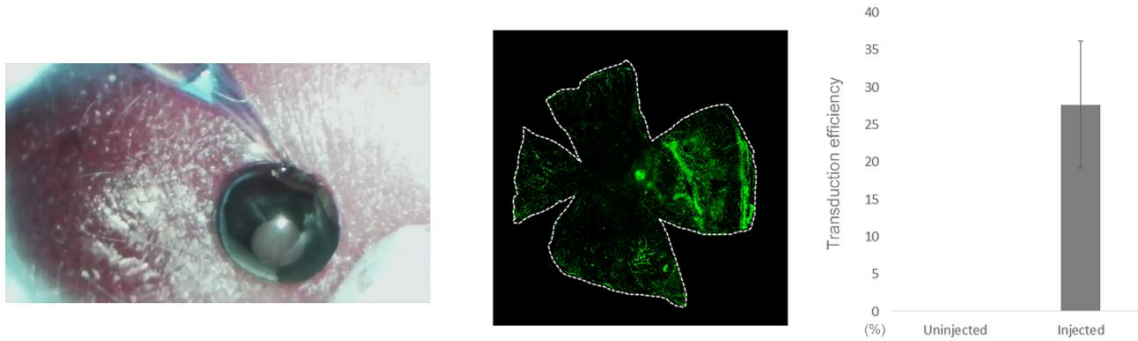


Figure 21. Representative data of Cas9-immunostaining in retinal flat mount. 14 days after Cas9+GR subretinal injection (left figure), the retinas were collected and stained for anti-Cas9 antibody (central figure, n=3). Image was assembled from multiple pictures. The transduced percentage was estimated by the fluorescent area/total retina area (right figure).

Genomic PCR analysis revealed the 400-bp truncated and 750-bp parental *mRho* fragments; uninjected, fellow retinae exhibited only the 750-bp fragment (Fig. 22).

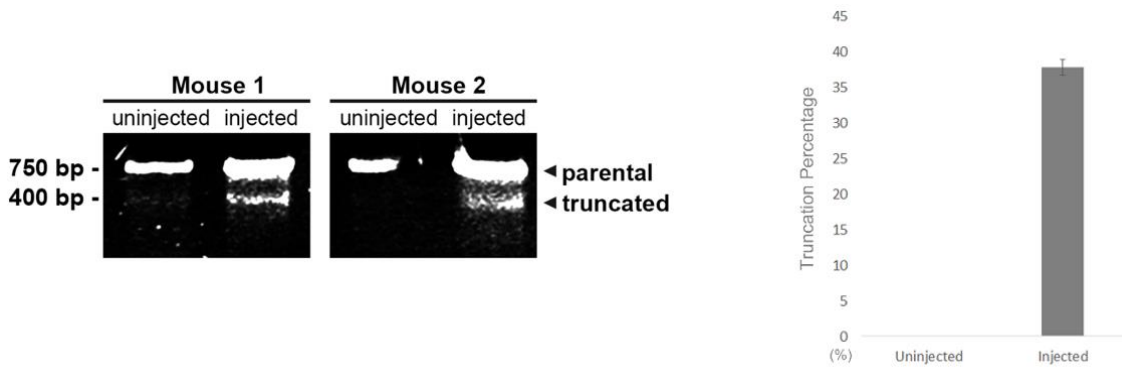


Figure 22. Representative data of PCR analysis of retinal genomic DNA from AAVs-Cas9+GR-injected right eyes and uninjected, fellow (left) eyes. (n=4, two mice data are shown).

Dideoxy-Sanger sequencing analysis of the 400-bp PCR amplicon confirmed that it was, in fact, truncated *mRho* exon 1, and that the large deletion had removed the start codon (Fig. 23). These data suggest that our CRISPRd dual-vector tool truncates *mRho* exon1 *in vivo*.

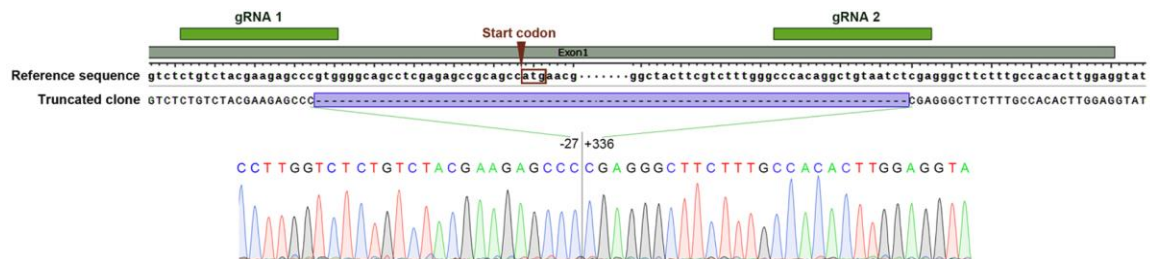


Figure 23. Representative data of mRho gene ablation validated by Sanger sequencing of PCR amplicon from Fig. 22.

We further determined if this *in vivo* AAVs-Cas9+GR-mediated gene ablation leads to decreased endogenous *mRho* levels in photoreceptors. Since there does not exist an antibody that can distinguish mRHO from *hRHO* protein, we extracted total retinal mRNA and used qPCR to evaluate the change in mRNA as a reflection of the change in protein.

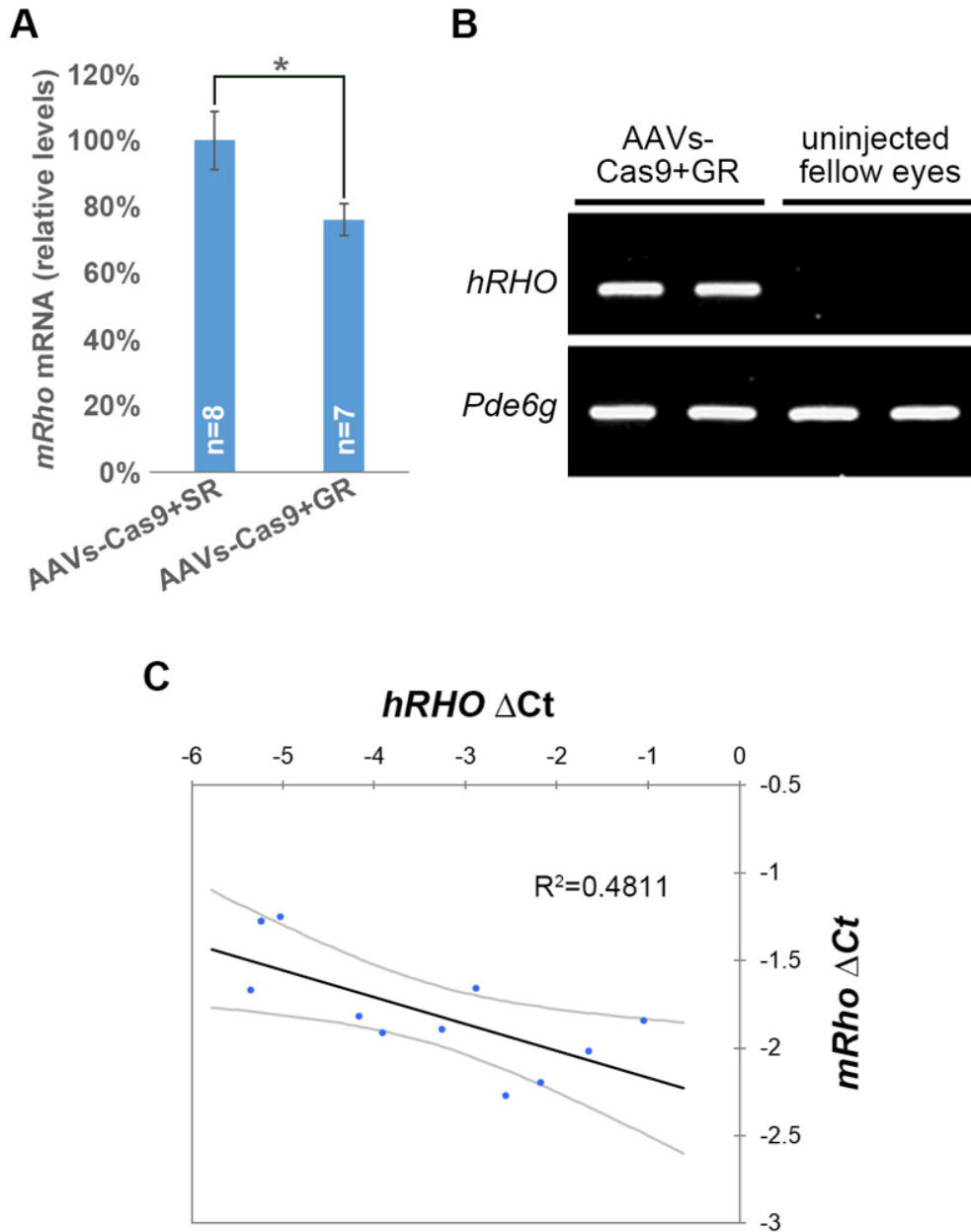


Figure 24. Gene ablation and replacement are co-localized in rod photoreceptors *in vivo*. A, Total retinal mRNA from injected eyes was analyzed by qPCR for *mRho* expression; values were normalized to *Pde6g*, a rod photoreceptor housekeeping gene, and control, AAVs-Cas9+SR were defined as 100%. Values are presented as mean \pm s.d. Unpaired two-sided t-test was used for the statistics (*, $p < 0.05$). B, RT-PCR of total mRNA isolated from whole retinas from two right eyes injected with AAVs-Cas9+GR and two uninjected fellow (left) eyes. C, Scatter plot of qPCR-derived Δ Ct values of *mRho* and *hRHO* mRNA isolated from 11 whole retinas from 11 left eyes injected with AAVs-Cas9+GR. The trend line is presented with 95% confidence interval.

Retinae treated with AAVs-Cas9+GR exhibited a 25% decrease in *mRho* mRNA compared to AAVs-Cas9+SR (Fig. 24A), thus demonstrating that gene ablation is occurring in rod cells transduced with AAVs-Cas9+GR. In addition, xenogeneic *hRHO* mRNA expression was clearly detectable in the injected eyes, indicating the transduction of AAV-GR into rod cells (Fig. 24B). We also found that *mRho* mRNA levels decreased as the *hRHO* mRNA increased based on a scatter plot of qPCR dCt values (Fig. 24C). This negative correlation (coefficient $r = -0.69$) between *mRho* and *hRHO* levels indicates that gene ablation consistently occurs in proportion to gene replacement, as our dual vector system was designed to achieve.

III. DISCUSSION

In this study, we compared the transgene driving efficiency of *mRho* promoters with different lengths. From the 4.2 kb to the shortest 0.5 kb promoter (with 0.5 kb descending), we found there is no significant difference based the fluorescence of EGFP reporter. This result implies the critical cis-element of promoter resides within the region close to the transcription start site. This result may also indicate that it is unnecessary to include excessive upper stream sequence of *mRho* promoter to reach maximum driving efficiency.

To encapsulate all the gene ablation and gene replacement components, dual AAV system is required to provide necessary capacity. However, to achieve gene ablation and gene replacement altogether, the two viruses have to be transduced into the same cell. It has already been reported that injecting reporter AAVs expressing GFP and RFP to the mouse retina can efficiently achieve high level of co-transduction¹⁴³. In our study, we further confirmed if this co-transduction allows gene ablation and gene replacement taken place together. By the negative correlation between *mRho* and *hRHO*, we concluded the transduced retina cells receive both viruses. (Fig. 25, upper set). Because if AAV-Cas9 and AAV-GR were not received by the same cell, we expect that when *hRHO* level changes there would be no fluctuation of *mRho* observed (Fig. 25, lower set).

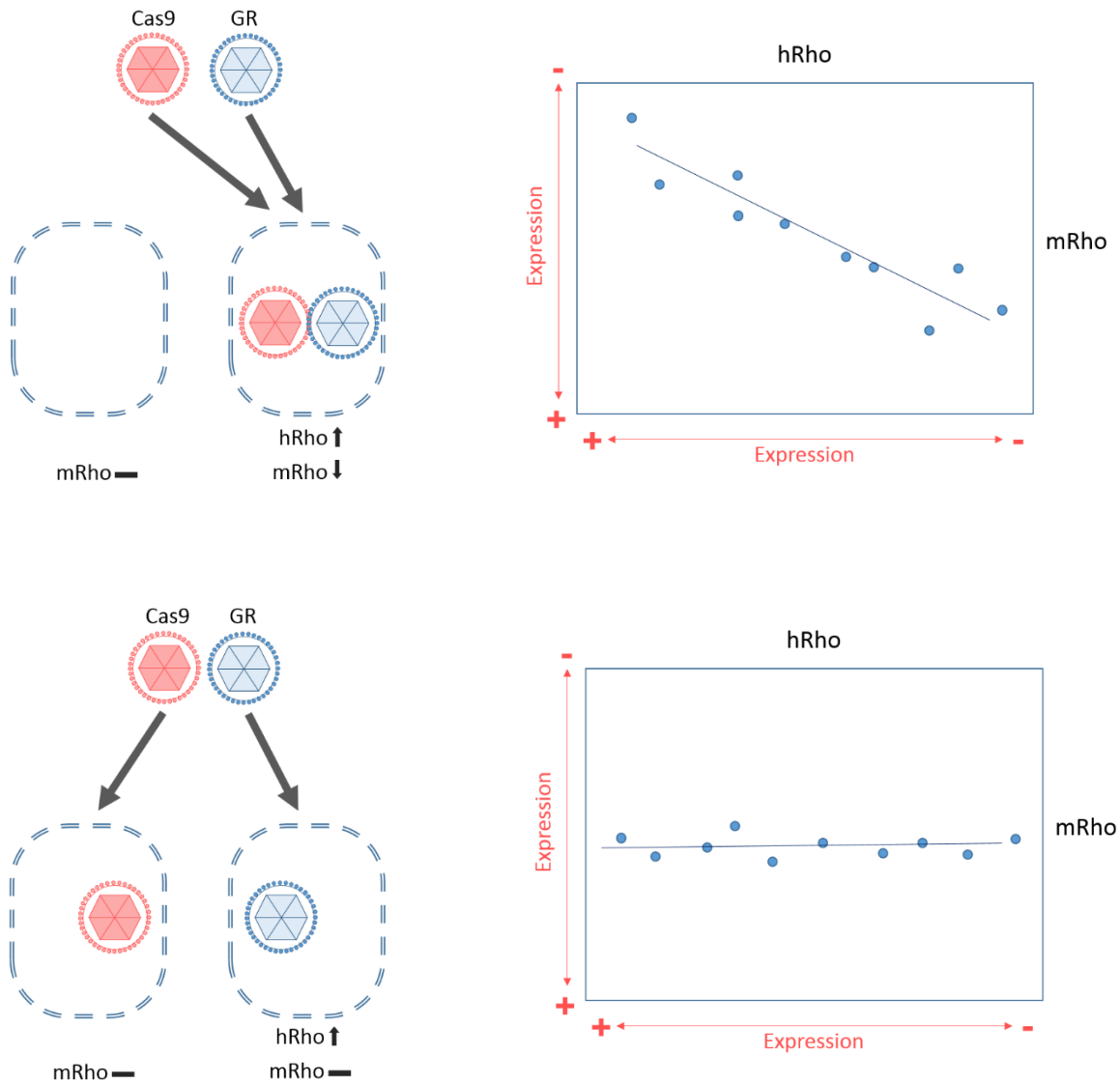


Figure 25. Schematic of two different AAVs distribution scenarios. Upper, if the two viruses were transduced into the same cell while the other cell receive no virus, the *mRho* level of the former cell should reduce and *hRHO* level should increase while nothing changes in the later cell. Lower, if the two viruses were received by two separate cells, the *mRho* level in both cells should not change. Only the *hRHO* level should increase in the cell which received GR virus.

CHAPTER 4: TEST OF ABLATE-AND-REPLACE VECTORS IN PRE-CLINICAL MODELS OF RETINITIS PIGMENTOSA

I. INTRODUCTION

The aim for this experiment is to test if our dual AAV, ablate-and-replace combination system has therapeutic efficacy in dominant retinal degenerative disorders, and also whether our dual vectors act in a mutation-independent fashion. To do this, we chose two knock-in mouse models of human RP caused *Rho* mutations: P23H on exon 1 and D190N on exon 3, which both localize to extracellular loops (Fig. 26).

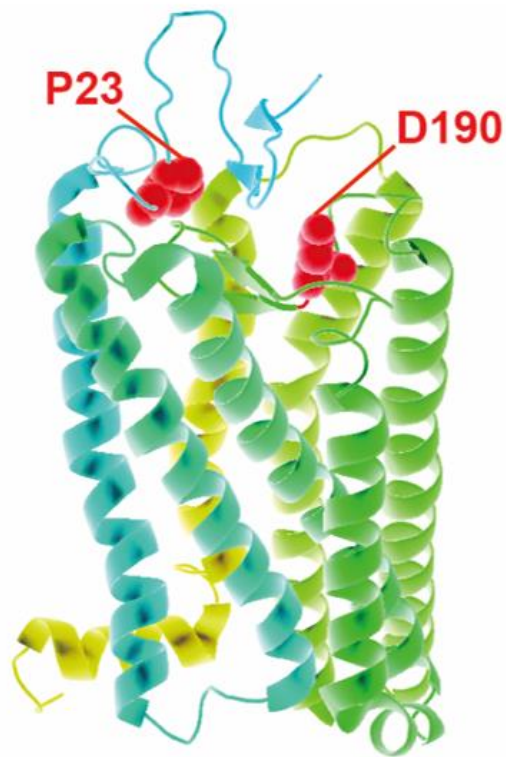
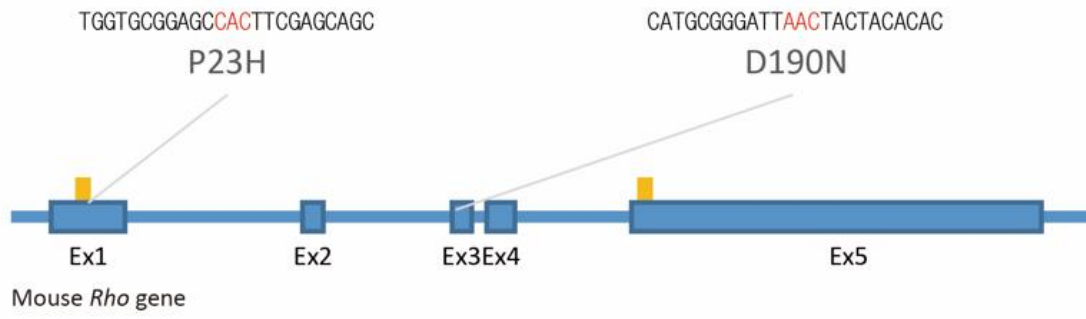


Figure 26. The amino acids of P23 and D190 on Rho structure.

II. RESULTS

The P23H mutation, which causes dominant-negative and gain-of-function phenotypes such as protein retention in the Golgi apparatus and the unfolded protein response^{39, 142}, is the most prevalent *hRHO* mutation in North America. The D190N mutation compromises RHO thermal stability and, therefore, leads to a gain-of-function increase in dark noise and slow yet progressive retinal degeneration¹⁶⁰⁻¹⁶³. For these two mutations, we tested one homozygote (*Rho*^{P23H/P23H}) and two heterozygote (*Rho*^{P23H/+} and *Rho*^{D190N/+}) models, since nearly all *RHO* mutant patients are heterozygous. Single subretinal injections of AAVs-Cas9+GR, AAVs-Cas9+SR or PBS were performed between postnatal days 1 and 3 (Fig. 27); left eyes were not injected. At P21 or later, retinal function was assessed by electroretinography (ERG), and then eyes were dissected and processed for histological analysis (Fig. 27).

ERG responses are characterized by a photoreceptor-mediated a-wave (negative deflection) followed by an inner retina-mediated b-wave (positive deflection). Importantly, we controlled for mouse-to-mouse variation by dividing a- and b-wave amplitudes for the injected (right) eyes by their respective amplitude for the uninjected fellow (left) eyes.

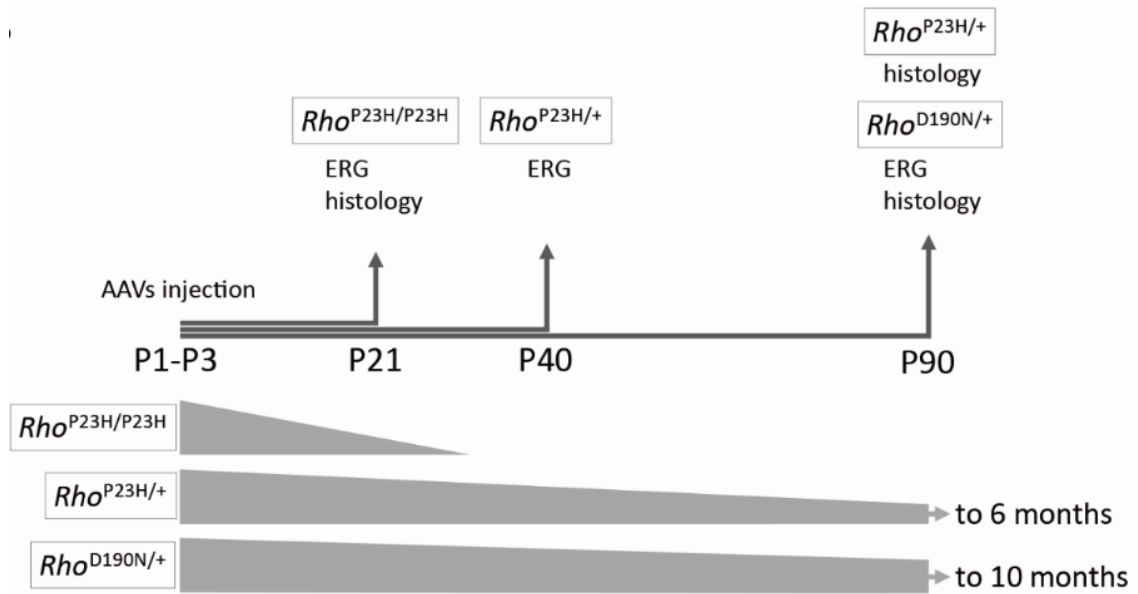


Figure 27. Experimental and disease progression timelines. Right eyes received a single 1.5-microliter subretinal injection of AAVs-Cas9+GR, AAVs-Cas9+SR or PBS between P1 and P3; left, fellow eyes were uninjected. On the indicated days, ERGs were performed and tissue prepared for histology. Approximate time windows for rod-driven photoreceptor degeneration in untreated mice are indicated for three genotypes.

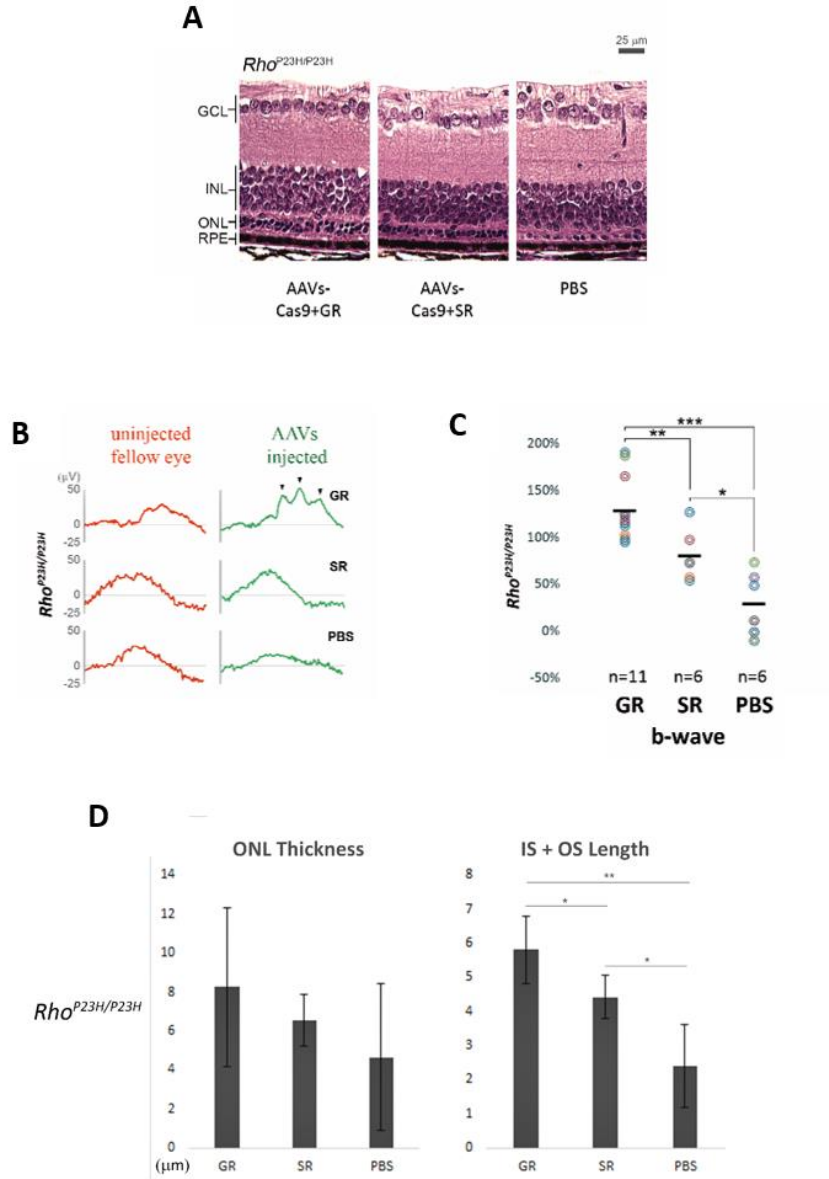


Figure 28. Therapeutic effect of *Rho*^{P23H/P23H} mice. (A) H&E stained retinal sections of right (injected) eyes from P21 *Rho*^{P23H/P23H} mice, which were injected with either AAVs-Cas9+GR, AAVs-Cas9+SR or PBS; images were taken about 200 micrometer from the optic nerve. GCL, ganglion cell layer; INL, inner nuclear layer; ONL, optic nuclear layer; RPE, retinal pigment epithelium. (B) Representative ERG traces of injected right eyes (green traces) and uninjected left, fellow eyes (red traces). Arrows, peaks of oscillatory potentials. (C) Percent change in ERG amplitudes. Each dot represents a b-wave amplitude for an injected, right eye that was normalized to the respective amplitude value of the uninjected fellow (left) eye. N values indicated on x axis; horizontal black lines, group means. Unpaired two-sided t-test was used for the statistics (*, $p < 0.05$; **, $p < 0.01$; ***, $p < 0.001$). In *Rho*^{P23H/P23H} mice, only b-wave data are shown, because a-waves are no longer detectable at P21.

To compare the number of surviving photoreceptors, thickness of the photoreceptor nuclei-containing outer nuclear layer (ONL) was approximated in histological images by counting the layers of photoreceptor nuclei (in wild-type mature retinae, ONL is 10-12 layers thick)¹⁶⁰. *Rho*^{P23H/P23H} homozygous mutant mice exhibit rapid and severe rod-driven retinal degeneration wherein rod cell death begins shortly after birth and results in complete loss of rods by P30⁴³. In fact, in control retinae injected with PBS, the ONL was only 0 to 1 layer thick at P21 (Fig. 28A). In contrast, retinae transduced with AAVs-Cas9+GR or AAVs-Cas9+SR typically had ONLs that were 2-3 and 1-2 layers thick, respectively (Fig. 28A). Such improvement is also reflected in the outer segment (OS) thickness (Fig. 28D). Compared to the PBS control group, the OS length is 142% and 85% longer in the AAVs-Cas9+GR and AAVs-Cas9+SR group, respectively. These data are consistent with the notion that rescue is more efficacious with our AAVs-Cas9+GR ablate-and-replace combination therapy compared to AAVs-Cas9+SR gene replacement. These qualitative structural data were validated by our quantitative ERG functional analysis (Fig. 28B). Specifically, the mean b-wave amplitude for the AAVs-Cas9+GR group was 130% (relative to uninjected fellow eyes) versus 80% and 30% for the AAVs-Cas9+SR and PBS groups, respectively; these differences were highly significant (Fig. 28C). In addition, the peaks of oscillatory potentials of the AAVs-Cas9+GR group were more pronounced compared to either of the controls (Fig. 28B, arrows). These functional data suggest that neural signaling is significantly more robust in AAVs-Cas9+GR-treated retinae. The fact that all of the individual b-wave amplitudes in the PBS group and most of those in the AAVs-Cas9+SR group were less than 100% (i.e., less than uninjected left eyes) (Fig. 28C) is likely due to surgical trauma, which is inevitable in early postnatal mouse eyes. That the

AAVs-Cas9+GR group showed greater b-wave amplitudes than the uninjected eye despite surgical trauma is a reflection of the robustness of the intervention. Since subretinal injections induce only insignificant damage in human retinae, efficacy could be even more robust in patients.

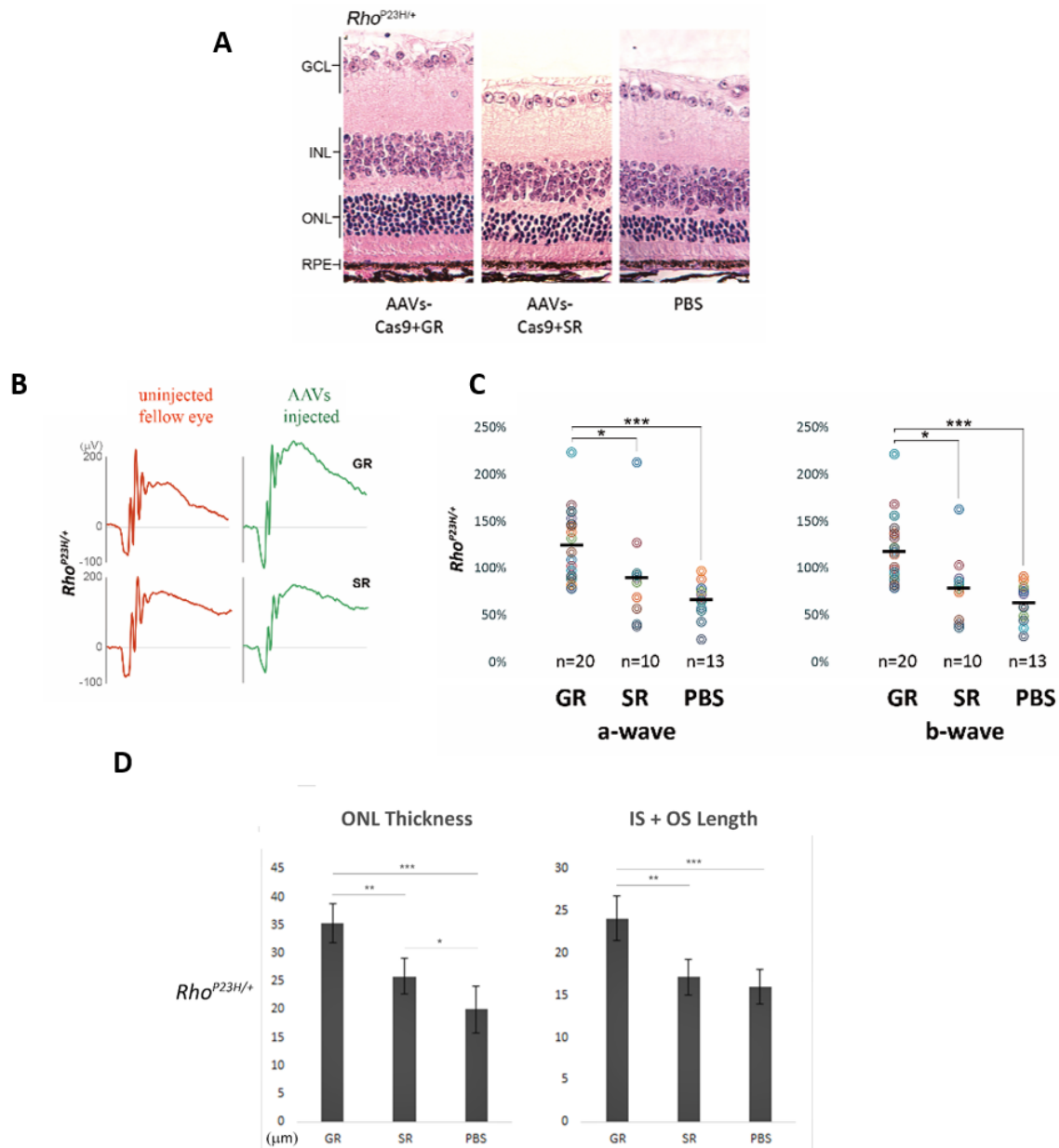


Figure 29. Therapeutic effect of $Rho^{P23H/+}$ mice. (A) H&E stained retinal sections of right (injected) eyes from P90 $Rho^{P23H/+}$ mice, which were injected with either AAVs-Cas9+GR, AAVs-Cas9+SR or PBS; images were taken about 200 micrometer from the optic nerve. GCL, ganglion cell layer; INL, inner nuclear layer; ONL, outer nuclear layer; RPE, retinal pigment epithelium. (B) Representative ERG traces of injected right eyes (green traces) and uninjected left, fellow eyes (red traces). Arrows, peaks of oscillatory potentials. (C) Percent change in ERG amplitudes. Each dot represents an a- or b-wave amplitude for an injected, right eye that was normalized to the respective amplitude value of the uninjected fellow (left) eye. N values indicated on x axis; horizontal black lines, group means. Unpaired two-sided t-test was used for the statistics (*, $p < 0.05$; **, $p < 0.01$; ***, $p < 0.001$).

In *Rho*^{P23H/+} and *Rho*^{D190N/+} mice, retinae were analyzed later than the *Rho*^{P23H/P23H} mutant since rod-driven retinal degeneration is dramatically slower in these heterozygotes: rod death is complete by about 6 and 10 months, respectively (Fig. 27). In P90 *Rho*^{P23H/+} retinae, AAVs-Cas9+GR treatment yielded 6-8 layer thick ONLs compared to 4-5 layers for AAVs-Cas9+SR treatment and 3-4 layers for PBS (Fig. 29A). The increase in OS thickness is more significant after AAVs-Cas9+GR treatment but is less efficacious in the AAVs-Cas9+SR group (Fig. 29D). In addition, AAVs-Cas9+GR-treatment significantly increased a- and b-wave amplitudes in *Rho*^{P23H/+} retinae compared to the AAVs-Cas9+SR and PBS controls (Fig. 29). Similarly, in P90 *Rho*^{D190N/+} mice, rescue by AAVs-Cas9+GR treatment was again statistically superior for both a- and b-waves (Fig. 30). These structural and functional efficacy data suggest that our ablate-and-replace combination, AAVs-Cas9+GR-treatment leads to significantly greater survival of functioning photoreceptors compared to AAVs-Cas9+SR-transduced retinae. The data also suggest that the treatment is mutation-independent. These results are consistent with our dual AAV vector design (Fig. 16) and analysis (Fig. 24).

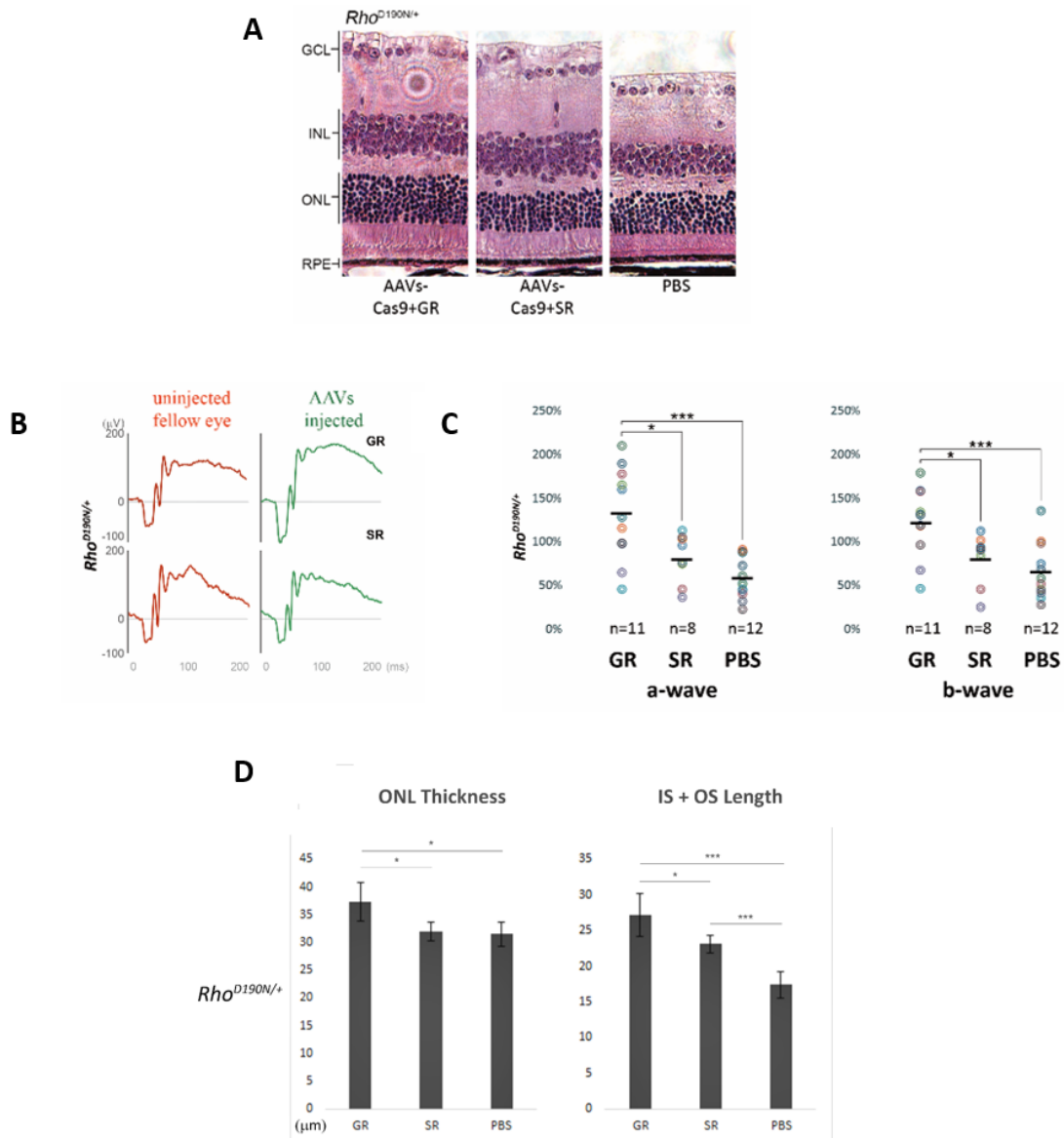


Figure 30. Therapeutic effect of *Rho*^{D190N/+} mice. (A) H&E stained retinal sections of right (injected) eyes from P90 *Rho*^{D190N/+} mice, which were injected with either AAVs-Cas9+GR, AAVs-Cas9+SR or PBS; images were taken about 200 micrometer from the optic nerve. GCL, ganglion cell layer; INL, inner nuclear layer; ONL, optic nuclear layer; RPE, retinal pigment epithelium. (B) Representative ERG traces of injected right eyes (green traces) and uninjected left, fellow eyes (red traces). Arrows, peaks of oscillatory potentials. (C) Percent change in ERG amplitudes. Each dot represents an a- or b-wave amplitude for an injected, right eye that was normalized to the respective amplitude value of the uninjected fellow (left) eye. N values indicated on x axis; horizontal black lines, group means. Unpaired two-sided t-test was used for the statistics (*, $p < 0.05$; **, $p < 0.01$; ***, $p < 0.001$).

III. DISCUSSION

Finding that gene replacement alone can only rescue the vision in homozygous *mRho*^{P23H/P23H} model but not the models of heterozygous P23H and D190N was unanticipated. This result is inconsistent with the previous findings on P23H and P347S mutation models^{143, 164}. However, it is worth noting that all of the previous animal models were established by transgenic expression of mutant *hRHO* in *mRHO*^{-/-}, *mRHO*^{+/+} or *mRHO*^{+/-} backgrounds instead of the mutation knock-in method. Our findings suggest that selecting genetic models to simulate gene therapy of adRP in mice is pivotal for therapeutic development.

Though AAV-delivered gene replacement is not integrating to the host genome, based on recent findings and clinical trials, the AAV-delivered gene replacement therapy of RPE65 has allowed the stable expression of retinal pigment epithelium (RPE) cells for 3+ years in humans and 9+ years in canine models¹⁶⁵⁻¹⁶⁷. We expect that this gene replacement effect can last even longer in photoreceptor cells, because—unlike RPE cells—photoreceptor cells do not divide. However, further experimentation is required to understand the persistence of the AAV transgene and the need for additional supplementation of gene replacement in the long run.

Our ablate-and-replace system has potential for other autosomal dominant diseases beyond retinitis pigmentosa. For example, Vitelliform Macular Dystrophy is a blinding macular disorder that may be caused by any one from more than 200 autosomal-dominant point mutations in the gene BESTROPHIN 1 (BEST 1), which encodes a calcium-dependent chloride channel¹⁶⁸⁻¹⁷⁰; Transthyretin amyloidosis is associated with 83 ad

mutations in the TTR gene¹⁷¹; and amyotrophic lateral sclerosis has more than 80 mutations on the SOD1 gene¹⁷². Instead of mutation-specific targeting, our system circumvents such heterogeneity.

IV. FUTURE DIRECTIONS

The current study provides evidence for the efficiency and feasibility of “ablate-and-replace” therapeutic strategy on rodent adRP models. However, for the clinical application, more tests are necessary to evaluate this strategy with human sequence. A *hRHO*-humanized mouse will be an ideal platform to test new, *hRHO*-targeting gRNAs for CRISPRd and to test new *hRHO* gene replacement underwent a new round of codon-modification to evade gRNA targeting.

CHAPTER 5: MATERIAL AND METHODS (FIRST PART)

Plasmids and AAV production

All gRNAs used in this study were designed by Benchling (<https://benchling.com/>). When selecting gRNAs, only those with excellent off-targeting scores (i.e. >80) were considered. The two gRNAs, labeled as gRNA1 and gRNA2, with the highest on-targeting scores were chosen and tested for use in this study (gRNA1 sequence: ctgtctacgaagagcccgtg; gRNA2 sequence: cccacaggctgtaatctcga). For *in vitro* gRNA specificity test, gRNA1+gRNA2 or gRNA2 alone expressing cassettes were cloned into pX459 (Addgene), which encodes SpCas9. For the production of the AAV-GR, gRNA1+gRNA2-expressing cassettes and a 2.2 kb *mRho* promoter-driven *hRHO* cDNA-expressing cassette were cloned into pZac2.1 vector (PL-C-PV0100, The Penn Vector Core, University of Pennsylvania). For the AAV-SR, gRNA sequences were replaced with scrambled sequences that do not exist in the mouse genome. For the AAV-Cas9, codon-optimized SpCas9 was cloned into pZac2.1 between the sCMV promoter and SPA sequence. The AAV2/8 (Y733F) was generated by The Penn Vector Core, University of Pennsylvania.

In vitro CRISPR digestion assay

To validate the targeting efficiency of our system, gRNA (25 ng/μl) was added to the reaction mixture alongside Cas9 protein (30 ng/μl, NEB) and template *mRho* DNA (20 ng/μl, 750 bp) covering both targeting sites of gRNA1 and gRNA2, and they were

subsequently incubated at 37° C for 2 hr. After Cas9/gRNA digestion, the mixture was analyzed by agarose gel electrophoresis.

Animals

Human mutation P23H knock-in and C57BL/6J mice were purchased from Jackson Labs to generate *Rho*^{P23H/+} and *Rho*^{P23H/P23H} mice. Another human mutation knock-in model, D190N, was established as described before¹⁶⁰. Animals were maintained on a 12-h light-dark cycle. Before ERG, animals were anesthetized with a mixture of ketamine hydrochloride (10 mg/100 g; Ketaset®, Fort Dodge Animal Health, Fort Dodge, IA, USA) and xylazine (1 mg/100 g, Anased®; Lloyd Laboratory, Shenandoah, IA, USA). As per regulations of the Institutional Animal Care and Use Committee (IACUC), animals sacrificed for histology were euthanized by placement in a CO2 chamber for 3 min followed by cervical dislocation. All efforts were made to minimize the number of animals used and their suffering. All mouse experiments were approved by the IACUC and conform to regulatory standards. All mice were used in accordance with the Statement for the Use of Animals in Ophthalmic and Vision Research of the Association for Research in Vision and Ophthalmology, as well as the Policy for the Use of Animals in Neuroscience Research established by the Society for Neuroscience.

Electroretinography

ERGs were performed at indicated time points as previously described¹⁶⁰. Briefly, animals were dark-adapted overnight, and their pupils were dilated with 0.5% tropicamide and 2.5% phenylephrine. Animals were then anesthetized with ketamine, and ERG responses were obtained using pulses of 3 cd × s/m² (white 6,500 K) light. ERG a- and b-wave magnitudes and maximal scotopic and photopic recordings were collected at P21 for *Rho*^{P23H/P23H}, P40 for *Rho*^{P23H/+}, and P90 for *Rho*^{D190N/+} mice.

Subretinal injection

AAV-Cas9 (1 × 10¹³ particles/ml) was premixed with AAV-GR or AAV-SR (1 × 10¹³ particles/ml). Mice at age P1-P3 were anesthetized according to established IACUC guidelines, and subretinal injections were performed with a single injection of 1.5 µl. The injection was done from the posterior part of the eye. All mice included for analysis had ideal bleb detachments at the retinal site of the injection as judged by postsurgical fundus examination. Mice with complete retinal detachment confirmed by both postsurgical fundus examination and ERG were then euthanized. The left eyes served as controls and remained uninjected.

Genomic DNA extraction and genomic PCR

Genomic DNA from retinae was extracted using the Blood & Tissue kit (QIAGEN). Genomic PCRs were performed using Phusion DNA polymerase (Fisher Scientific). Primers for the detection of gene truncation and NHEJ were as follows: Forward: tacctaaggcctccaccg; Reverse: ttgccaatgaataagctggg. PCR amplicons generated from 3T3 cell culture or gross retinal DNA samples were further subcloned by the TOPO-TA cloning kit (Invitrogen) and analyzed by Sanger sequencing.

Cell culture and plasmid transfection

Mouse fibroblast 3T3 cell line was purchased from ATCC. The mycoplasma contamination test was performed every month. The cells were seeded in a 6-well plate at 1×10^6 cells/well. When the cells reached 75% confluency, the pX459 plasmids (2.5 μ g) of CRISPRd or CRISPRs were transfected into 3T3 cells by Lipofectamine 2000 (Invitrogen). The cell culture was further purified by puromycin selection at 2 μ g/ml starting at 48 hours after transfection. DNA extraction was carried out after two weeks of selection.

Immunostaining

Mice were euthanized, and eyes were enucleated and placed in 4% paraformaldehyde for 1 h at room temperature. The optic nerve, cornea, and lens were removed. The whole eyecup was then flattened by means of four radial cuts extending

out from the optic nerve and mounted with mounting medium (Vectashield, Vector Laboratories). Anti-Cas9 primary antibody (1:200 Abcam ab191468) and secondary antibody-conjugated Alexa 488 (Invitrogen, A11017) staining were performed according to the manufacturer's instruction. Visualization was achieved by fluorescence microscopy, and bright-field imaging was used to visualize the whole retina (Leica DM 5000B microscope). Pictures were taken using the Leica Application Suite Software (Leica Microsystems).

Histology

Mice were euthanized, and eyes were enucleated and fixed. H&E histology was carried out as previously described¹⁶⁰.

Real-time PCR and relative mRNA quantification

Retinas were harvested at the indicated time and lysed with TRIZOL reagent (Invitrogen). Total RNA was isolated according to the manufacturer's instructions. DNase I (Invitrogen) treatment was then performed to prevent genomic DNA contamination. The reverse transcription reaction was conducted by Superscript III Reverse Transcription kit, and a random hexamer (Invitrogen) was used to generate cDNA. Real-time PCR method was performed using Maxima SYBR Green/ROX qPCR Master Mix (Fisher Scientific) with StepOne Real-time PCR System (Invitrogen) to quantify gene expression levels. The *mRho* and *hRHO* mRNA expression level was determined and normalized with the rod

photoreceptor cell housekeeping gene, Pde6g. The PCR products were validated by melting curve and agarose gel electrophoresis. The following primers were used: *mRho* forward: 5'- TGGGCCACAGGCTGTAATCTC-3'; *mRho* reverse: 5'- GAAGACCACACCCATGATAGCGTGA-3'; *hRHO* forward: 5'- CTTTGCCAAGAGCGCCG-3'; *hRHO* reverse: 5'- AGCAGAGGCCTCATCGTCA-3'. Pde6g forward: 5'- ACCACCTAAGTTTAAGCAGCGGCA-3'; Pde6g reverse: 5'- CGTGCAGCTCTAGGTGATTGAAG-3'.

Statistics

An unpaired, two-sided t-test was used for the comparisons of mRNA levels and ERG response.

CHAPTER 6: ESTABLISHMENT OF GENE CORRECTION TOOLSET FOR DOYNE HONEY

COMB DYSTROPHY

I. INTRODUCTION

Though many hypotheses have been proposed, it is still unclear how the *EFEMP1*^{R345W} mutant protein can cause drusen formation and lead to the disease. With the fact that *EFEMP1* is expressed exclusively by RPE cells in the retina, we hypothesize that the expression of *EFEMP1*^{R345W} may change RPE physiology. Because of the onset of this disease is usually around 30's to 40's and drusen formation is a slow, progressive process, that cellular, physiological phenotype may be subtle. In order to precisely reflect the *EFEMP1*^{R345W} -induced phenotype, we tended to create an isogenic cell line pair in which, the only difference is the single nucleotide mutation of *EFEMP1*^{R345W}. Since DHRD is a monogenic disease, we expect that this rigorous phenotyping clarify the consequence of mutant *EFEMP1* expression in RPE cells.

The ^{R345W} mutation is a C>T mutation on exon 10 of *EFEMP1* gene. To create an isogenic cell line, we obtained DHRD patient fibroblast-derived iPSC cells. We expected to perform gene correction by CRISPR-induced homology directed repair. The yield iPSC which carries wildtype *EFEMP1* sequence can thus serve as isogenic, wildtype control of this experiment.

II. RESULTS

To create a double strand break at the *EFEMP1* mutation site, we designed three different gRNAs to target the *EFEMP1* mutation locus on exon 10 (Fig. 31). The design was done by Benchling website.

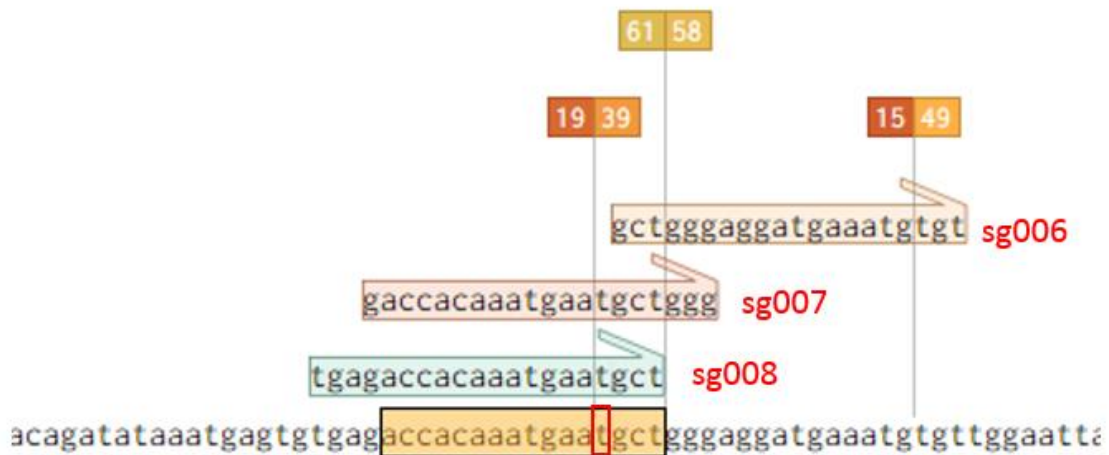


Figure 31. gRNA targeting sites. Three gRNAs sg006, sg007 and sg008 (from top to bottom) targeting the *EFEMP1*^{R345W} mutation were designed by Benchling.

These three gRNAs, sg006, sg007 and sg008 were tested *in vitro* for targeting efficiency (Fig. 32). By mixing SpCas9 protein and each of these gRNA individually with wildtype or mutant templates, more digested fragments instead of parental band in the sg008 group was observed, indicating highest targeting efficiency among all gRNAs. However, we noticed that no one of the gRNA can specifically target the mutant sequence,

since appreciable cutting has also been detected in the groups treated with wildtype sequence.

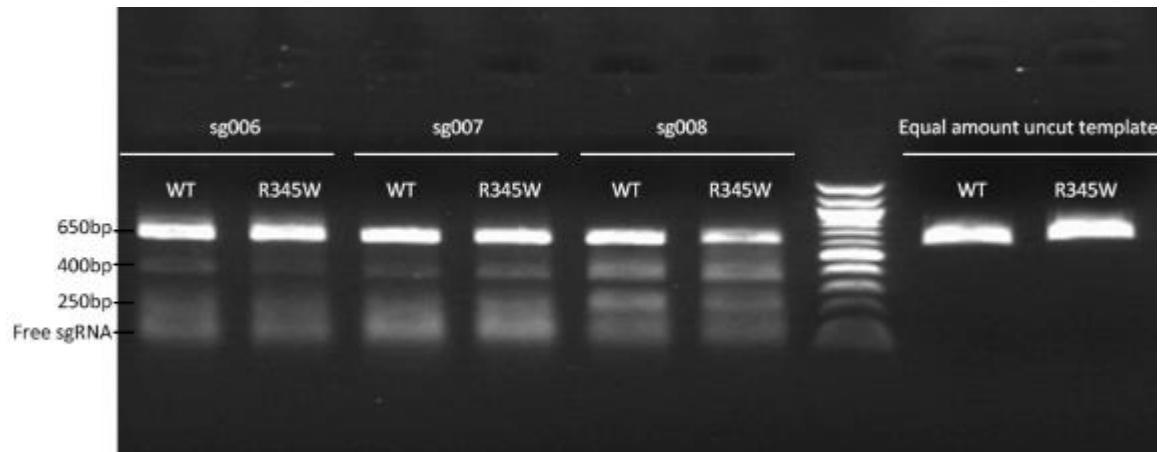


Figure 32. *In vitro* gRNA targeting. Three gRNAs sg006, sg007 and sg008 were used to challenge dsDNA fragment bearing wildtype or R345W mutation sequence. The 650bp band is the parental sequence of the uncut template. If cut, the parental band should be digested into two bands with size around 400bp and 250bp.

To facilitate homology dependent repair (HDR) to happen, addition of donor template is necessary when inducing double strand break at the mutation site by Cas9/gRNA. We designed a 128bp single-stranded oligodeoxynucleotide (ssODN) (Fig. 33). Compared to the mutant sequence, this ssODN contains three mismatches: one to correct C>T mutation and the other two contributes to two silent mutations, which were set to allow colony screening by restriction fragment length polymorphism (RFLP). The mini homology arm on each side of this ssODN are 60bp long. The expected sequence after gene correction can be recognized by restriction enzyme ScrFI.

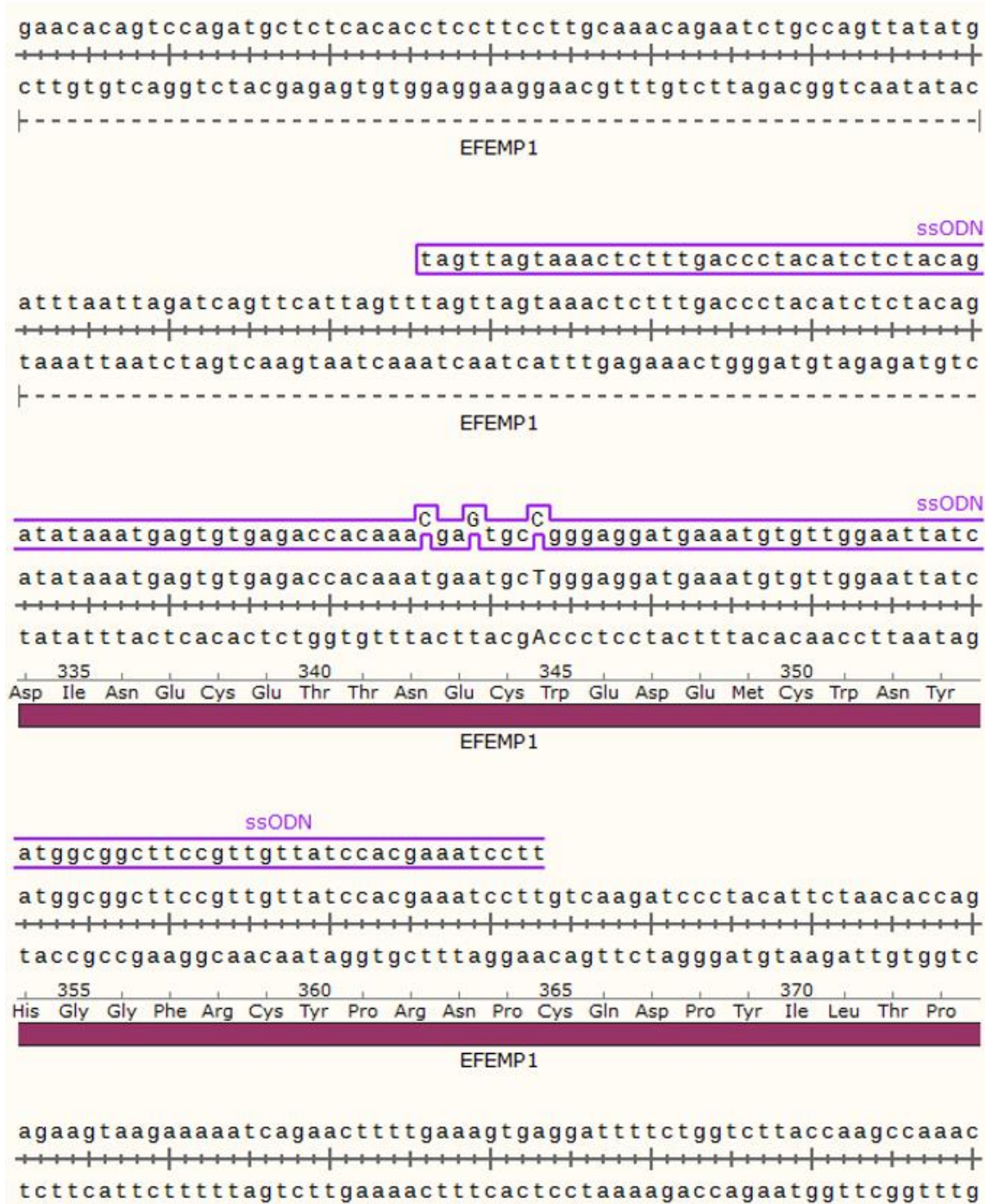
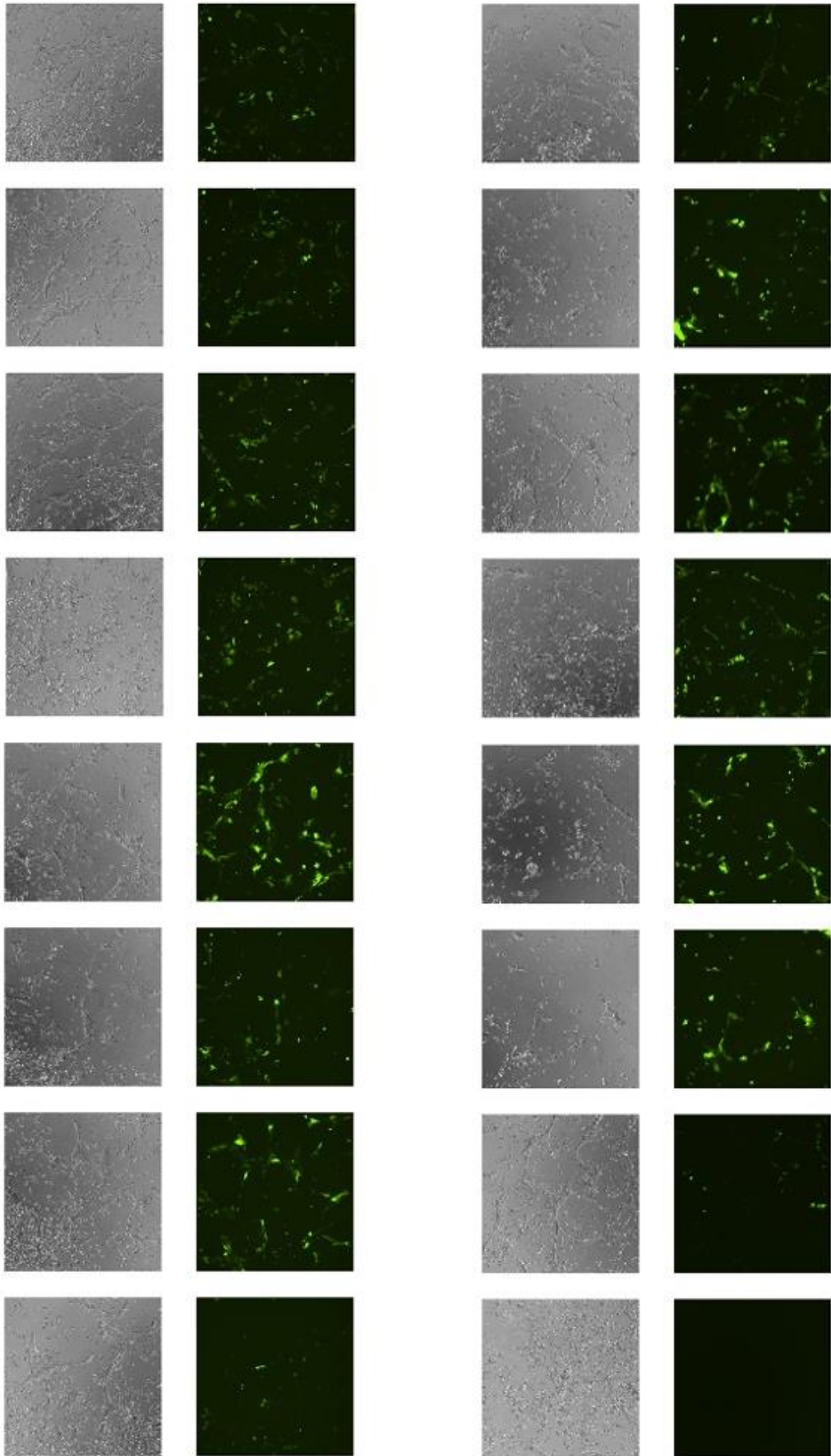


Figure 33. Donor template design. The donor template (ssODN) used to facilitate homology directed repair contains three different mismatches comparing to the *EFEMP1*^{R345W} sequence. Despite one mismatch to correct the R345W mutation, the other two mismatches were created to enable restriction fragment length polymorphism for colony screening.

We chose Lonza nucleofector 4D to perform the transfection of Cas9/gRNA and donor template. To optimize the transfection efficiency of the patient iPSC, we tested different nucleofection protocols with different nucleofection reagents and conditions (Fig. 34).



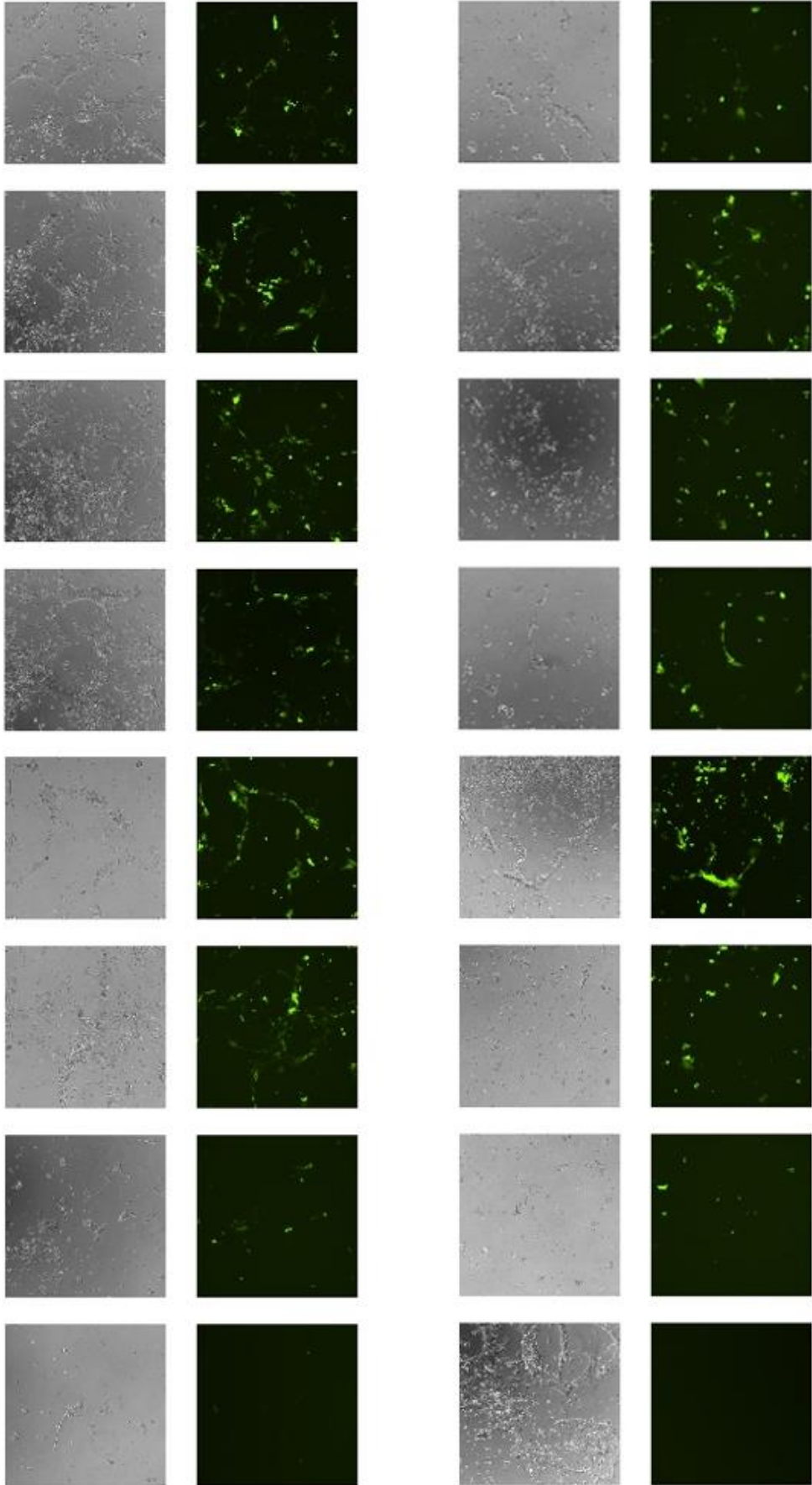


Figure 34. Optimization of nucleofection program. The iPSC cells were mixed with plasmid pMAX-GFP in Amaxa solution P3 (first array) or P4 (second array). The nucleofection was carried out using programs CA-137, CM-138, CM-137, CM-150, DS-150, DS-120, EH-100, EO-100, DN-100, DS-138, DS-137, DS-130, EN-138, EN150, EW-113 and CB150 (from top to bottom, left to right). The fluorescence was detected on the next day.

The iPS cells were treated with ROCK inhibitor to prevent apoptosis. Right before nucleofection, the iPSC was detached by accutase from the dish and dispersed into single cell suspension. The cells were then mixed with P3 or P4 buffer for nucleofection and put pmax-GFP at a ratio 0.5ul in each well of the strip. Each of the wells contains 2×10^5 cells. The cells were then nucleofected by CA-137, CM-138, CM-137, CM-150, DS-150, DS-120, EH-100, EO-100, DN-100, DS-138, DS-137, DS-130, EN-138, EN150, EW-113 and CB150 programs. The fluorescence and cell survivability were recorded on the next day.

All the conditions gave low survival rate (Fig. 34). The intensity of green fluorescence of CM-138, DS-150 and DS-130 were higher than average. Based on the fluorescence intensity and the survival rate of the cells, we concluded DS-150 with P3 reagent is the best condition for efficient nucleofection for our patient iPSC.

For the gene correction of R345W mutation, the patient iPSC was mixed with SpCas9 protein 1ug, gRNA 300ng and ssODN 500pmol in Solution P3 reagent and then nucleofected by DS-150 program. The resulted cells were split into single colony and expanded for one week. The colonies were screened by RFLP assay. Positive colony were further confirmed by Sanger sequencing (Fig. 35). Gene-corrected colony without artifact mutations were chose for the future experiment.

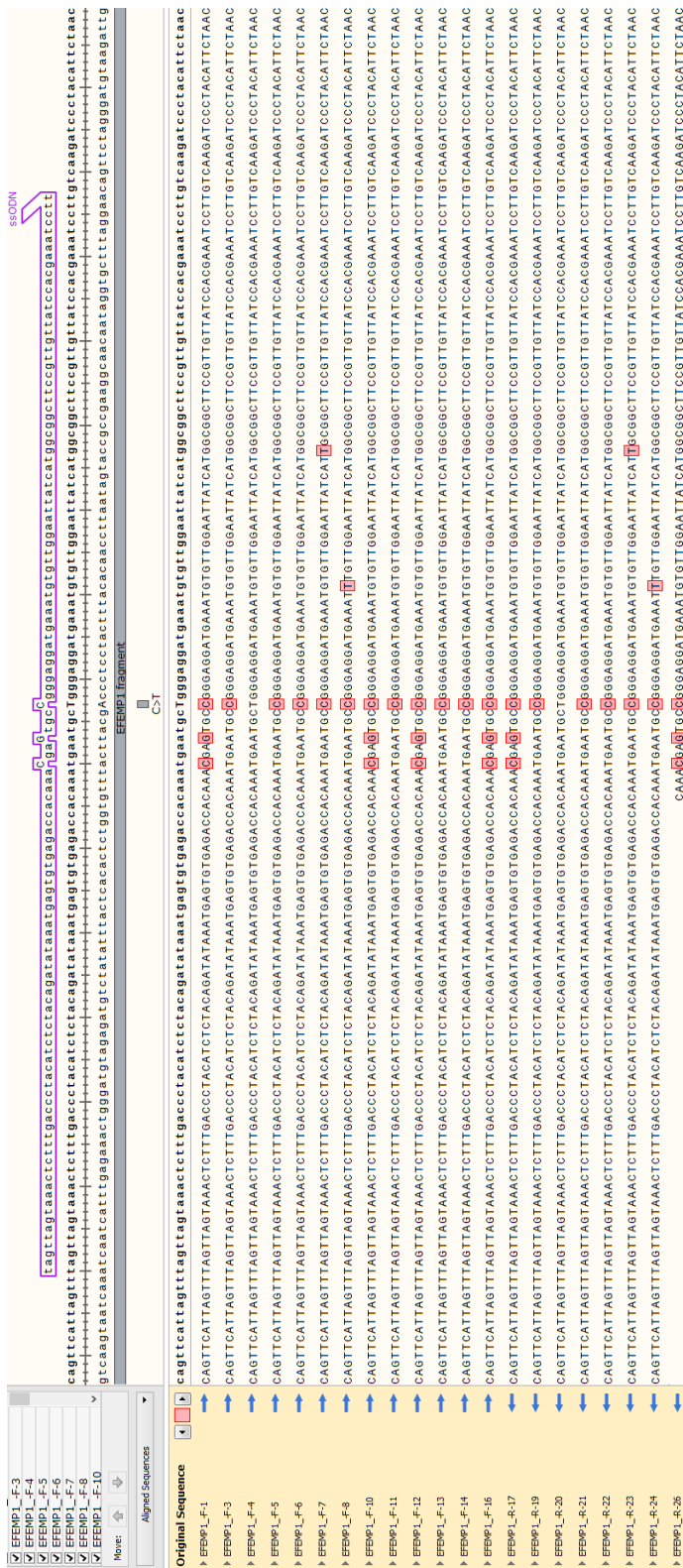


Figure 35. Sequencing result of iPSC colonies after gene correction. The iPSC colonies after nucleofection were manually picked and expanded. Sanger sequencing was used to verify the corrected sequence.

III. DISCUSSION

Though it has been reported that mismatches with in the 3' end region of gRNA can disable the targeting^{173, 174}. However, in our study, even though the wildtype nucleotide cytosine is differ from that in the sg006, sg007 or sg008, all of these three still mediates the digestion of the wildtype template. This result may imply an unreliability of mutation-specific targeting by CRISPR based on single nucleotide difference. For many genetic diseases which only have single nucleotide mutation, using CRISPR to perform *in vivo*, gene ablation therapy may arise safety concerns, since the wildtype allele may be targeted as well. A CRISPR-based *in vitro* therapy combined with cell transplantation therapy may be a more practical route to treat non-neuronal diseases.

CHAPTER 7: IPSC REPROGRAMING AND RPE DIFFERENTIATION

I. INTRODUCTION

For the precise phenotyping of *EFEMP1*^{R345W} mutation, RPE cells will be the best cell model to study the physiological change. However, due to the limited availability of autopsy RPE cells and the difficulty of genetic manipulation on primary RPE cells, we chose to obtain RPE cells from DHRD patient iPSC. The possibility of *in vitro* differentiation of RPE from iPSC was first described in 2009¹⁷⁵. In this study, the RPE cells were differentiated by this protocol with slight modification.

II. RESULTS

DHRD patient skin biopsy was collected by a surgeon. This 5 mm skin biopsy was placed in culture dishes for two week to allow fibroblast to migrate to the cover slide. These fibroblast were propagated and transduced by Sendai viruses expressing OCT3/4, SOX2, cMYC and KLF4. The iPSC colonies formed in the cell culture were picked up for colonial expansion. The quality of these iPSC colonies were confirmed by immunostaining of iPSC markers TRA-1-60, SOX2, SSEA4 and OCT4 (Fig. 36 and 37).

The nuclear expression of SOX2 and OCT4 was clearly detected, as well as the cytoplasmic expression of TRA-1-60 and SSEA4. The colony edge remained clear and clear indicating no sign of differentiation.

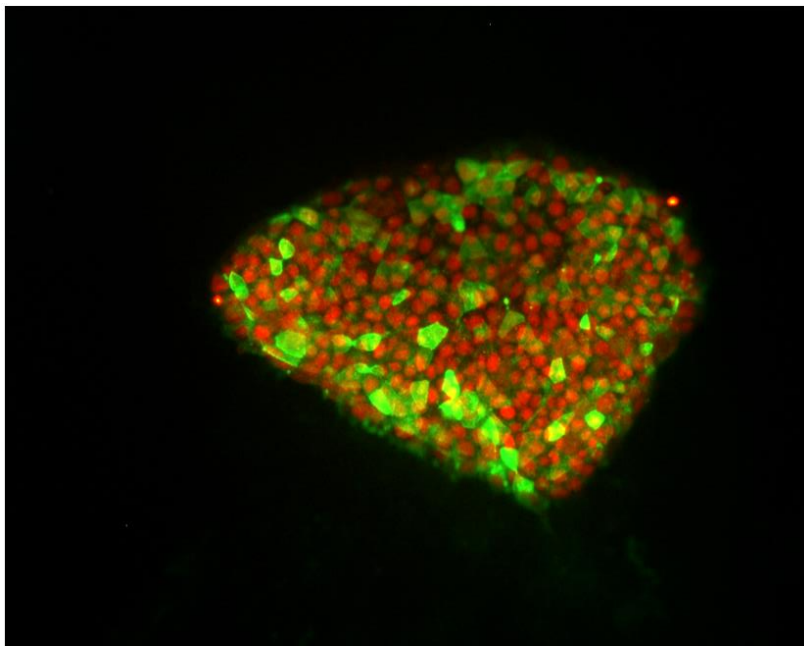


Figure 36. Immunostaining of TRA-1-60 and SOX2. TRA-1-60 (green) and SOX2 (red) were detected in iPSC culture.

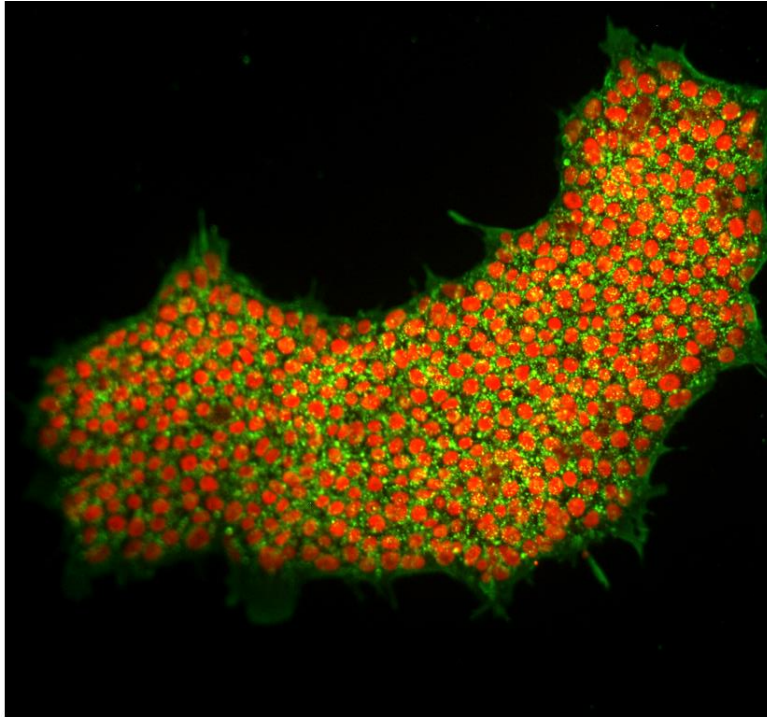


Figure 37. Immunostaining of SSEA4 and OCT4. SSEA4 (green) and OCT4 (red) were detected in iPSC culture.

To differentiate iPSC colony into RPE cells, the iPSC were grown to 90% confluency before the treatment of nicotinamide. After differentiating in nicotinamide-containing medium for two weeks, the differentiating medium were further enriched by activin A for the next two weeks of culture. Sporadic, tiny black spots in the cell culture started to appear in the last week of incubation.

These black, pigmented cell colonies were manually picked up and transferred to another culture plate for expansion and maturation (Fig. 38).

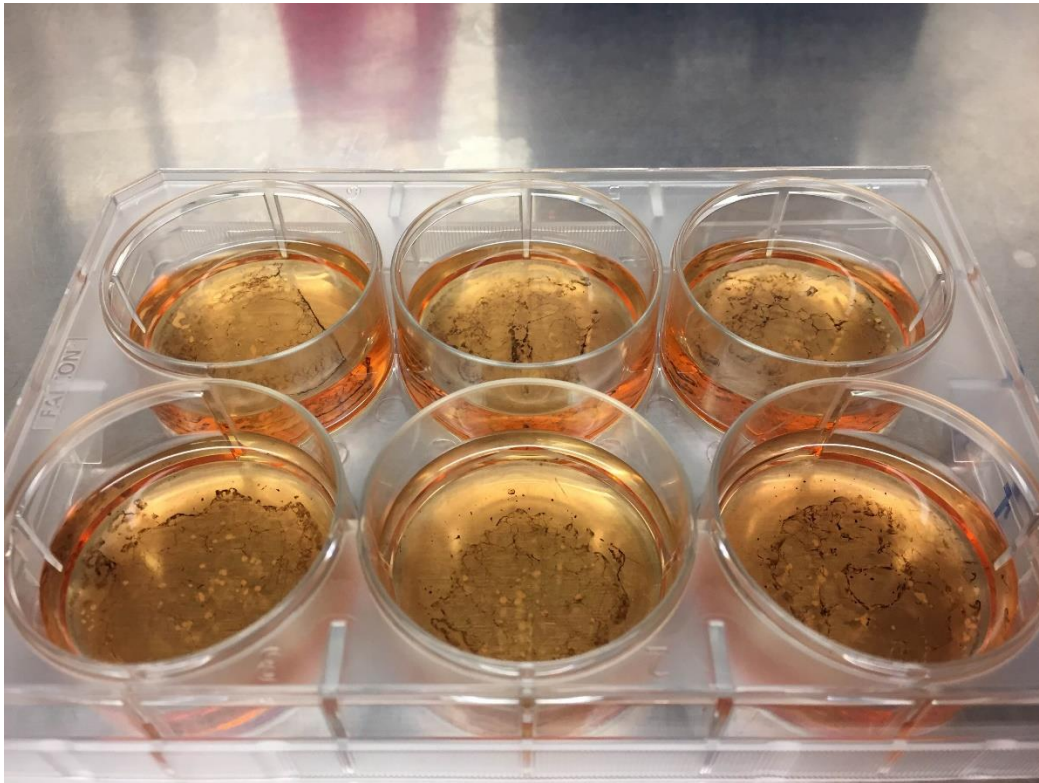


Figure 38. iPSC culture of RPE differentiation before and after colonial enrichment.

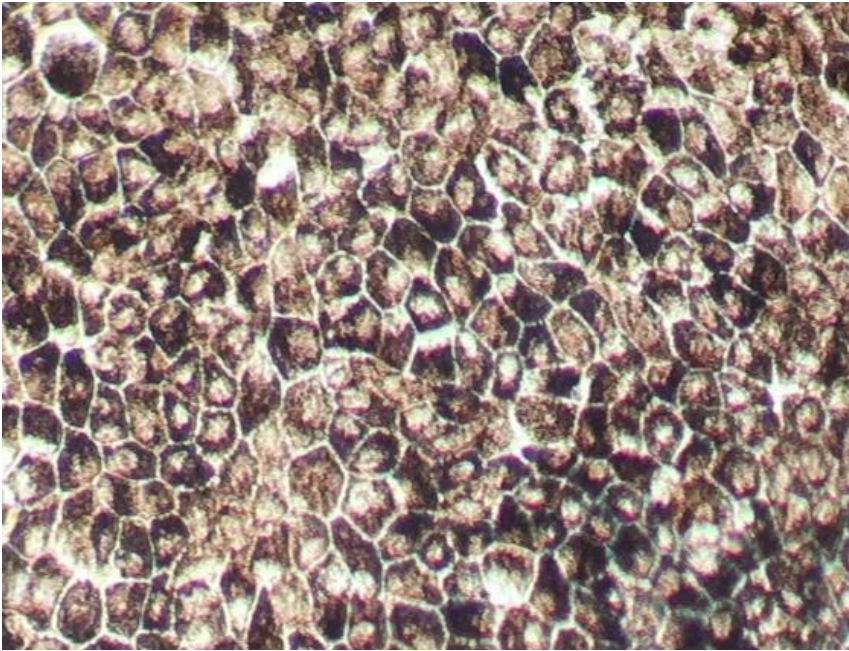
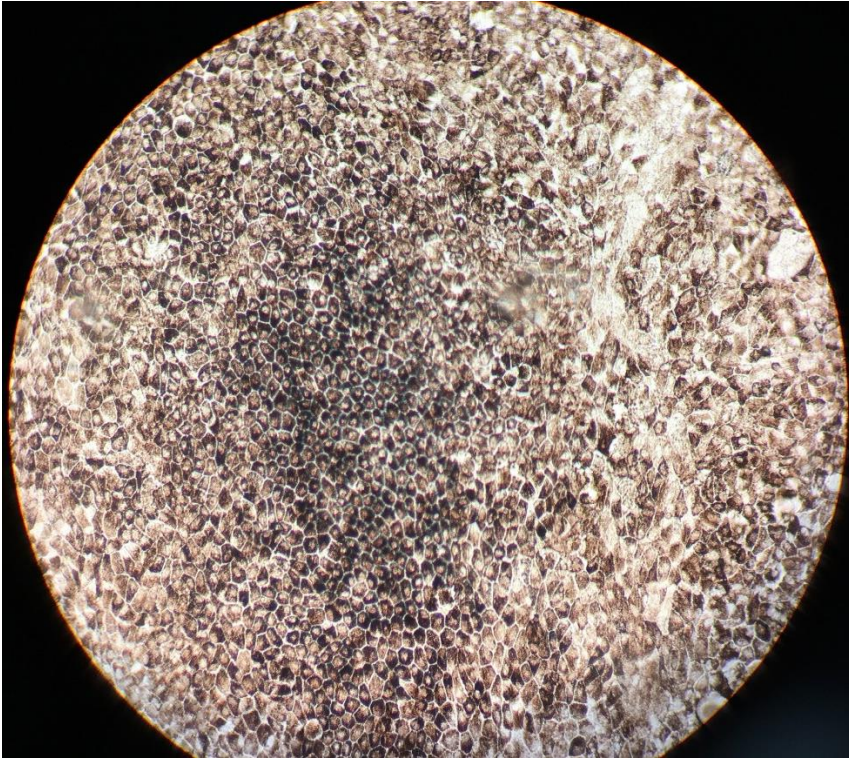


Figure 39. Morphology of iPSC-derived RPE after 200 days of differentiation.

After 100-200 days of culture, the cells became pigmented (Fig. 39). Hexagon shape morphology was observed under microscope. This morphology resembles what observed in primary RPE cell culture from autopsy⁷⁸.

These RPE cell were further characterized by immunostaining of RPE specific marker BEST1 (Fig. 40).

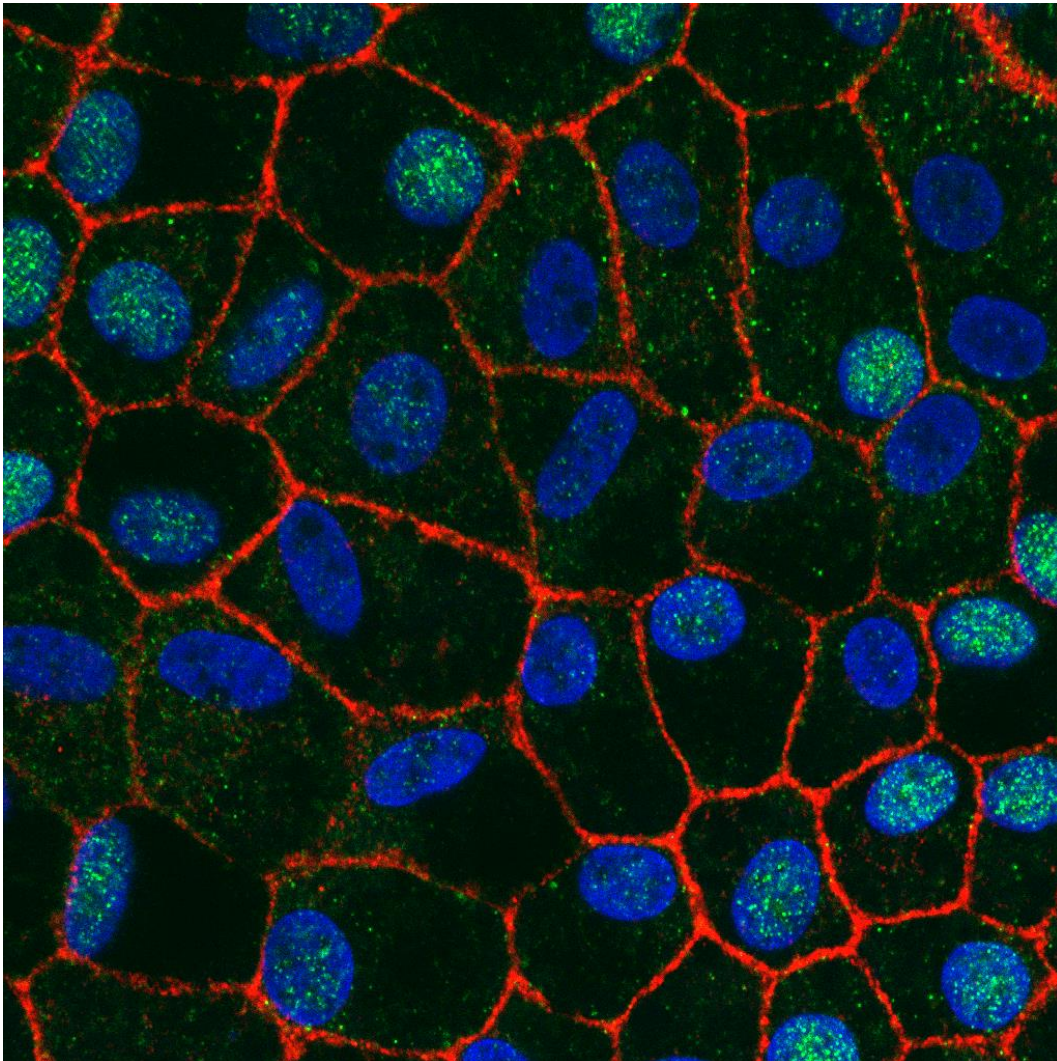


Figure 40. Immunostaining of RPE marker. Anti-BEST1 (red) and DAPI (blue) were used to stain iPSC-derived RPE.

III. Discussion

There have been different differentiation protocols published. The most recent version comprises many growth factors, including IGF, Noggin and bFGF in addition to nicotinamide and activin A¹⁷⁶. The RPE derived from iPSC treated with this protocol is reported to appear in as little as 14 days of treatment. However, this protocol is not reproducible in our lab and the result is variable among different iPSC clones based on our lab's experience. The current study followed a simplified but more reliable version published by Buchholz et al. in 2009¹⁷⁷, which primarily depends on the incubation with merely nicotinamide and activin A. However, a fly in the ointment, this protocol requires 4-6 weeks of incubation to see pigmented RPE cells in the cell culture. Nevertheless, both of the protocols requires a differentiation time over than three months to obtain mature RPE cells and each round of subculture/passaging requires another three months for re-maturation. A faster differentiation protocol would be very beneficial to boost RPE research.

CHAPTER 8: PHENOTYPING OF PATIENT IPSC-DERIVED RPE

I. INTRODUCTION

There has been some proposed hypotheses toward RPE pathogenesis. Accumulation of misfolded EFEMP1 proteins within the endoplasmic reticulum (ER) may activate a signaling pathway termed the unfolded protein response (UPR). This response, which is conserved from yeast to mammals, leads to the stress-responsive gene expression to increase ER protein processing capacity and boost ability to degrade misfolded proteins aggregating within the ER¹⁷⁸. UPR may induce the expression of VEGF, which is also discovered in DHRD and RPE^{179, 180}.

In addition to UPR, aberrant immune response has also been suggested to involve in the pathogenesis of AMD disease^{181, 182}. NLRP3 inflammasome has been found to be upregulated in AMD patient RPE cells. This upregulation induced the release of proinflammatory cytokines IL-1b and IL-18.

II. RESULTS

ER stress/unfolded protein response (UPR) markers GRP78 (Bip) and XBP-1a as well as VEGF were reported to increase when overexpressing mutant EFEMP1 in ARPE19 cell line⁵³. To validate the involvement of UPR, we screened the UPR biomarkers, sXBP1, usXBP1, total XBP1, ATF4, CHOP, GRP778/Bip, GRP94, EDEM and VEGF expression using real-time PCR in the patient iPSC-derived RPE cells (Fig. 41). The cell clones were divided into three groups: Untreated mutant, gene corrected and wildtype control.

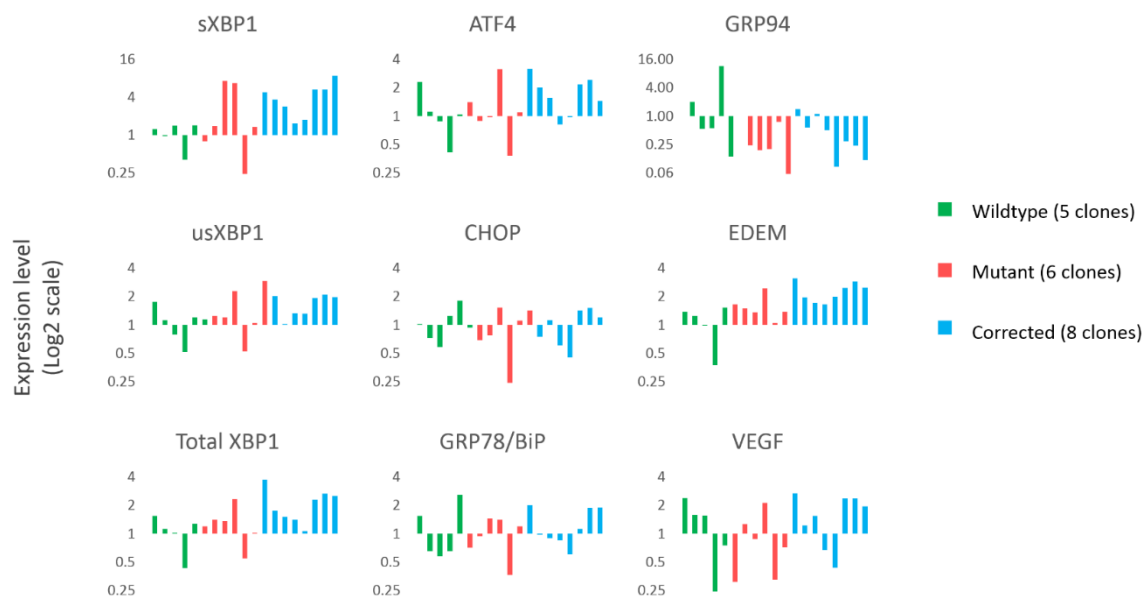


Figure 41. Real-time analysis of unfolded protein response biomarkers. The patient iPSC-derived RPE cells from the three groups, wildtype, *EFEMP1*^{+/R345W} mutant and gene corrected *EFEMP1*^{+/+} were analyzed for unfolded protein response biomarkers and VEGF expression. The dCT values were normalized by beta-actin.

Every group consists 5-8 clones of RPE derived from patient or healthy donors. We expected the expression of these markers to be low in the wildtype control group and high in the mutant group. Likewise, after gene correction the cell should behave similar to wildtype control, with low expression of UPR markers. However, we detected low expression of all markers in all the clones. The trends of each markers didn't match the pattern we expected, either. We concluded that UPR is not as activated by mutant EFEMP1 expression.

Next, we validated if mutant EFEMP1 can induce aberrant immune response in RPE cells or not. Since cytokine release is a common outcome of nearly all kinds of immune-related pathways (NLRP3 and NF- κ B), we screened cytokine release of IL-1 and IL-18 in the culture supernatant of the iPSC-derived RPE clones (Fig. 42).

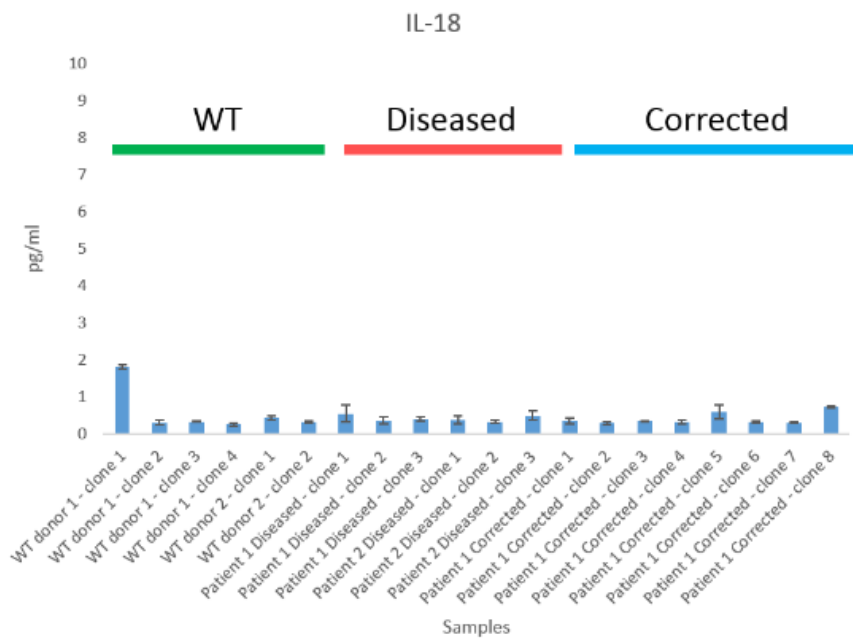
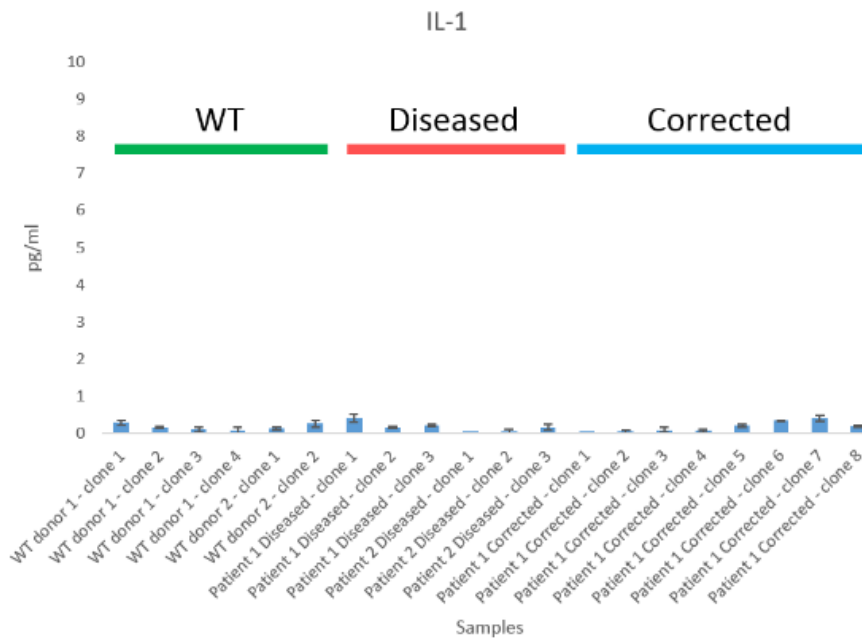


Figure 42. ELISA analysis of pro-inflammatory cytokines. The supernatant from patient iPSC-derived RPE culture were analyzed for cytokine IL-1 and IL-18 release. (n=2)

Surprisingly, no IL-1 or IL-18 was detected in all the screened clones (Fig. 42). All the cytokines level were very low in the supernatant, close to background. Only clone 1 in the wildtype group has appreciable but little IL-18 expression. This wildtype donor was obtained from patient with URSHER syndrom, which does not share clinical similarity with AMD or DHRD.

We abandoned existing hypotheses since those cannot explain what was observed in our disease model. We in turn, used untargeted mass-spectrophotometer to analyze the proteomics outcome of gene correction (Fig. 43).

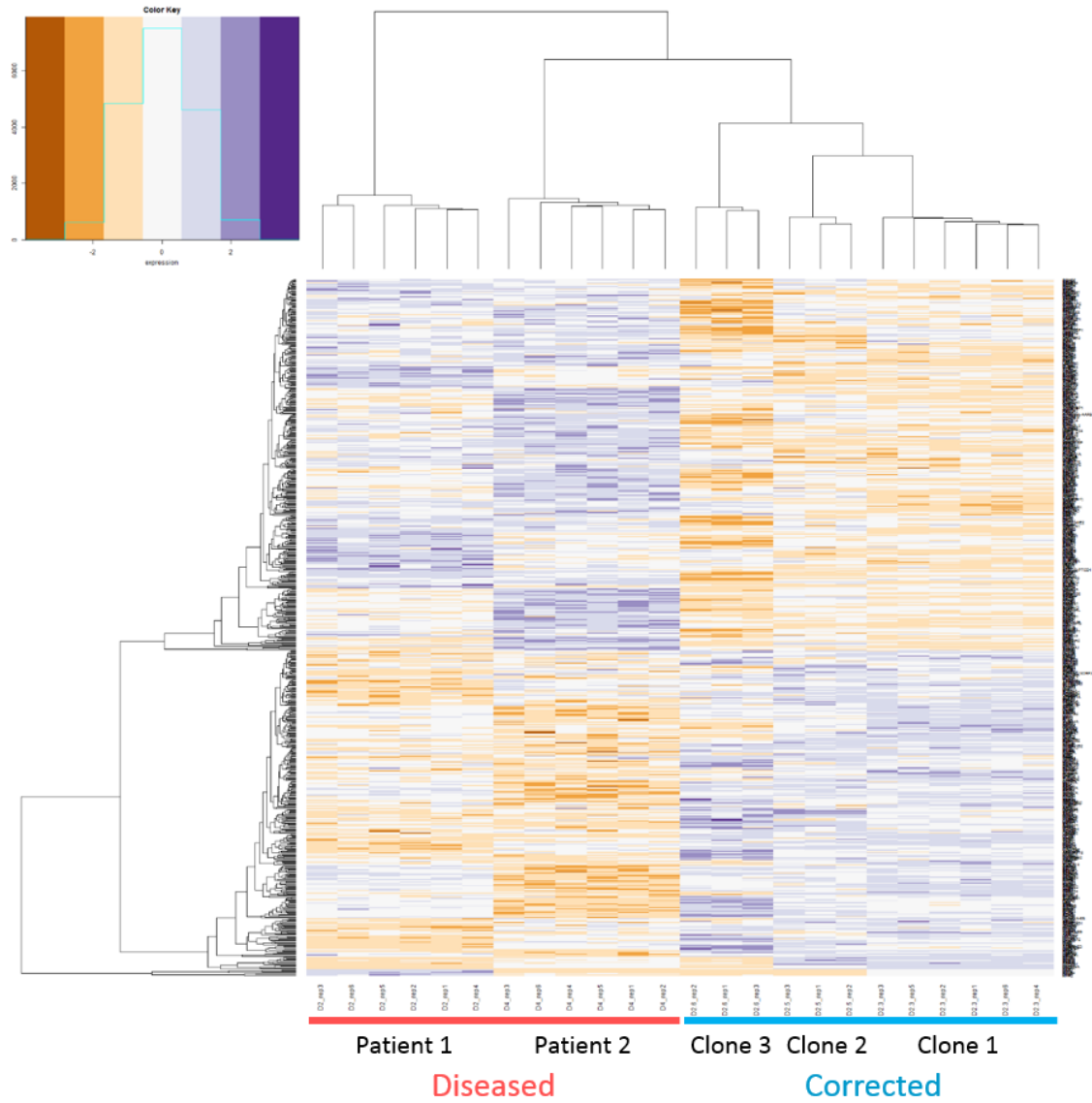


Figure 43. Proteomics analysis on patient-iPSC-derived RPEs by LC-MS/MS. (Heatmap and dendrogram)

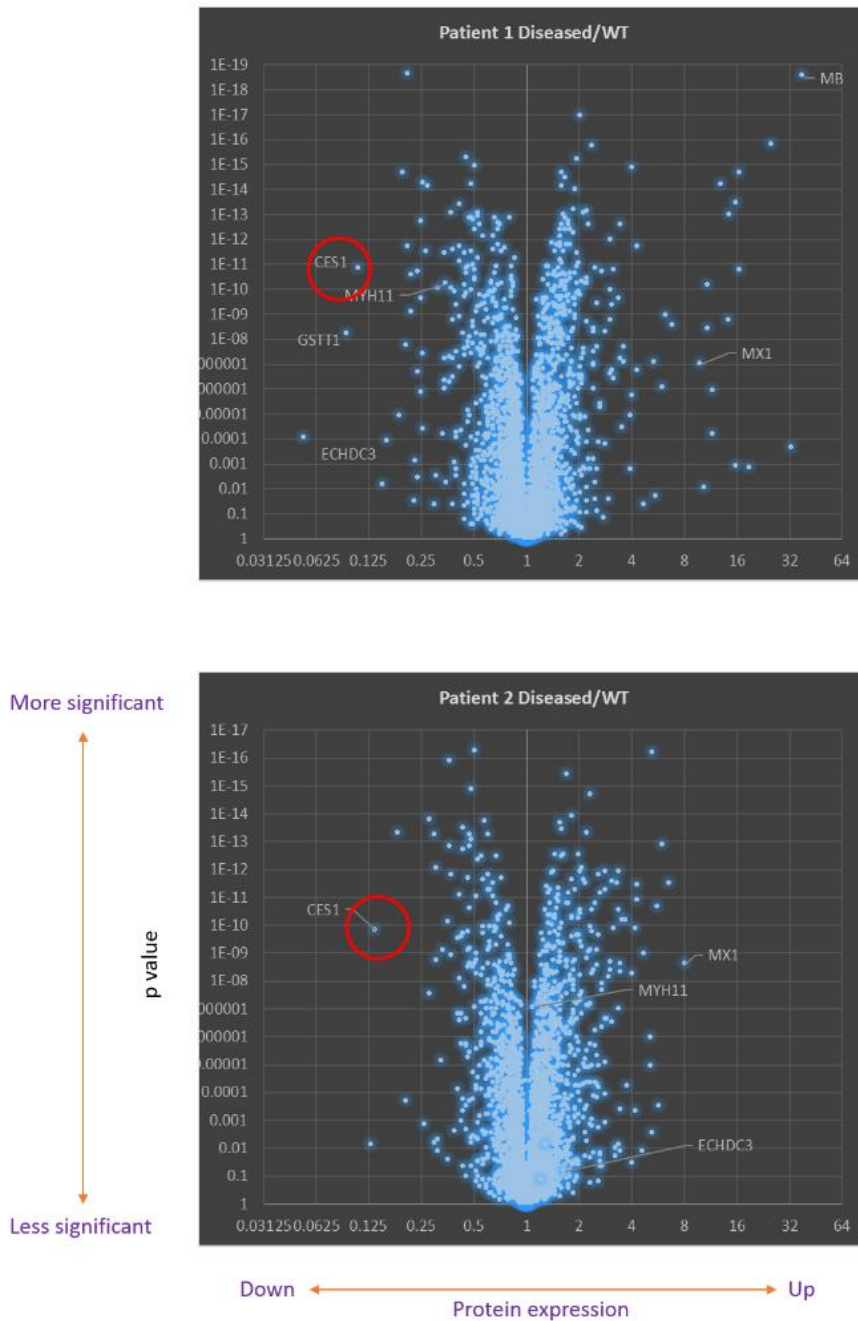


Figure 44. Volcano plot comparing proteomic profiles between patient and wildtype iPSC-derived PREs. A base-2 log scale is used for the abscissa (X axis), ranging from 0.03125 to 64. A base-10 log scale is used for the ordinate (Y axis), ranging from 1 to 1E-17.

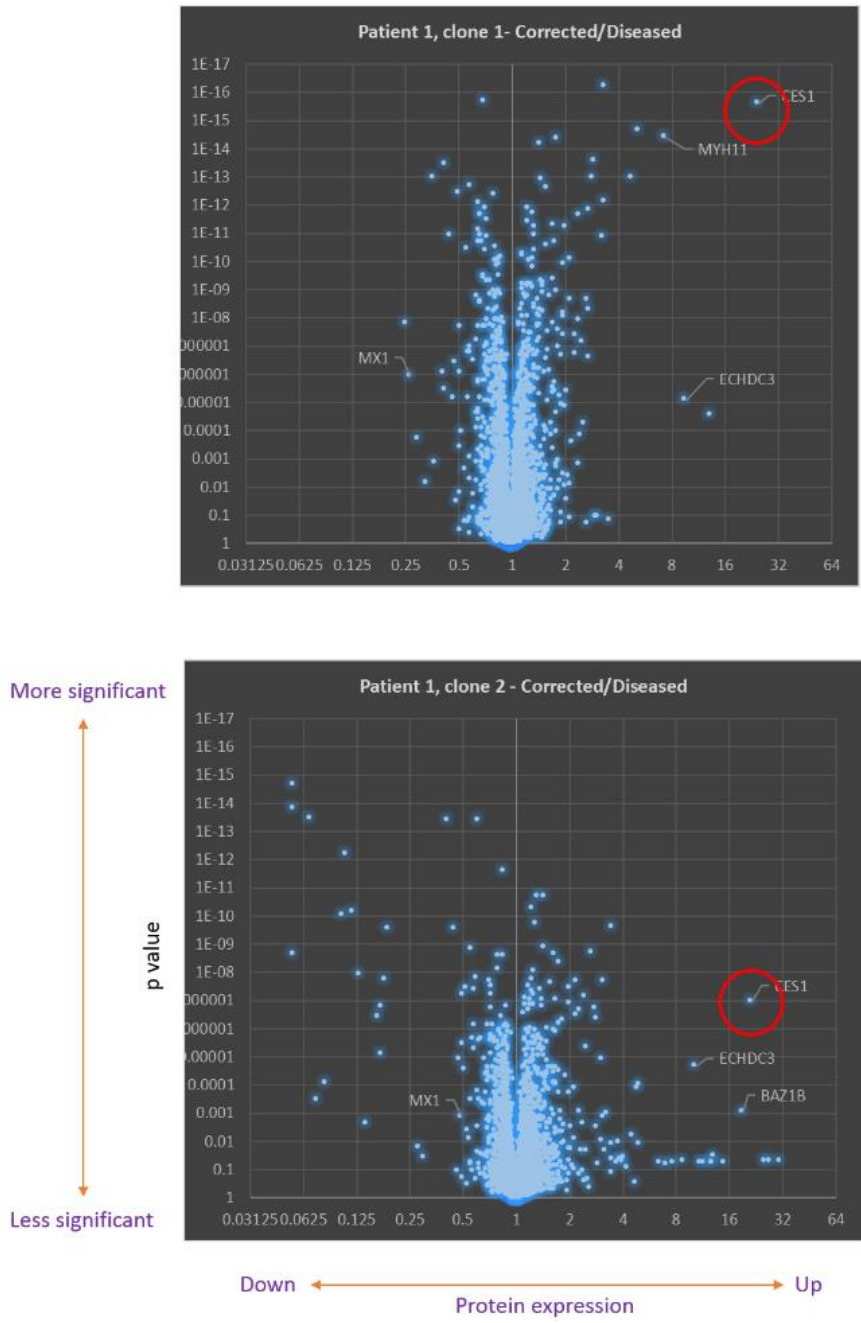


Figure 45. Volcano plot comparing proteomic profiles between gene-corrected and mutant iPSC-derived RPEs. A base-2 log scale is used for the abscissa (X axis), ranging from 0.03125 to 64. A base-10 log scale is used for the ordinate (Y axis), ranging from 1 to 1E-17.

By comparing the protein expression profiles, we found CES1 protein expression level is significantly decreased in patient RPE cells when compared to wildtype RPE cells ($p < 1 \times 10E-9$) (Fig. 44). This findings is consistent between two DHRD patients. After using CRISPR to correct the R345W (C>T) mutation, the CES1 expression level is then restored (Fig. 45). We concluded CES1 expression level is affected by the mutant *EFEMP1*.

Since CES1 has been reported to be a rate-limiting step of cholesterol efflux process, we further analyze the protein expression level related to cholesterol transport and catabolism. However, no significant change has been found in any transporter or catalytic enzyme, but only CES1 is affected (Fig. 46).

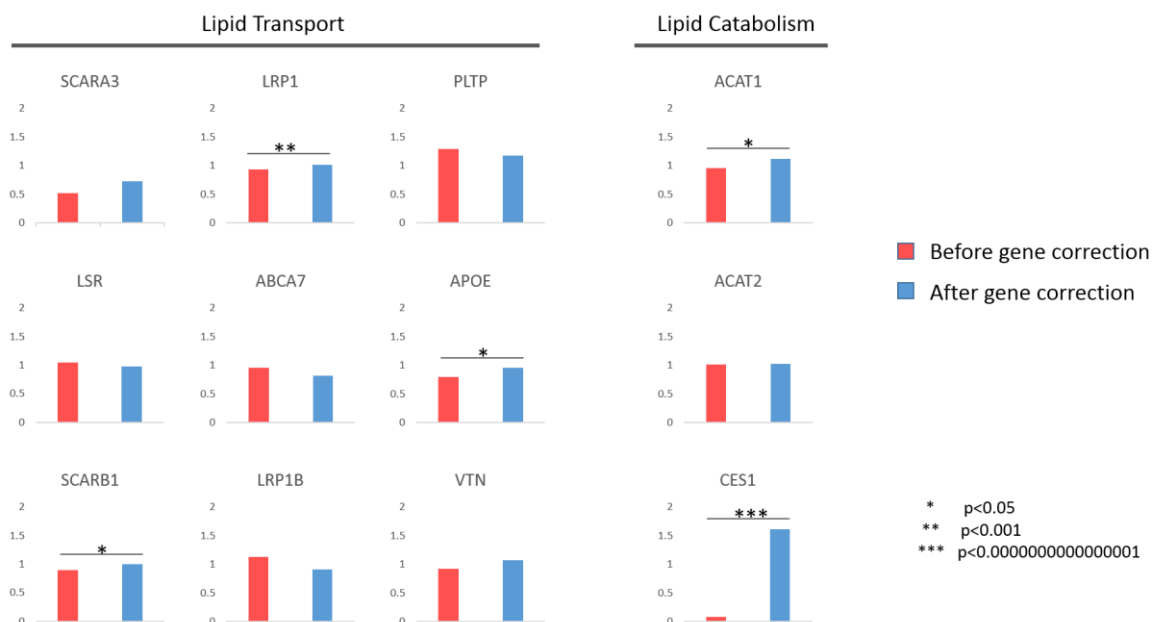


Figure 46. Protein level changes after gene correction. Protein involved in lipid transport and catabolism were analyzed by LC-MS/MS for differential expression.

III. Discussion

Though it has been reported over-expression of *EFEMP1*^{R345W} in ARPE19 can lead to UPR⁵³, in our experiment, we did not see any sign of UPR response in the patient RPE cells. Given that the patient iPSC-derived RPE is more authentic than the immortalized APRE-19 cell line, this result implies that the UPR detected in ARPE19 can be artifact resulted from excessive gene expression. Besides UPR, VEGF is elevated in RPE cell culture, according to Roybal et al.⁵³, which is not detected in our disease model, either. Because VEGF is also a common target of UPR pathway shared with hypoxia factor, HIF-1 signaling¹⁸³, lacking of VEGF response also indirectly indicates the dormancy of UPR.

Photo-oxidative stress¹⁸⁴⁻¹⁸⁶, lipid peroxidation¹⁸⁷⁻¹⁸⁹, Toll-like receptor¹⁹⁰⁻¹⁹² and alternative complement pathways have been proposed to compose a sophisticated immunopathogenesis toward AMD. Induction of inflammation and release of pro-inflammatory cytokines IL-1 and IL-18 is discovered to be a common consequence of these pathways. However, the absence of these cytokines in our RPE culture indicates that the way *EFEMP1*^{R345W} causes disease is independent to these pathways.

Excessive lipid droplet deposition in RPE cells has also been reported in both AMD patient RPE cells¹⁹³ and iPSC-derived RPE cells from both AMD and DHRD patients^{193, 194}, these findings strongly suggest dysregulation of lipid transport or catabolism in these disease. CES1 belongs to the carboxylesterase family of enzymes that was first identified in liver^{195, 196}. CES1, with an alternative name as cholesterol ester hydrolase (CEH), is responsible for the mobilization of cholesteryl ester in macrophage¹⁹⁷ (Fig. 47). Cholesteryl ester is the form of cholesterol for long-term storage in the cell. When input

from outside source, free cholesterol is converted to cholesteryl ester and stored in lipid droplets. This conversion is usually mediated by ACAT1 and ACAT2 enzymes (Fig. 47). In contrast, the efflux of cholesterol which requires the mobilization of cholesteryl ester. This conversion is mediated by a multiple enzyme process, in which CES1 is indispensable (Fig. 47).

Though the role of CES1 has never been studied in RPE cells, it has been suggested to participate in the efflux of cholesterol in foam cells during the regression phase (reverse cholesterol transport) of atherosclerosis^{197, 198}.

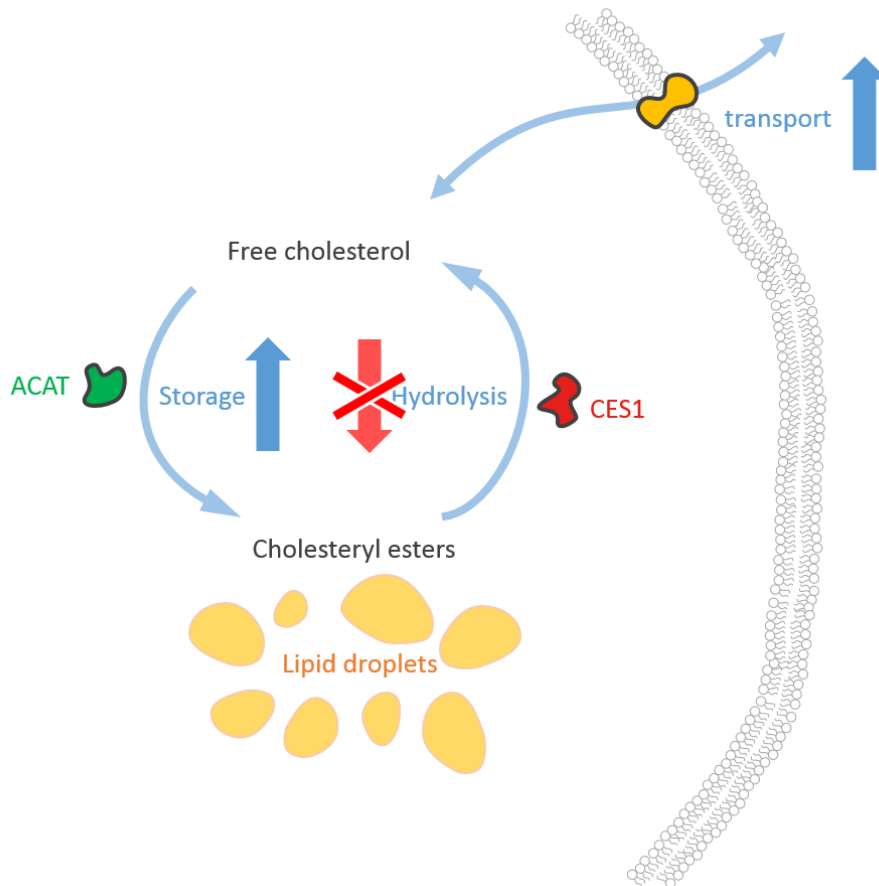


Figure 47. Hypothesis illustration of potential mechanism resulting intracellular lipid accumulation.

The accumulation of lipid in RPE can be possibly due to increased influx and decreased efflux of cholesterol. However, in our study no transporter protein or influx protein was affected by gene correction of *EFEMP1*^{R345W} mutation, indicating the efflux of cholesterol, which is controlled by CES1, may play a significant role in the disease development.

IV. FUTURE DIRECTIONS

Though the data from current study reveal the involvement of CES1 in the disease development, it is not clear how EFEMP1^{R345W} mutant protein can affect the expression level of CES1. EFEMP1 is an extracellular matrix protein and does not participate in gene transcription. Given that the two genes reside in different chromosomes (Chr 2 and 16), intergenic interaction between two genes is not likely to be the correct explanation.

However, further investigation is needed to determine whether the reduction of CES1 is resulted from increased degradation or decreased production that may be indirectly affected by EFEMP1^{R345W} mutant protein.

CHAPTER 9: MATERIAL AND METHODS (SECOND PART)

Design of the gRNA and donor template

All gRNAs used in this study were designed by Benchling (<https://benchling.com/>). When selecting gRNAs, only those covering the C>T mutation were considered. Three gRNAs, labeled as sg006, sg007 and sg008 with sequence 5'- gctgggaggatgaaatgtgt -3', 5'- gaccacaaatgaatgctggg -3' and 5'- tgagaccacaaatgaatgct -3' were selected for *in vitro* testing. For gene correction of *EFEMP1*^{R345W} mutation, donor template with sequence 5'- tagttagtaaactctttgacctacatctctacagatataaatgagtgtgagaccacaaaCgaGtgcCgggaggatgaaatg tgttgaattatcatggcggcttccgtgttatccacgaaatcctt was added when performing CRISPR. In total three nucleotides are different from the mutant sequence. Despite the cytosine at the mutated nucleotide, another cytosine and guanine (upper case) were created by silent mutations were included to enable colony screening by restriction fragment length polymorphism after nucleofection. The homology arms on each side is 60-mer long.

In vitro CRISPR digestion assay

To validate the targeting efficiency of our system, gRNA (25 ng/μl) was added to the reaction mixture alongside Cas9 protein (30 ng/μl, NEB) and template *EFEMP1*^{R345W} DNA (20 ng/μl, 750 bp) covering all three targeting sites of sg006, sg007 and sg008. The mixture was subsequently incubated at 37° C for 2 hr. After Cas9/gRNA digestion, the mixture was analyzed by agarose gel electrophoresis.

Genomic DNA extraction and genomic PCR

Genomic DNA from retinæ was extracted using the Blood & Tissue kit (QIAGEN). Genomic PCRs were performed using Phusion DNA polymerase (Fisher Scientific). Primers for the detection of gene truncation and NHEJ were as follows: Forward: 5'-tttgctggcctttgctcac -3'; Reverse: 5'- acatttccccgaaaagtgccca -3'. PCR amplicons generated from iPSC cell culture or gross retinal DNA samples were further subcloned by the TOPO-TA cloning kit (Invitrogen) and analyzed by Sanger sequencing.

Cell culture and nucleofection

Patient fibroblasts were transduced by sendai vectors to create iPS cell lines according to previously established protocols¹⁹⁹⁻²⁰¹. The methods used to induce undifferentiated iPS cells to differentiate into RPE-like cells have been described in detail¹⁷⁷. In brief, iPS cells cultured on matrigel were transduced with viral vectors carrying transcription factors OCT4, SOX2, KLF4 and MYC. The cells were further incubated in mTeSR medium under 5% CO₂ at 37°C. To perform CRISPR-mediated gene correction, 1 x 10⁶ cells, SpCas9 protein 5µg (2.5µl), gRNA 1500ng (1µl) and ssODN 1000pmol (2µl) were mixed with Amaxa solution P3 to a final volume at 20 µl. After incubation at room temperature for 10 mins, the cells were nucleofected using Lonza 4D nucleofector by DS150 program. After the nucleofection, the cells were immediately transferred to 6 cm dishes. After 48 hours of incubation, the cells were transferred to 10 cm dish for colony

picking. Restriction fragment length polymorphism with ScrFI was used to screen the positively gene-corrected clones. For the differentiation of iPSC cells into RPE, iPSC cells were grown to 90% confluency. For the first phase of differentiation, the cells were put in medium with 100 mM Nicotinamide in DMEM for 14 days. In the second phase, cells were treated with medium contains additional 100 ng/ml activin A for another 14 days before turning back to phase I medium. The pigmented spots in cell culture, which contains RPE cells, were transferred in to another culture plate. The cells were then propagated and enriched in RPE medium which contains N1 supplement and THT²⁰².

Name	Sigma	Amount	Storage
MEM, α modification	M-4526	500 mL	+4°C
N1 supplement	N-6530	5 mL	+4°C
Glutamine-penicillin-streptomycin	G-1146	5 mL	-20°C
Non essential amino acids	M-7145	5 mL	+4°C
THT*			-80°C
Taurine	T-0625	125 mg	
Hydrocortisone	H-0396	10 μ g	
Triiodo-thyronin	T-5516	0.0065 μ g	
Fetal bovine serum, heat inactivated*†		5% or 15%	-80°C

* THT is made by dissolving taurine-hydrocortisone-triiodo-thyronin in 1-1.5 mL PBS before making the medium. Multiple aliquots are made and stored at -80°C to simplify culturing preparation of the culture medium.

† Fetal bovine serum is not obtained from Sigma-Aldrich.

Figure 48. Medium and components used for RPE differentiation.

Immunostaining

Four antibodies against pluripotency markers (TRA-1-60, SSEA4, NANOG and SOX2 [ASK-306, Applied StemCell, Menlo Park, CA, USA]) were used to characterize the iPSC reprogrammed from the patient fibroblasts. Secondary antibodies conjugated Alexa Fluor 488 goat anti-rabbit or Alexa Fluor 555 goat anti-mouse IgG (1:1,000; Invitrogen; Life

Technologies). For the characterization of RPE cells, anti-BEST1 primary antibody was used. DAPI (4',6-diamidino-2-phenylindole) was used to stain nuclei. Images for all antibody labels were taken under the same settings with a fluorescence microscope (Leica DM 5000 B).

Mass spectrophotometry

For the sample preparation, each cell pellet was homogenized with 1% NP-40 lysis buffer with protease and phosphatase cocktails. Enhanced BCA Protein Quantification assay was used to determine the total protein amount of each sample. Proteins from 50 µg of serum filtrate were purified by mini S-trap columns (<http://www.proteome.com/s-trap/>) and digested on column by trypsin. The Thermo Quantitative Fluorometric Peptide Assay was used to quantify peptide concentrations prior to TMT labeling. 40µg peptides were labeled with TMT 6plex isobaric reagent and mixed for high pH reverse phase peptide fractionation. Thermo Orbitrap Fusion Tribrid Mass Spectrometer was used for MS/MS analysis (MS3 data acquisition method). Technical replications were run according to the table on the right. Each set was run in triplicates. Proteome Discoverer software (version PD 2.1) was used to search the acquired MS/MS data against human protein database downloaded from the UniProt website and generate TMT ratios. Positive identification was set at 5% peptide FDR. Also, at least 1 unique peptide has to be identified per protein. Duplicated protein identifications from database were removed. Total of 4605 human proteins were quantified and included in the final data. TMT ratios (each tag/common reference) were calculated by PD 2.1 and normalized by total peptide amount. Qlucore

Omic Explorer & Prism 6 Software were used to perform correlation and statistical analysis. KNN imputation was used for missing values.

Real-time PCR and relative mRNA quantification

RPE cells were harvested at the indicated time and lysed with TRIZOL reagent (Invitrogen). Total RNA was isolated according to the manufacturer's instructions. DNase I (Invitrogen) treatment was then performed to prevent genomic DNA contamination. The reverse transcription reaction was conducted by Superscript III Reverse Transcription kit, and a random hexamer (Invitrogen) was used to generate cDNA. Real-time PCR method was performed using Maxima SYBR Green/ROX qPCR Master Mix (Fisher Scientific) with StepOne Real-time PCR System (Invitrogen) to quantify gene expression levels. The expression level of unfolded protein response biomarkers were determined and normalized with actin. The PCR products were validated by melting curve and agarose gel electrophoresis. The following primers were used:

Target	Primer sequence (5' -> 3')
sXBP1	CTGAGTCCGAATCAGGTGCAG
	ATCCATGGGGAGATGTTCTGG
usXBP1	CAGCACTCAGACTACGTGCA
	ATCCATGGGGAGATGTTCTGG
Total XBP1	TGGCCGGGTCTGCTGAGTCCG
	ATCCATGGGGAGATGTTCTGG
ATF4	GTTCTCCAGCGACAAGGCTA
	ATCCTGCTTGCTGTTGTTGG
CHOP	AGAACCAGGAAACGGAAACAGA
	TCTCCTTCATGCGCTGCTTT
BiP	TGTTCAACCAATTATCAGCAAATC
	TTCTGCTGTATCCTCTTACCAGT
GRP94	GAAACGGATGCCTGGTGG
	GCCCCTTCTCCTGGGTC
EDEM	CAAGTGTTGGGTACGCCACG
	AAAGAAGCTCTCCATCCGGTC
VEGF	TGCAGATTATGCGGATCAAACC
	TGCATTACATTTGTTGTGCTGTAG
b-actin	TCCACCTTCCAGCAGATGTG
	GCATTTGCGGTGGACGAT

Figure 49. Primers list for real-time PCR.

Statistics

An unpaired, two-sided t-test was used for the comparisons of mRNA levels response.

Reference:

1. Malhotra, A, Minja, FJ, Crum, A, and Burrowes, D (2011). Ocular anatomy and cross-sectional imaging of the eye. *Semin Ultrasound CT MR* **32**: 2-13.
2. Palczewski, K (2014). Chemistry and biology of the initial steps in vision: the Friedenwald lecture. *Invest Ophthalmol Vis Sci* **55**: 6651-6672.
3. Palczewski, K (2012). Chemistry and biology of vision. *J Biol Chem* **287**: 1612-1619.
4. Kefalov, VJ, and Arshavsky, VY (2014). FASEB Science Research Conference on Biology and Chemistry of Vision. *FASEB J* **28**: 2395-2397.
5. Tang, PH, Kono, M, Koutalos, Y, Ablonczy, Z, and Crouch, RK (2013). New insights into retinoid metabolism and cycling within the retina. *Prog Retin Eye Res* **32**: 48-63.
6. Cote, RH (2004). Characteristics of photoreceptor PDE (PDE6): similarities and differences to PDE5. *Int J Impot Res* **16 Suppl 1**: S28-33.
7. Yarfitz, S, and Hurley, JB (1994). Transduction mechanisms of vertebrate and invertebrate photoreceptors. *J Biol Chem* **269**: 14329-14332.
8. Stryer, L (1991). Visual excitation and recovery. *J Biol Chem* **266**: 10711-10714.
9. Kiser, PD, and Palczewski, K (2010). Membrane-binding and enzymatic properties of RPE65. *Prog Retin Eye Res* **29**: 428-442.
10. Fung, BK, Hurley, JB, and Stryer, L (1981). Flow of information in the light-triggered cyclic nucleotide cascade of vision. *Proc Natl Acad Sci U S A* **78**: 152-156.
11. Baehr, W, Devlin, MJ, and Applebury, ML (1979). Isolation and characterization of cGMP phosphodiesterase from bovine rod outer segments. *J Biol Chem* **254**: 11669-11677.
12. Arshavsky, V, and Bownds, MD (1992). Regulation of deactivation of photoreceptor G protein by its target enzyme and cGMP. *Nature* **357**: 416-417.
13. Rivas, MA, and Vecino, E (2009). Animal models and different therapies for treatment of retinitis pigmentosa. *Histol Histopathol* **24**: 1295-1322.
14. Palczewski, K, McDowell, JH, Jakes, S, Ingebritsen, TS, and Hargrave, PA (1989). Regulation of rhodopsin dephosphorylation by arrestin. *J Biol Chem* **264**: 15770-15773.
15. Torre, V, Matthews, HR, and Lamb, TD (1986). Role of calcium in regulating the cyclic GMP cascade of phototransduction in retinal rods. *Proc Natl Acad Sci U S A* **83**: 7109-7113.
16. Lagnado, L, and Baylor, D (1992). Signal flow in visual transduction. *Neuron* **8**: 995-1002.
17. Koutalos, Y (1992). High-pH form of bovine rhodopsin. *Biophys J* **61**: 272-275.
18. Sohocki, MM, Daiger, SP, Bowne, SJ, Rodriguez, JA, Northrup, H, Heckenlively, JR, *et al.* (2001). Prevalence of mutations causing retinitis pigmentosa and other inherited retinopathies. *Hum Mutat* **17**: 42-51.
19. Tang, Z, Zhang, Y, Wang, Y, Zhang, D, Shen, B, Luo, M, *et al.* (2017). Progress of stem/progenitor cell-based therapy for retinal degeneration. *J Transl Med* **15**: 99.
20. Stroupe, KT, Stelmack, JA, Tang, XC, Reda, DJ, Moran, D, Rinne, S, *et al.* (2008). Economic evaluation of blind rehabilitation for veterans with macular diseases in the Department of Veterans Affairs. *Ophthalmic Epidemiol* **15**: 84-91.
21. McKusick, VA (2007). Mendelian Inheritance in Man and its online version, OMIM. *Am J Hum Genet* **80**: 588-604.
22. Amladi, S (2003). Online Mendelian Inheritance in Man 'OMIM'. *Indian J Dermatol Venereol Leprol* **69**: 423-424.
23. Fahim, AT, Daiger, SP, and Weleber, RG (1993). Nonsyndromic Retinitis Pigmentosa Overview. In: Adam, MP, *et al.* (eds). *GeneReviews*((R)): Seattle (WA).
24. Stieger, K, and Lorenz, B (2010). Gene therapy for vision loss -- recent developments. *Discov Med* **10**: 425-433.

25. Athanasiou, D, Aguila, M, Bellingham, J, Li, W, McCulley, C, Reeves, PJ, *et al.* (2018). The molecular and cellular basis of rhodopsin retinitis pigmentosa reveals potential strategies for therapy. *Prog Retin Eye Res* **62**: 1-23.
26. Daiger, SP, Bowne, SJ, and Sullivan, LS (2014). Genes and Mutations Causing Autosomal Dominant Retinitis Pigmentosa. *Cold Spring Harb Perspect Med* **5**.
27. Rivolta, C, Sharon, D, DeAngelis, MM, and Dryja, TP (2002). Retinitis pigmentosa and allied diseases: numerous diseases, genes, and inheritance patterns. *Hum Mol Genet* **11**: 1219-1227.
28. Nishiguchi, KM, and Rivolta, C (2012). Genes associated with retinitis pigmentosa and allied diseases are frequently mutated in the general population. *PLoS One* **7**: e41902.
29. Dryja, TP, and Berson, EL (1995). Retinitis pigmentosa and allied diseases. Implications of genetic heterogeneity. *Invest Ophthalmol Vis Sci* **36**: 1197-1200.
30. Wang, DY, Chan, WM, Tam, PO, Baum, L, Lam, DS, Chong, KK, *et al.* (2005). Gene mutations in retinitis pigmentosa and their clinical implications. *Clin Chim Acta* **351**: 5-16.
31. Paquet-Durand, F, Azadi, S, Hauck, SM, Ueffing, M, van Veen, T, and Ekstrom, P (2006). Calpain is activated in degenerating photoreceptors in the rd1 mouse. *J Neurochem* **96**: 802-814.
32. Doonan, F, Donovan, M, and Cotter, TG (2005). Activation of multiple pathways during photoreceptor apoptosis in the rd mouse. *Invest Ophthalmol Vis Sci* **46**: 3530-3538.
33. Rohrer, B, Pinto, FR, Hulse, KE, Lohr, HR, Zhang, L, and Almeida, JS (2004). Multidestructive pathways triggered in photoreceptor cell death of the rd mouse as determined through gene expression profiling. *J Biol Chem* **279**: 41903-41910.
34. Sharma, AK, and Rohrer, B (2004). Calcium-induced calpain mediates apoptosis via caspase-3 in a mouse photoreceptor cell line. *J Biol Chem* **279**: 35564-35572.
35. Audo, I, Sahel, JA, Mohand-Said, S, Lancelot, ME, Antonio, A, Moskova-Doumanova, V, *et al.* (2010). EYS is a major gene for rod-cone dystrophies in France. *Hum Mutat* **31**: E1406-1435.
36. Weng, J, Mata, NL, Azarian, SM, Tzekov, RT, Birch, DG, and Travis, GH (1999). Insights into the function of Rim protein in photoreceptors and etiology of Stargardt's disease from the phenotype in abcr knockout mice. *Cell* **98**: 13-23.
37. Lu, Z, Hu, X, Liu, F, Soares, DC, Liu, X, Yu, S, *et al.* (2017). Ablation of EYS in zebrafish causes mislocalisation of outer segment proteins, F-actin disruption and cone-rod dystrophy. *Sci Rep* **7**: 46098.
38. Han, Z, Conley, SM, and Naash, MI (2014). Gene therapy for Stargardt disease associated with ABCA4 gene. *Adv Exp Med Biol* **801**: 719-724.
39. Mendes, HF, van der Spuy, J, Chapple, JP, and Cheetham, ME (2005). Mechanisms of cell death in rhodopsin retinitis pigmentosa: implications for therapy. *Trends Mol Med* **11**: 177-185.
40. Sung, CH, Schneider, BG, Agarwal, N, Papermaster, DS, and Nathans, J (1991). Functional heterogeneity of mutant rhodopsins responsible for autosomal dominant retinitis pigmentosa. *Proc Natl Acad Sci U S A* **88**: 8840-8844.
41. Sung, CH, Davenport, CM, and Nathans, J (1993). Rhodopsin mutations responsible for autosomal dominant retinitis pigmentosa. Clustering of functional classes along the polypeptide chain. *J Biol Chem* **268**: 26645-26649.
42. Gorbatyuk, MS, Knox, T, LaVail, MM, Gorbatyuk, OS, Noorwez, SM, Hauswirth, WW, *et al.* (2010). Restoration of visual function in P23H rhodopsin transgenic rats by gene delivery of BiP/Grp78. *Proc Natl Acad Sci U S A* **107**: 5961-5966.
43. Sakami, S, Maeda, T, Bereta, G, Okano, K, Golczak, M, Sumaroka, A, *et al.* (2011). Probing mechanisms of photoreceptor degeneration in a new mouse model of the

- common form of autosomal dominant retinitis pigmentosa due to P23H opsin mutations. *J Biol Chem* **286**: 10551-10567.
44. Olsson, JE, Gordon, JW, Pawlyk, BS, Roof, D, Hayes, A, Molday, RS, *et al.* (1992). Transgenic mice with a rhodopsin mutation (Pro23His): a mouse model of autosomal dominant retinitis pigmentosa. *Neuron* **9**: 815-830.
 45. Heon, E, Piguet, B, Munier, F, Sneed, SR, Morgan, CM, Forni, S, *et al.* (1996). Linkage of autosomal dominant radial drusen (malattia leventinese) to chromosome 2p16-21. *Arch Ophthalmol* **114**: 193-198.
 46. Tarttelin, EE, Gregory-Evans, CY, Bird, AC, Weleber, RG, Klein, ML, Blackburn, J, *et al.* (2001). Molecular genetic heterogeneity in autosomal dominant drusen. *J Med Genet* **38**: 381-384.
 47. Toto, L, Parodi, MB, Baralle, F, Casari, G, Ravalico, G, and Romano, M (2002). Genetic heterogeneity in Malattia Leventinese. *Clin Genet* **62**: 399-403.
 48. Gaillard, MC, Wolfensberger, TJ, Uffer, S, Mantel, I, Pournaras, JA, Schorderet, DF, *et al.* (2005). [Optical coherence tomography in Malattia Leventinese]. *Klin Monbl Augenheilkd* **222**: 180-185.
 49. Hogan, MJ (1972). Role of the retinal pigment epithelium in macular disease. *Trans Am Acad Ophthalmol Otolaryngol* **76**: 64-80.
 50. Guymer, RH, McNeil, R, Cain, M, Tomlin, B, Allen, PJ, Dip, CL, *et al.* (2002). Analysis of the Arg345Trp disease-associated allele of the EFEMP1 gene in individuals with early onset drusen or familial age-related macular degeneration. *Clin Exp Ophthalmol* **30**: 419-423.
 51. Marmorstein, L (2004). Association of EFEMP1 with malattia leventinese and age-related macular degeneration: a mini-review. *Ophthalmic Genet* **25**: 219-226.
 52. Narendran, N, Guymer, RH, Cain, M, and Baird, PN (2005). Analysis of the EFEMP1 gene in individuals and families with early onset drusen. *Eye (Lond)* **19**: 11-15.
 53. Roybal, CN, Marmorstein, LY, Vander Jagt, DL, and Abcouwer, SF (2005). Aberrant accumulation of fibulin-3 in the endoplasmic reticulum leads to activation of the unfolded protein response and VEGF expression. *Invest Ophthalmol Vis Sci* **46**: 3973-3979.
 54. Corbelli, E, Corvi, F, Carnevali, A, Querques, L, Zucchiatti, I, Bandello, F, *et al.* (2016). Optical Coherence Tomography Angiography Demonstration of Choroidal Neovascularization in Malattia Leventinese. *Ophthalmic Surg Lasers Imaging Retina* **47**: 602-604.
 55. Serra, R, Coscas, F, Messaoudi, N, Srour, M, and Souied, E (2017). Choroidal Neovascularization in Malattia Leventinese Diagnosed Using Optical Coherence Tomography Angiography. *Am J Ophthalmol* **176**: 108-117.
 56. Sohn, EH, Patel, PJ, MacLaren, RE, Adatia, FA, Pal, B, Webster, AR, *et al.* (2011). Responsiveness of choroidal neovascular membranes in patients with R345W mutation in fibulin 3 (Doyme honeycomb retinal dystrophy) to anti-vascular endothelial growth factor therapy. *Arch Ophthalmol* **129**: 1626-1628.
 57. Klein, R, Klein, BE, and Linton, KL (1992). Prevalence of age-related maculopathy. The Beaver Dam Eye Study. *Ophthalmology* **99**: 933-943.
 58. Vingerling, JR, Dielemans, I, Hofman, A, Grobbee, DE, Hijmering, M, Kramer, CF, *et al.* (1995). The prevalence of age-related maculopathy in the Rotterdam Study. *Ophthalmology* **102**: 205-210.
 59. Hulleman, JD (2016). Malattia Leventinese/Doyme Honeycomb Retinal Dystrophy: Similarities to Age-Related Macular Degeneration and Potential Therapies. *Adv Exp Med Biol* **854**: 153-158.

60. Heiba, IM, Elston, RC, Klein, BE, and Klein, R (1994). Sibling correlations and segregation analysis of age-related maculopathy: the Beaver Dam Eye Study. *Genet Epidemiol* **11**: 51-67.
61. Sarks, JP, Sarks, SH, and Killingsworth, MC (1994). Evolution of soft drusen in age-related macular degeneration. *Eye (Lond)* **8 (Pt 3)**: 269-283.
62. Marmorstein, LY, Munier, FL, Arsenijevic, Y, Schorderet, DF, McLaughlin, PJ, Chung, D, *et al.* (2002). Aberrant accumulation of EFEMP1 underlies drusen formation in Malattia Leventinese and age-related macular degeneration. *Proc Natl Acad Sci U S A* **99**: 13067-13072.
63. Loffler, KU, and Lee, WR (1986). Basal linear deposit in the human macula. *Graefes Arch Clin Exp Ophthalmol* **224**: 493-501.
64. Marshall, GE, Konstas, AG, Reid, GG, Edwards, JG, and Lee, WR (1992). Type IV collagen and laminin in Bruch's membrane and basal linear deposit in the human macula. *Br J Ophthalmol* **76**: 607-614.
65. Knupp, C, Munro, PM, Luther, PK, Ezra, E, and Squire, JM (2000). Structure of abnormal molecular assemblies (collagen VI) associated with human full thickness macular holes. *J Struct Biol* **129**: 38-47.
66. Reale, E, Groos, S, Eckardt, U, Eckardt, C, and Luciano, L (2009). New components of 'basal laminar deposits' in age-related macular degeneration. *Cells Tissues Organs* **190**: 170-181.
67. Lommatzsch, A, Hermans, P, Muller, KD, Bornfeld, N, Bird, AC, and Pauleikhoff, D (2008). Are low inflammatory reactions involved in exudative age-related macular degeneration? Morphological and immunohistochemical analysis of AMD associated with basal deposits. *Graefes Arch Clin Exp Ophthalmol* **246**: 803-810.
68. Curcio, CA, Johnson, M, Huang, JD, and Rudolf, M (2009). Aging, age-related macular degeneration, and the response-to-retention of apolipoprotein B-containing lipoproteins. *Prog Retin Eye Res* **28**: 393-422.
69. Schaumberg, DA, Christen, WG, Hankinson, SE, and Glynn, RJ (2001). Body mass index and the incidence of visually significant age-related maculopathy in men. *Arch Ophthalmol* **119**: 1259-1265.
70. Klein, R, Knudtson, MD, Cruickshanks, KJ, and Klein, BE (2008). Further observations on the association between smoking and the long-term incidence and progression of age-related macular degeneration: the Beaver Dam Eye Study. *Arch Ophthalmol* **126**: 115-121.
71. Curcio, CA, Millican, CL, Bailey, T, and Kruth, HS (2001). Accumulation of cholesterol with age in human Bruch's membrane. *Invest Ophthalmol Vis Sci* **42**: 265-274.
72. Burns, RP, and Feeney-Burns, L (1980). Clinico-morphologic correlations of drusen of Bruch's membrane. *Trans Am Ophthalmol Soc* **78**: 206-225.
73. Feeney-Burns, L, Hilderbrand, ES, and Eldridge, S (1984). Aging human RPE: morphometric analysis of macular, equatorial, and peripheral cells. *Invest Ophthalmol Vis Sci* **25**: 195-200.
74. Curcio, CA, and Millican, CL (1999). Basal linear deposit and large drusen are specific for early age-related maculopathy. *Arch Ophthalmol* **117**: 329-339.
75. Qian, TW, and Xu, X (2017). [Research progress of treatment strategies for retinitis pigmentosa]. *Zhonghua Yan Ke Za Zhi* **53**: 148-153.
76. Huang, XF (2018). Current Pharmacological Concepts in the Treatment of the Retinitis Pigmentosa. *Adv Exp Med Biol* **1074**: 439-445.
77. DiCarlo, JE, Mahajan, VB, and Tsang, SH (2018). Gene therapy and genome surgery in the retina. *J Clin Invest* **128**: 2177-2188.

78. Li, Y, Tsai, YT, Hsu, CW, Erol, D, Yang, J, Wu, WH, *et al.* (2012). Long-term safety and efficacy of human-induced pluripotent stem cell (iPS) grafts in a preclinical model of retinitis pigmentosa. *Mol Med* **18**: 1312-1319.
79. Wang, NK, Tosi, J, Kasanuki, JM, Chou, CL, Kong, J, Parmalee, N, *et al.* (2010). Transplantation of reprogrammed embryonic stem cells improves visual function in a mouse model for retinitis pigmentosa. *Transplantation* **89**: 911-919.
80. Federico, M (1999). Lentiviruses as gene delivery vectors. *Curr Opin Biotechnol* **10**: 448-453.
81. Voelker, R (2018). Gene Therapy for Vision Loss. *JAMA* **319**: 434.
82. Surace, EM, and Auricchio, A (2008). Versatility of AAV vectors for retinal gene transfer. *Vision Res* **48**: 353-359.
83. Abbasi, J (2017). Spark Advances Gene Therapy for Inherited Vision Loss. *JAMA* **318**: 116.
84. (2014). Chapter 3 - Restoring Vision to the Blind: Gene Therapy for Vision Loss. *Transl Vis Sci Technol* **3**: 5.
85. Grieger, JC, and Samulski, RJ (2012). Adeno-associated virus vectorology, manufacturing, and clinical applications. *Methods Enzymol* **507**: 229-254.
86. Bartel, MA, Weinstein, JR, and Schaffer, DV (2012). Directed evolution of novel adeno-associated viruses for therapeutic gene delivery. *Gene Ther* **19**: 694-700.
87. Kumar-Singh, R (2008). Barriers for retinal gene therapy: separating fact from fiction. *Vision Res* **48**: 1671-1680.
88. Samulski, RJ, Srivastava, A, Berns, KI, and Muzyczka, N (1983). Rescue of adeno-associated virus from recombinant plasmids: gene correction within the terminal repeats of AAV. *Cell* **33**: 135-143.
89. Sonntag, F, Schmidt, K, and Kleinschmidt, JA (2010). A viral assembly factor promotes AAV2 capsid formation in the nucleolus. *Proc Natl Acad Sci U S A* **107**: 10220-10225.
90. Lusby, E, Fife, KH, and Berns, KI (1980). Nucleotide sequence of the inverted terminal repetition in adeno-associated virus DNA. *J Virol* **34**: 402-409.
91. King, JA, Dubielzig, R, Grimm, D, and Kleinschmidt, JA (2001). DNA helicase-mediated packaging of adeno-associated virus type 2 genomes into preformed capsids. *EMBO J* **20**: 3282-3291.
92. Vandenberghe, LH, and Auricchio, A (2012). Novel adeno-associated viral vectors for retinal gene therapy. *Gene Ther* **19**: 162-168.
93. Kronenberg, S, Kleinschmidt, JA, and Bottcher, B (2001). Electron cryo-microscopy and image reconstruction of adeno-associated virus type 2 empty capsids. *EMBO Rep* **2**: 997-1002.
94. Bartlett, JS, Wilcher, R, and Samulski, RJ (2000). Infectious entry pathway of adeno-associated virus and adeno-associated virus vectors. *J Virol* **74**: 2777-2785.
95. Rabinowitz, JE, and Samulski, RJ (2000). Building a better vector: the manipulation of AAV virions. *Virology* **278**: 301-308.
96. Grieger, JC, Johnson, JS, Gurda-Whitaker, B, Agbandje-McKenna, M, and Samulski, RJ (2007). Surface-exposed adeno-associated virus Vp1-NLS capsid fusion protein rescues infectivity of noninfectious wild-type Vp2/Vp3 and Vp3-only capsids but not that of fivefold pore mutant virions. *J Virol* **81**: 7833-7843.
97. Ferrari, FK, Samulski, T, Shenk, T, and Samulski, RJ (1996). Second-strand synthesis is a rate-limiting step for efficient transduction by recombinant adeno-associated virus vectors. *J Virol* **70**: 3227-3234.
98. Smith, RH (2008). Adeno-associated virus integration: virus versus vector. *Gene Ther* **15**: 817-822.

99. Samulski, RJ, Zhu, X, Xiao, X, Brook, JD, Housman, DE, Epstein, N, *et al.* (1991). Targeted integration of adeno-associated virus (AAV) into human chromosome 19. *EMBO J* **10**: 3941-3950.
100. Hallek, M, Girod, A, Braun-Falco, M, Wendtner, CM, Bogedain, C, and Horer, M (1998). Recombinant adeno-associated virus vectors. *IDrugs* **1**: 561-573.
101. Cheung, AK, Hoggan, MD, Hauswirth, WW, and Berns, KI (1980). Integration of the adeno-associated virus genome into cellular DNA in latently infected human Detroit 6 cells. *J Virol* **33**: 739-748.
102. McCarty, DM, Fu, H, Monahan, PE, Toulson, CE, Naik, P, and Samulski, RJ (2003). Adeno-associated virus terminal repeat (TR) mutant generates self-complementary vectors to overcome the rate-limiting step to transduction in vivo. *Gene Ther* **10**: 2112-2118.
103. Bainbridge, JW, Tan, MH, and Ali, RR (2006). Gene therapy progress and prospects: the eye. *Gene Ther* **13**: 1191-1197.
104. Dudus, L, Anand, V, Acland, GM, Chen, SJ, Wilson, JM, Fisher, KJ, *et al.* (1999). Persistent transgene product in retina, optic nerve and brain after intraocular injection of rAAV. *Vision Res* **39**: 2545-2553.
105. Auricchio, A, Kobinger, G, Anand, V, Hildinger, M, O'Connor, E, Maguire, AM, *et al.* (2001). Exchange of surface proteins impacts on viral vector cellular specificity and transduction characteristics: the retina as a model. *Hum Mol Genet* **10**: 3075-3081.
106. Rabinowitz, JE, Rolling, F, Li, C, Conrath, H, Xiao, W, Xiao, X, *et al.* (2002). Cross-packaging of a single adeno-associated virus (AAV) type 2 vector genome into multiple AAV serotypes enables transduction with broad specificity. *J Virol* **76**: 791-801.
107. Zincarelli, C, Soltys, S, Rengo, G, and Rabinowitz, JE (2008). Analysis of AAV serotypes 1-9 mediated gene expression and tropism in mice after systemic injection. *Mol Ther* **16**: 1073-1080.
108. Dalkara, D, Byrne, LC, Klimczak, RR, Visel, M, Yin, L, Merigan, WH, *et al.* (2013). In vivo-directed evolution of a new adeno-associated virus for therapeutic outer retinal gene delivery from the vitreous. *Sci Transl Med* **5**: 189ra176.
109. Kaiser, J (2003). Gene therapy. Seeking the cause of induced leukemias in X-SCID trial. *Science* **299**: 495.
110. Cavazzana-Calvo, M, Hacein-Bey, S, de Saint Basile, G, Gross, F, Yvon, E, Nusbaum, P, *et al.* (2000). Gene therapy of human severe combined immunodeficiency (SCID)-X1 disease. *Science* **288**: 669-672.
111. Bennett, J, Ashtari, M, Wellman, J, Marshall, KA, Cyckowski, LL, Chung, DC, *et al.* (2012). AAV2 gene therapy readministration in three adults with congenital blindness. *Sci Transl Med* **4**: 120ra115.
112. Moiseyev, G, Chen, Y, Takahashi, Y, Wu, BX, and Ma, JX (2005). RPE65 is the isomerohydrolase in the retinoid visual cycle. *Proc Natl Acad Sci U S A* **102**: 12413-12418.
113. Stone, EM (2007). Leber congenital amaurosis - a model for efficient genetic testing of heterogeneous disorders: LXIV Edward Jackson Memorial Lecture. *Am J Ophthalmol* **144**: 791-811.
114. Lorenz, B, Poliakov, E, Schambeck, M, Friedburg, C, Preising, MN, and Redmond, TM (2008). A comprehensive clinical and biochemical functional study of a novel RPE65 hypomorphic mutation. *Invest Ophthalmol Vis Sci* **49**: 5235-5242.
115. Lorenz, B, Gyurus, P, Preising, M, Bremser, D, Gu, S, Andrassi, M, *et al.* (2000). Early-onset severe rod-cone dystrophy in young children with RPE65 mutations. *Invest Ophthalmol Vis Sci* **41**: 2735-2742.

116. Gu, SM, Thompson, DA, Srikumari, CR, Lorenz, B, Finckh, U, Nicoletti, A, *et al.* (1997). Mutations in RPE65 cause autosomal recessive childhood-onset severe retinal dystrophy. *Nat Genet* **17**: 194-197.
117. Narfstrom, K, Katz, ML, Bragadottir, R, Seeliger, M, Boulanger, A, Redmond, TM, *et al.* (2003). Functional and structural recovery of the retina after gene therapy in the RPE65 null mutation dog. *Invest Ophthalmol Vis Sci* **44**: 1663-1672.
118. Le Meur, G, Stieger, K, Smith, AJ, Weber, M, Deschamps, JY, Nivard, D, *et al.* (2007). Restoration of vision in RPE65-deficient Briard dogs using an AAV serotype 4 vector that specifically targets the retinal pigmented epithelium. *Gene Ther* **14**: 292-303.
119. Bennicelli, J, Wright, JF, Komaromy, A, Jacobs, JB, Hauck, B, Zelenai, O, *et al.* (2008). Reversal of blindness in animal models of leber congenital amaurosis using optimized AAV2-mediated gene transfer. *Mol Ther* **16**: 458-465.
120. Acland, GM, Aguirre, GD, Ray, J, Zhang, Q, Aleman, TS, Cideciyan, AV, *et al.* (2001). Gene therapy restores vision in a canine model of childhood blindness. *Nat Genet* **28**: 92-95.
121. Simonelli, F, Maguire, AM, Testa, F, Pierce, EA, Mingozzi, F, Bennicelli, JL, *et al.* (2010). Gene therapy for Leber's congenital amaurosis is safe and effective through 1.5 years after vector administration. *Mol Ther* **18**: 643-650.
122. Wang, L, Nichols, TC, Read, MS, Bellinger, DA, and Verma, IM (2000). Sustained expression of therapeutic level of factor IX in hemophilia B dogs by AAV-mediated gene therapy in liver. *Mol Ther* **1**: 154-158.
123. Snyder, RO, Miao, C, Meuse, L, Tubb, J, Donahue, BA, Lin, HF, *et al.* (1999). Correction of hemophilia B in canine and murine models using recombinant adeno-associated viral vectors. *Nat Med* **5**: 64-70.
124. Nathwani, AC, Davidoff, A, Hanawa, H, Zhou, JF, Vanin, EF, and Nienhuis, AW (2001). Factors influencing in vivo transduction by recombinant adeno-associated viral vectors expressing the human factor IX cDNA. *Blood* **97**: 1258-1265.
125. Herzog, RW, Yang, EY, Couto, LB, Hagstrom, JN, Elwell, D, Fields, PA, *et al.* (1999). Long-term correction of canine hemophilia B by gene transfer of blood coagulation factor IX mediated by adeno-associated viral vector. *Nat Med* **5**: 56-63.
126. Herzog, RW, Hagstrom, JN, Kung, SH, Tai, SJ, Wilson, JM, Fisher, KJ, *et al.* (1997). Stable gene transfer and expression of human blood coagulation factor IX after intramuscular injection of recombinant adeno-associated virus. *Proc Natl Acad Sci U S A* **94**: 5804-5809.
127. Mount, JD, Herzog, RW, Tillson, DM, Goodman, SA, Robinson, N, McClelland, ML, *et al.* (2002). Sustained phenotypic correction of hemophilia B dogs with a factor IX null mutation by liver-directed gene therapy. *Blood* **99**: 2670-2676.
128. Urnov, FD, Rebar, EJ, Holmes, MC, Zhang, HS, and Gregory, PD (2010). Genome editing with engineered zinc finger nucleases. *Nat Rev Genet* **11**: 636-646.
129. Carroll, D (2011). Genome engineering with zinc-finger nucleases. *Genetics* **188**: 773-782.
130. Redman, M, King, A, Watson, C, and King, D (2016). What is CRISPR/Cas9? *Arch Dis Child Educ Pract Ed* **101**: 213-215.
131. Marraffini, LA, and Sontheimer, EJ (2008). CRISPR interference limits horizontal gene transfer in staphylococci by targeting DNA. *Science* **322**: 1843-1845.
132. Barrangou, R, Fremaux, C, Deveau, H, Richards, M, Boyaval, P, Moineau, S, *et al.* (2007). CRISPR provides acquired resistance against viruses in prokaryotes. *Science* **315**: 1709-1712.
133. Gaj, T, Gersbach, CA, and Barbas, CF, 3rd (2013). ZFN, TALEN, and CRISPR/Cas-based methods for genome engineering. *Trends Biotechnol* **31**: 397-405.

134. Wood, AJ, Lo, TW, Zeitler, B, Pickle, CS, Ralston, EJ, Lee, AH, *et al.* (2011). Targeted genome editing across species using ZFNs and TALENs. *Science* **333**: 307.
135. Wang, M, Sun, Z, Zou, Z, Ding, F, Li, L, Wang, H, *et al.* (2018). Efficient targeted integration into the bovine Rosa26 locus using TALENs. *Sci Rep* **8**: 10385.
136. Tesson, L, Usal, C, Menoret, S, Leung, E, Niles, BJ, Remy, S, *et al.* (2011). Knockout rats generated by embryo microinjection of TALENs. *Nat Biotechnol* **29**: 695-696.
137. Barrangou, R (2015). The roles of CRISPR-Cas systems in adaptive immunity and beyond. *Curr Opin Immunol* **32**: 36-41.
138. Hsu, PD, Lander, ES, and Zhang, F (2014). Development and applications of CRISPR-Cas9 for genome engineering. *Cell* **157**: 1262-1278.
139. Wu, X, Kriz, AJ, and Sharp, PA (2014). Target specificity of the CRISPR-Cas9 system. *Quant Biol* **2**: 59-70.
140. Chira, S, Gulei, D, Hajitou, A, Zimta, AA, Cordelier, P, and Berindan-Neagoe, I (2017). CRISPR/Cas9: Transcending the Reality of Genome Editing. *Mol Ther Nucleic Acids* **7**: 211-222.
141. Hartong, DT, Berson, EL, and Dryja, TP (2006). Retinitis pigmentosa. *Lancet* **368**: 1795-1809.
142. Lewin, AS, Rossmiller, B, and Mao, H (2014). Gene augmentation for adRP mutations in RHO. *Cold Spring Harb Perspect Med* **4**: a017400.
143. Millington-Ward, S, Chadderton, N, O'Reilly, M, Palfi, A, Goldmann, T, Kilty, C, *et al.* (2011). Suppression and replacement gene therapy for autosomal dominant disease in a murine model of dominant retinitis pigmentosa. *Mol Ther* **19**: 642-649.
144. Gorbatyuk, MS, Gorbatyuk, OS, LaVail, MM, Lin, JH, Hauswirth, WW, and Lewin, AS (2012). Functional rescue of P23H rhodopsin photoreceptors by gene delivery. *Adv Exp Med Biol* **723**: 191-197.
145. Gorbatyuk, M, Justilien, V, Liu, J, Hauswirth, WW, and Lewin, AS (2007). Preservation of photoreceptor morphology and function in P23H rats using an allele independent ribozyme. *Exp Eye Res* **84**: 44-52.
146. Gorbatyuk, MS, Pang, JJ, Thomas, J, Jr., Hauswirth, WW, and Lewin, AS (2005). Knockdown of wild-type mouse rhodopsin using an AAV vectored ribozyme as part of an RNA replacement approach. *Mol Vis* **11**: 648-656.
147. Mao, H, Gorbatyuk, MS, Rossmiller, B, Hauswirth, WW, and Lewin, AS (2012). Long-term rescue of retinal structure and function by rhodopsin RNA replacement with a single adeno-associated viral vector in P23H RHO transgenic mice. *Hum Gene Ther* **23**: 356-366.
148. Bakondi, B, Lv, W, Lu, B, Jones, MK, Tsai, Y, Kim, KJ, *et al.* (2016). In Vivo CRISPR/Cas9 Gene Editing Corrects Retinal Dystrophy in the S334ter-3 Rat Model of Autosomal Dominant Retinitis Pigmentosa. *Mol Ther* **24**: 556-563.
149. Latella, MC, Di Salvo, MT, Cocchiarella, F, Benati, D, Grisendi, G, Comitato, A, *et al.* (2016). In vivo Editing of the Human Mutant Rhodopsin Gene by Electroporation of Plasmid-based CRISPR/Cas9 in the Mouse Retina. *Mol Ther Nucleic Acids* **5**: e389.
150. Jinek, M, Chylinski, K, Fonfara, I, Hauer, M, Doudna, JA, and Charpentier, E (2012). A programmable dual-RNA-guided DNA endonuclease in adaptive bacterial immunity. *Science* **337**: 816-821.
151. Cong, L, Ran, FA, Cox, D, Lin, S, Barretto, R, Habib, N, *et al.* (2013). Multiplex genome engineering using CRISPR/Cas systems. *Science* **339**: 819-823.
152. Ran, FA, Hsu, PD, Wright, J, Agarwala, V, Scott, DA, and Zhang, F (2013). Genome engineering using the CRISPR-Cas9 system. *Nat Protoc* **8**: 2281-2308.
153. Lin, WY, Wilson, JH, and Lin, Y (2013). Repair of chromosomal double-strand breaks by precise ligation in human cells. *DNA Repair (Amst)* **12**: 480-487.

154. Mandal, PK, Ferreira, LM, Collins, R, Meissner, TB, Boutwell, CL, Friesen, M, *et al.* (2014). Efficient ablation of genes in human hematopoietic stem and effector cells using CRISPR/Cas9. *Cell Stem Cell* **15**: 643-652.
155. Long, C, Amoasii, L, Mireault, AA, McAnally, JR, Li, H, Sanchez-Ortiz, E, *et al.* (2016). Postnatal genome editing partially restores dystrophin expression in a mouse model of muscular dystrophy. *Science* **351**: 400-403.
156. Nelson, CE, Hakim, CH, Ousterout, DG, Thakore, PI, Moreb, EA, Castellanos Rivera, RM, *et al.* (2016). In vivo genome editing improves muscle function in a mouse model of Duchenne muscular dystrophy. *Science* **351**: 403-407.
157. Tabebordbar, M, Zhu, K, Cheng, JKW, Chew, WL, Widrick, JJ, Yan, WX, *et al.* (2016). In vivo gene editing in dystrophic mouse muscle and muscle stem cells. *Science* **351**: 407-411.
158. Betermier, M, Bertrand, P, and Lopez, BS (2014). Is non-homologous end-joining really an inherently error-prone process? *PLoS Genet* **10**: e1004086.
159. Suzuki, K, Tsunekawa, Y, Hernandez-Benitez, R, Wu, J, Zhu, J, Kim, EJ, *et al.* (2016). In vivo genome editing via CRISPR/Cas9 mediated homology-independent targeted integration. *Nature* **540**: 144-149.
160. Sancho-Pelluz, J, Tosi, J, Hsu, CW, Lee, F, Wolpert, K, Tabacaru, MR, *et al.* (2012). Mice with a D190N mutation in the gene encoding rhodopsin: a model for human autosomal-dominant retinitis pigmentosa. *Mol Med* **18**: 549-555.
161. Tsui, I, Chou, CL, Palmer, N, Lin, CS, and Tsang, SH (2008). Phenotype-genotype correlations in autosomal dominant retinitis pigmentosa caused by RHO, D190N. *Curr Eye Res* **33**: 1014-1022.
162. Liu, MY, Liu, J, Mehrotra, D, Liu, Y, Guo, Y, Baldera-Aguayo, PA, *et al.* (2013). Thermal stability of rhodopsin and progression of retinitis pigmentosa: comparison of S186W and D190N rhodopsin mutants. *J Biol Chem* **288**: 17698-17712.
163. Park, SP, Lee, W, Bae, EJ, Greenstein, V, Sin, BH, Chang, S, *et al.* (2014). Early structural anomalies observed by high-resolution imaging in two related cases of autosomal-dominant retinitis pigmentosa. *Ophthalmic Surg Lasers Imaging Retina* **45**: 469-473.
164. Mao, H, James, T, Jr., Schwein, A, Shabashvili, AE, Hauswirth, WW, Gorbatyuk, MS, *et al.* (2011). AAV delivery of wild-type rhodopsin preserves retinal function in a mouse model of autosomal dominant retinitis pigmentosa. *Hum Gene Ther* **22**: 567-575.
165. Acland, GM, Aguirre, GD, Bennett, J, Aleman, TS, Cideciyan, AV, Bencicelli, J, *et al.* (2005). Long-term restoration of rod and cone vision by single dose rAAV-mediated gene transfer to the retina in a canine model of childhood blindness. *Mol Ther* **12**: 1072-1082.
166. Jacobson, SG, Cideciyan, AV, Roman, AJ, Sumaroka, A, Schwartz, SB, Heon, E, *et al.* (2015). Improvement and decline in vision with gene therapy in childhood blindness. *N Engl J Med* **372**: 1920-1926.
167. Swain, GP, Prociuk, M, Bagel, JH, O'Donnell, P, Berger, K, Drobotz, K, *et al.* (2014). Adeno-associated virus serotypes 9 and rh10 mediate strong neuronal transduction of the dog brain. *Gene Ther* **21**: 28-36.
168. Yang, T, Justus, S, Li, Y, and Tsang, SH (2015). BEST1: the Best Target for Gene and Cell Therapies. *Mol Ther* **23**: 1805-1809.
169. Johnson, AA, Guziewicz, KE, Lee, CJ, Kalathur, RC, Pulido, JS, Marmorstein, LY, *et al.* (2017). Bestrophin 1 and retinal disease. *Prog Retin Eye Res* **58**: 45-69.
170. Marmorstein, LY, Wu, J, McLaughlin, P, Yocom, J, Karl, MO, Neussert, R, *et al.* (2006). The light peak of the electroretinogram is dependent on voltage-gated calcium channels and antagonized by bestrophin (best-1). *J Gen Physiol* **127**: 577-589.
171. Chakraborty, R, Muchtar, E, and Gertz, MA (2016). Newer Therapies for Amyloid Cardiomyopathy. *Curr Heart Fail Rep* **13**: 237-246.

172. Wang, L, Yi, F, Fu, L, Yang, J, Wang, S, Wang, Z, *et al.* (2017). CRISPR/Cas9-mediated targeted gene correction in amyotrophic lateral sclerosis patient iPSCs. *Protein Cell* **8**: 365-378.
173. Zheng, T, Hou, Y, Zhang, P, Zhang, Z, Xu, Y, Zhang, L, *et al.* (2017). Profiling single-guide RNA specificity reveals a mismatch sensitive core sequence. *Sci Rep* **7**: 40638.
174. Zhang, XH, Tee, LY, Wang, XG, Huang, QS, and Yang, SH (2015). Off-target Effects in CRISPR/Cas9-mediated Genome Engineering. *Mol Ther Nucleic Acids* **4**: e264.
175. Buchholz, DE, Hikita, ST, Rowland, TJ, Friedrich, AM, Hinman, CR, Johnson, LV, *et al.* (2009). Derivation of functional retinal pigmented epithelium from induced pluripotent stem cells. *Stem Cells* **27**: 2427-2434.
176. Buchholz, DE, Pennington, BO, Croze, RH, Hinman, CR, Coffey, PJ, and Clegg, DO (2013). Rapid and efficient directed differentiation of human pluripotent stem cells into retinal pigmented epithelium. *Stem Cells Transl Med* **2**: 384-393.
177. Idelson, M, Alper, R, Obolensky, A, Ben-Shushan, E, Hemo, I, Yachimovich-Cohen, N, *et al.* (2009). Directed differentiation of human embryonic stem cells into functional retinal pigment epithelium cells. *Cell Stem Cell* **5**: 396-408.
178. Harding, HP, Calton, M, Urano, F, Novoa, I, and Ron, D (2002). Transcriptional and translational control in the Mammalian unfolded protein response. *Annu Rev Cell Dev Biol* **18**: 575-599.
179. Roybal, CN, Yang, S, Sun, CW, Hurtado, D, Vander Jagt, DL, Townes, TM, *et al.* (2004). Homocysteine increases the expression of vascular endothelial growth factor by a mechanism involving endoplasmic reticulum stress and transcription factor ATF4. *J Biol Chem* **279**: 14844-14852.
180. Abcouwer, SF, Marjon, PL, Loper, RK, and Vander Jagt, DL (2002). Response of VEGF expression to amino acid deprivation and inducers of endoplasmic reticulum stress. *Invest Ophthalmol Vis Sci* **43**: 2791-2798.
181. Wang, Y, Hanus, JW, Abu-Asab, MS, Shen, D, Ogilvy, A, Ou, J, *et al.* (2016). NLRP3 Upregulation in Retinal Pigment Epithelium in Age-Related Macular Degeneration. *Int J Mol Sci* **17**.
182. Fernandez-Godino, R, Garland, DL, and Pierce, EA (2015). A local complement response by RPE causes early-stage macular degeneration. *Hum Mol Genet* **24**: 5555-5569.
183. Pereira, ER, Frudd, K, Awad, W, and Hendershot, LM (2014). Endoplasmic reticulum (ER) stress and hypoxia response pathways interact to potentiate hypoxia-inducible factor 1 (HIF-1) transcriptional activity on targets like vascular endothelial growth factor (VEGF). *J Biol Chem* **289**: 3352-3364.
184. Tseng, WA, Thein, T, Kinnunen, K, Lashkari, K, Gregory, MS, D'Amore, PA, *et al.* (2013). NLRP3 inflammasome activation in retinal pigment epithelial cells by lysosomal destabilization: implications for age-related macular degeneration. *Invest Ophthalmol Vis Sci* **54**: 110-120.
185. Kauppinen, A, Niskanen, H, Suuronen, T, Kinnunen, K, Salminen, A, and Kaarniranta, K (2012). Oxidative stress activates NLRP3 inflammasomes in ARPE-19 cells--implications for age-related macular degeneration (AMD). *Immunol Lett* **147**: 29-33.
186. Hollyfield, JG, Bonilha, VL, Rayborn, ME, Yang, X, Shadrach, KG, Lu, L, *et al.* (2008). Oxidative damage-induced inflammation initiates age-related macular degeneration. *Nat Med* **14**: 194-198.
187. Krohne, TU, Stratmann, NK, Kopitz, J, and Holz, FG (2010). Effects of lipid peroxidation products on lipofuscinogenesis and autophagy in human retinal pigment epithelial cells. *Exp Eye Res* **90**: 465-471.

188. Hoppe, G, O'Neil, J, Hoff, HF, and Sears, J (2004). Products of lipid peroxidation induce missorting of the principal lysosomal protease in retinal pigment epithelium. *Biochim Biophys Acta* **1689**: 33-41.
189. Catala, A (2011). Lipid peroxidation of membrane phospholipids in the vertebrate retina. *Front Biosci (Schol Ed)* **3**: 52-60.
190. Kumar, MV, Nagineni, CN, Chin, MS, Hooks, JJ, and Detrick, B (2004). Innate immunity in the retina: Toll-like receptor (TLR) signaling in human retinal pigment epithelial cells. *J Neuroimmunol* **153**: 7-15.
191. Kleinman, ME, Yamada, K, Takeda, A, Chandrasekaran, V, Nozaki, M, Baffi, JZ, *et al.* (2008). Sequence- and target-independent angiogenesis suppression by siRNA via TLR3. *Nature* **452**: 591-597.
192. Kleinman, ME, Kaneko, H, Cho, WG, Dridi, S, Fowler, BJ, Blandford, AD, *et al.* (2012). Short-interfering RNAs induce retinal degeneration via TLR3 and IRF3. *Mol Ther* **20**: 101-108.
193. Golestaneh, N, Chu, Y, Xiao, YY, Stoleru, GL, and Theos, AC (2017). Dysfunctional autophagy in RPE, a contributing factor in age-related macular degeneration. *Cell Death Dis* **8**: e2537.
194. Galloway, CA, Dalvi, S, Hung, SSC, MacDonald, LA, Latchney, LR, Wong, RCB, *et al.* (2017). Drusen in patient-derived hiPSC-RPE models of macular dystrophies. *Proc Natl Acad Sci U S A* **114**: E8214-E8223.
195. Ghosh, S, Mallonee, DH, Hylemon, PB, and Grogan, WM (1995). Molecular cloning and expression of rat hepatic neutral cholesteryl ester hydrolase. *Biochim Biophys Acta* **1259**: 305-312.
196. Ghosh, S (2000). Cholesteryl ester hydrolase in human monocyte/macrophage: cloning, sequencing, and expression of full-length cDNA. *Physiol Genomics* **2**: 1-8.
197. Crow, JA, Middleton, BL, Borazjani, A, Hatfield, MJ, Potter, PM, and Ross, MK (2008). Inhibition of carboxylesterase 1 is associated with cholesteryl ester retention in human THP-1 monocyte/macrophages. *Biochim Biophys Acta* **1781**: 643-654.
198. Slocum, C, Kramer, C, and Genco, CA (2016). Immune dysregulation mediated by the oral microbiome: potential link to chronic inflammation and atherosclerosis. *J Intern Med* **280**: 114-128.
199. Nakamura, N, Saeki, K, Mitsumoto, M, Matsuyama, S, Nishio, M, Saeki, K, *et al.* (2012). Feeder-free and serum-free production of hepatocytes, cholangiocytes, and their proliferating progenitors from human pluripotent stem cells: application to liver-specific functional and cytotoxic assays. *Cell Reprogram* **14**: 171-185.
200. Jin, ZB, Okamoto, S, Xiang, P, and Takahashi, M (2012). Integration-free induced pluripotent stem cells derived from retinitis pigmentosa patient for disease modeling. *Stem Cells Transl Med* **1**: 503-509.
201. Fusaki, N, Ban, H, Nishiyama, A, Saeki, K, and Hasegawa, M (2009). Efficient induction of transgene-free human pluripotent stem cells using a vector based on Sendai virus, an RNA virus that does not integrate into the host genome. *Proc Jpn Acad Ser B Phys Biol Sci* **85**: 348-362.
202. Maminishkis, A, Chen, S, Jalickee, S, Banzon, T, Shi, G, Wang, FE, *et al.* (2006). Confluent monolayers of cultured human fetal retinal pigment epithelium exhibit morphology and physiology of native tissue. *Invest Ophthalmol Vis Sci* **47**: 3612-3624.